UNIVERSITY OF OKLAHOMA

GRADUATE COLLEGE

STUDY TOWARDS IMPROVING THE EFFICIENCY OF MATRIX ACIDIZING IN OIL-BEARING CARBONATE FORMATIONS

A DISSERTATION

SUBMITTED TO THE GRADUATE FACULTY

in partial fulfillment of the requirements for the

Degree of

DOCTOR OF PHILOSOPHY

By

MOHAMED MUSTAFA ELMABRUK ELSAFIH
Norman, Oklahoma
2021

STUDY TOWARDS IMPROVING THE EFFICIENCY OF MATRIX ACIDIZING IN

OIL-BEARING CARBONATE FORMATIONS

A DISSERTATION APPROVED FOR THE
MEWBOURNE SCHOOL OF PETROLEUM AND GEOLOGICAL ENGINEERING

BY THE COMMITTEE CONSISTING OF

Dr. Mashhad Fahes, Chair

Dr. Matthias Nollert

Dr. Catalin Teodoriu

Dr. Xingru Wu

Dr. Hamidreza Karami

Dedication

To my father, *Mustafa Elsafih*

To my mother, *Fathia Elsafih*

To my *brothers and sisters*

To my wife, *Najah Abuojaylah*

To my son, *Ebraheem Elsafih*

To my daughter, *Joury Elsafih*

To my coming baby, *Eyad Elsafih*

Acknowledgment

All praise be to Allah, Lord of the Worlds, who helped me to complete this dissertation. I highly appreciate and acknowledge the massive contribution of my advisor Dr. Mashhad who, without her, this work could not be achieved. Her knowledge, motivation, and guidance helped me conducting experiments, analyze results, and writing a dissertation. My sincere gratitude goes to my wife (Najah), son (Ebraheem), and daughter (Joury) for their sacrifices and support. I am thankful to my parents, brothers, and sisters for their love and help. I would like to thank my dissertation committee for contributing to my committee, their comments, and their feedback. My thanks and appreciation to Dr. Mathias Nollert, Dr. Catalin Teodoriu, Dr. Xingru Wu, and Dr. Hamidreza Karami. My special thanks to Dr. Catalin Teodoriu for his help during laboratory experiments. His experience and knowledge helped me overcoming technical issues and running experiments in the lab. My sincere thanks also go to Gary Stowe for his help and support in labs. I also would like to thank Bryan Scarborough for his contribution to the early stage of this research.

Table of Contents

List of Tables

List of Figures

Abstract

Matrix acidizing in carbonate formations is a common technique to improve well productivity. Since more than 60% of the world's reservoir formations are carbonates, enhancing the process of acidizing can have a significant impact on hydrocarbon production. To improve the outcome of this stimulation technique from both the technical and economic points of view, an optimization of the acidizing process is essential. Improving the acidizing process can be achieved by: (1) Investigating the formation of acid-oil emulsions and understanding their behavior and stability over time, (2) Analyzing how the addition of de-emulsifiers would affect the performance of acidizing treatment, and (3) Studying how the presence of oil and the formation of acid-oil emulsions affect the acid optimum injection conditions of rate and volume with the consideration of possible field applications in terms of permeability and reservoir pressure. All these investigations are conducted in this study at the laboratory scale.

In this work, a series of laboratory experiments are conducted to better understand the process of matrix acidizing in three approaches; First, acid-oil emulsion viscosity and stability are analyzed of their effect on productivity after treatment. Second, the importance of additives such as de-emulsifiers and surfactants is studied and quantified in terms of their influence on enhancing acid treatment performance. Third, factors controlling the acid optimum injection rate are analyzed. These factors include fluid saturation, reservoir pressure, and formation permeability. Such specific improvements over the three dimensions mentioned above would enhance the acid treatment, resulting in creating an optimum wormhole with minimum skin and improved well deliverability.

1. Chapter 1: Introduction

1.1 Matrix Acidizing

Matrix acidizing has been used extensively since the first attempt in 1930 (Kalfayan 2008). The main goal of acidizing is improving well productivity by reducing formation damage around the wellbore. While acidizing in sandstone dissolves particles inside the pores, the acid creates wormholes with massive permeability in carbonates. This acidizing process is conducted by injecting acid into the formation at a specific rate, volume, and concentration. Injection pressure in matrix acidizing must be below the fracturing pressure of the formation to avoid fracturing it. Matrix acidizing is the most common stimulation technique in carbonate formations, where hydrochloric acid (HCl) is injected to react with the formation (mostly Calcium Carbonate) and create wormholes (Daccord et al. 1989; Daccord et al. 1993). The chemical reaction happens as in Equation 1.1, where Calcium Chloride ($CaCl_2$), Carbon Dioxide (CO_2), and water (HO_2) are the reaction products:

$$2HCl + CaCO_3 \rightarrow CaCl_2 + CO_2 + H_2O \qquad (1.1)$$

1.2 Problem Statement

It is common to inject acidic stimulation fluids into oil-bearing formations to enhance well productivity. However, to achieve the targeted results, the process of acidizing must be optimized. The injection of acid can generate acid-in-oil emulsions that are highly stable, highly viscous, and it can result in severe damage to well performance if not considered as a part of the design of the stimulation job. In some cases, additives are added to the acid to reduce the risk of emulsions. In other cases, a pre-flush is injected to displace the oil from the near-wellbore region to reduce acid-oil contact. However, the concept of emulsion risk inside the formation is still controversial; many operators and researchers do not think that enough shear-mixing can occur in the pore space to

form stable emulsions. The result is inconsistent use of acid additives when the cost of these additives is not justified. This concern of additives cost raises especially in small independent companies operating in small fields, as we observed in a recent field case we studied.

A critical aspect of the process of optimizing acid jobs is the acid injection rate, which is affected by many factors such as formation permeability, reservoir pressure, fluid saturation, and rock dimensions. If these factors are not critically considered, the acid injection parameters identified in laboratory settings would be unsuitable when scaled for reservoir conditions, thus, leading to ineffective acid jobs that are costly and do not maximize well deliverability.

1.3 Research Motivations and Objectives

According to Schlumberger market analysis in 2007, A massive proportion of the world's oil reserves are found in carbonate reservoirs in places such as Libya, Middle East, Russia, Kazakhstan, and North America, as shown in Figure 1.1. An example of one of the largest carbonate reservoirs in the world is the Ghawar field in Saudi Arabia. More attention to such an important resource is required. With the oil prices being low and unstable over the recent years, more cost optimization is needed in oil service jobs such as acidizing. As the vast majority of acid treatment companies are using de-emulsifiers in their routine schedule, it is helpful to better assess the impact on project economics by looking at the benefits of using de-emulsifiers to overcome acid-oil emulsions, compared to not using them but allowing the formation of emulsions. With the motivation of better understanding the mechanisms that impact the efficiency of the acidizing process in carbonate formations, this study aims to accomplish the following:

- Investigate the formation and stability of acid-oil emulsions during the acidizing process and analyze their effect on well deliverability after acid treatment.
- Analyze the effect of acid additives on the process of acidizing.

- ❖ Study the effect of the presence of an oil saturation on the efficiency of the acidizing process under various conditions of permeability and backpressure.
- ❖ Study the effect of de-emulsifiers on the performance and efficiency of the acidizing process.

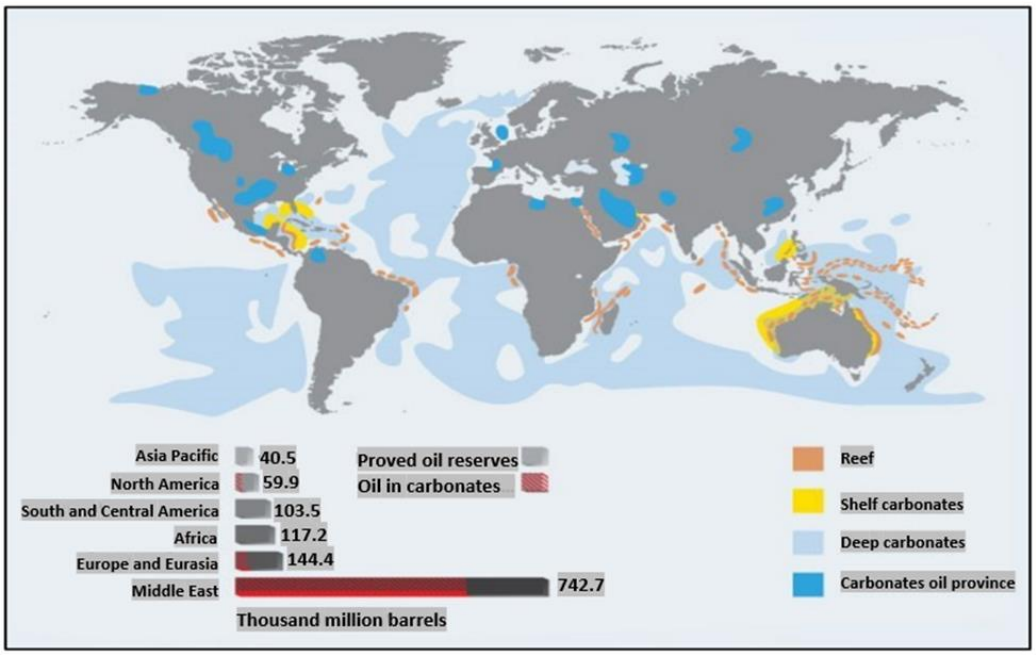

Figure 1.1: Carbonate formations distribution in the world (Schlumberger 2007)

1.4 Research Scope and Methodology

This study is divided into two stages of research to achieve the objectives outlined in section 1.3. These stages include a critical literature review and experimental work. The scope and methodology of each stage are described in the following:

1. Critical Literature Review: This stage aims to provide a comprehensive review of all published work where an experimental investigation of matrix acidizing in carbonate formations is performed. More attention is given to cases where the impact of oil is considered. The review covers the following highlights: the formation of acid-oil emulsions during the acidizing process, emulsion's behavior in terms of stability and

viscosity over time, the effect of additives on the acidizing treatment, optimizing acid injection rate and volume, and factors affecting the optimization of the acidizing process.

2. Experimental Work: This stage includes conducting a systematic and structured set of experiments where a massive amount of data is collected and analyzed to better understand the acidizing process. Four types of experiments were conducted as follows:
   A. Acid-crude emulsions were investigated over time to document the changes in the viscosity and density of the sludge using bottle tests. Core flooding was performed on crude-saturated samples to see how such emulsions affect oil flow post-acidizing. Crude oil from a field in Texas was obtained for this study, and Indiana Limestone cores were used in the flooding tests.
   B. Experiments were conducted to quantify the effect of de-emulsifiers on oil flow performance after acidizing. Nine different de-emulsifiers were investigated to identify the most effective one in eliminating the emulsion. Bottle tests were then conducted to study the stability and viscosity of three fluid systems considering those prone to emulsions versus those that do not carry an emulsion risk. A core flooding experiment was designed that replicates the process of well stimulation and backflow of oil production.
   C. A systematic experimental study was designed to evaluate the impact of multi-phase flow, permeability, and pressure on the acidizing process when injecting 15 wt.% HCl into crude-oil saturated Indiana Limestone cores.
   D. Experiments were conducted to evaluate the effect of adding de-emulsifiers on the efficiency of the acidizing process.

1.5 Research Hypotheses

Based on the fact of the presence of oil in carbonate formations during acidizing, the following hypotheses are considered for this research:

- Acid-oil emulsions are real and have a significant influence on flow assurance.
- De-emulsifiers need to be balanced in terms of type and volume to improve the acidizing efficiency and not affect flow assurance.

1.6 Dissertation Structure

The dissertation is structured into seven chapters. Chapter 1 provides an overview of matrix acidizing in oil-bearing carbonate formations and underlines the problems associated with the presence of oil in the formation. The motivations, objectives, scope, methodology, and hypotheses of this work are also discussed. In Chapter 2, a general overview of carbonate rocks and the principles of matrix acidizing is provided. A comprehensive literature review of prior research conducted in the area of matrix acidizing in carbonate formations and the characterization of gaps in the available research is illustrated in Chapter 3. Chapter 4 outlines part A of the experimental work conducted to confirm the formation of acid-oil emulsions during acidizing and analyzing their viscosity and stability behavior over time. Chapter 5 covers part B of the experimental work, where the effect of using de-emulsifiers on the performance of the acidizing process is quantified. Chapter 6 describes parts C and D of the experimental work conducted to study the effect of two-phase flow on optimizing the acidizing process under various conditions of permeability and pressure, including the impact of de-emulsifiers on the process. Finally, Chapter 7 summarizes conclusions and proposes recommendations that can help to improve acidizing in oil-bearing carbonate formations.

2. Chapter 2: General Overview

2.1 Overview of Matrix Acidizing in Carbonate Formations

2.1.1 Carbonate Formations

Carbonate formations are kinds of sedimentary rocks that are mainly composed of carbonate minerals. Carbonates are commonly classified into two main types, which are Limestone and Dolomite. While the Limestone is composed of Calcite ($CaCO_3$), the Dolomite composition is more complicated because it forms when Calcite reacts with Magnesium (Mg^{+2}) according to the chemical reaction in Equation 2.1. This process is called "Dolomitization," which causes contraction in rocks and produces porosity (Mazzullo et al. 1996).

$$2\ CaCO_3 + Mg^{+2} \rightarrow CaMg\ (CO_3)_2 + Ca^{+2} \qquad (2.1)$$

Although the classifications of carbonate formations seem to be simple, the reality of their presence in nature is more complicated, where other minerals such as Iron and Silicon are usually present. It is often difficult to determine the exact nature of the rock. The inclusion of Iron minerals and Siliceous material may complicate the structure of carbonates (Feazel et al. 2004). Depending on the concentration of Siliceous components, such rocks are known as Sandy or Shaly Limestones. Figure 2.1 shows a schematic classification of carbonates as a function of the composition (William 1962). As described by Economides et al. (1994) in their book "Petroleum Production Systems," the reactions of the Hydrochloric acid (HCl) with Calcite and Dolomite are as follows:

- *Calcite*

Hydrochloric Acid + Calcite → Calcium Chloride + Carbon Dioxide + Water

$$2HCl + CaCO_3 \rightarrow CaCl_2 + CO_2 + H_2O \qquad (2.2)$$

❖ *Dolomite*

Hydrochloric Acid + Dolomite → Calcium Chloride + Carbon Dioxide + Magnesium Chloride + Water

$$4HCl + CaMg(CO_3)_2 \rightarrow CaCl_2 + 2CO_2 + MgCl_2 + 2H_2O \qquad (2.3)$$

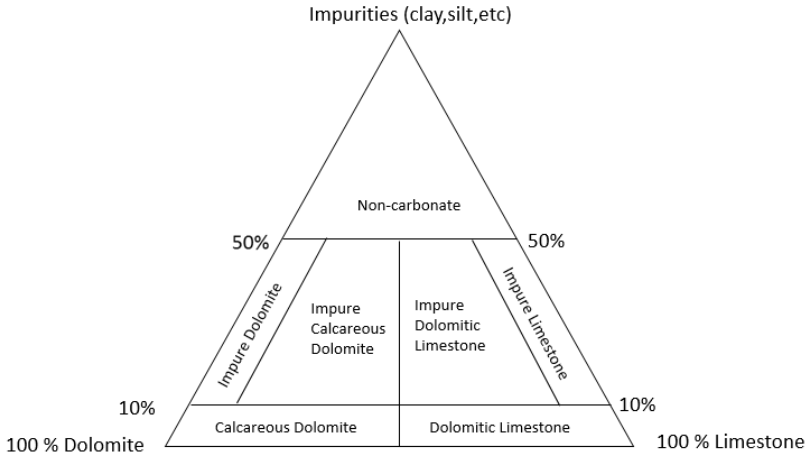

Figure 2.1: Carbonate rocks composition (William 1962)

2.1.2 Matrix Acidizing

Matrix acidizing is the process of injecting a significant amount of acid into the wellbore, typically after well completion, to remove formation damage and restore or improve permeability (Williams et al. 1979). That happens by injecting the acid at a pressure that is below fracturing pressure. In carbonate formations, the reaction between the acid and the formation results in creating wormholes which can significantly increase hydrocarbon flow towards the wellbore. While in sandstone formations, the improvement of permeability occurs when the acid removes the near wellbore damage caused by drilling, completion, and production operations. Although Matrix acidizing is considered a risky process by many operators in the oil and gas industry, it has been

proven that this technique can highly improve productivity at a relatively low cost (Rae and Di-Lullo 2003).

2.1.3 Why Is Acidizing in Carbonates Different Than in Sandstones?

The primary objective of acidizing stimulation is to remove or bypass formation damage around the wellbore. However, both chemical and physical aspects of carbonate acidizing are very different from sandstone acidizing. The different composition of the rock causes the reaction rate to be much faster in carbonates. Hydrofluoric (HF) acid is commonly used in sandstones, while Hydrochloric acid (HCl) is used in carbonates. The different nature of porosity and permeability (vuggy, fractured porosity in carbonates vs. intergranular porosity in sandstones), in addition to the faster reaction rate, causes the acid in carbonates to follow preferential flow paths called "wormholes," thus bypassing rather than dissolving damage (Economides et al. 1994). The difference in the dissolution path between carbonates and sandstones is showing in Figures 2.2 and 2.3.

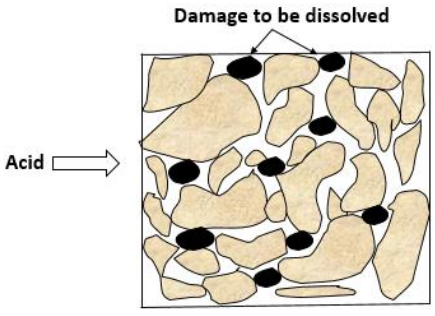

Figure 2.2: HF acid injection in Sandstones

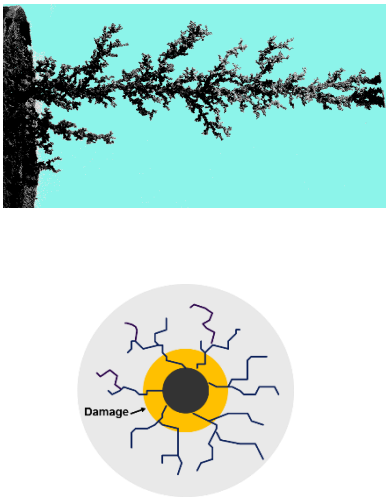

Figure 2.3: HCl acid injection in Carbonates (Modified after Buijse 2000)

2.2 The Phenomenon of Worm-holing in Carbonates

As the name suggests, wormholes in carbonate acidizing are the paths built due to HCl acid reacting with Calcite, as shown in Figure 2.4. Physically, what happens is called a "dissolution process," where small pores grow at a much lower rate than the large pores' rate (Akanni et al. 2017). According to Hoefner and Fogler (1989), the structure of wormholes depends on three main factors: injection rate, Damkohler Number, and Peclet Number. These three factors are explained as follows:

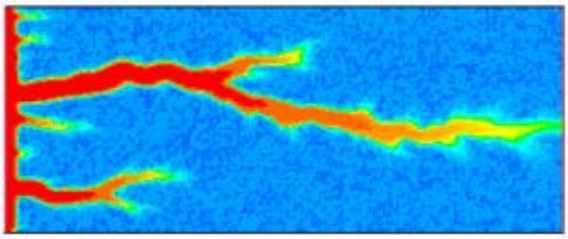

Figure 2.4: Wormhole shaping (Akanni et al. 2017)

2.2.1 Injection Rate

One of the most critical factors that shape the wormholes in acidizing is the rate at which acid is injected. Older studies recommended injecting acid at the highest possible rate below fracturing pressure (Williams et al. 1979; Paccaloni and Tambini 1993). However, some experimental studies revealed favorable results at lower acid injection rates (Daccord et al. 1989). The change in injection rate results in a different wormhole structure. While the optimum injection rate creates the longest wormhole for a given amount of acid injected, very low or very high rates result in face dissolution, as shown in Figure 2.5.

2.2.2 Dimensionless Numbers

2.2.2.1 Damkohler Number

Generally, the Damkohler number (D_a) is a dimensionless number defined as the ratio of the reaction rate to the convective mass transport rate. For a general chemical reaction, the Damkohler number is expressed by Equation 2.4:

$$D_a = kC_0^{n-1}t \qquad (2.4)$$

Where:

k : Kinetics reaction rate constant

C_0: Initial concentration

n: Reaction order

t : Time

As for the HCl reaction with carbonates, Wang et al. (1993) defined the Damkohler number experimentally according to Equation 2.5:

$$D_a = \frac{E_f C_o^{n-1}}{u} \qquad (2.5)$$

Where:

E_f: Forward reaction rate constant

u : Acid flux, which is the volumetric flow rate per area

According to their experimental analysis, Wang et al. (1993) introduced the concept of "transition area." When the wormhole propagates, there is a critical pore cross-sectional area where the reaction is taking place, defined by Equation 2.6:

$$A_T = 20D_a^{1.5}(KL_a)^{1.5} \qquad (2.6)$$

Where:

A_T: Transition pore area

K : Average permeability

L_a: Average length

Then, the transition pore size (r_T) is given by Equation 2.7:

$$r_T = \left(\frac{A_T}{\pi}\right)^{1/2} \qquad (2.7)$$

From Equations 2.6 and 2.7, the Damkohler number decreases as the transition area decreases, and that happens when the acid flux increases or the reaction rate decreases. Therefore, if the largest pore radius in the rock is greater than or equal to the transition area pore radius, a major wormhole will form due to those large pores being propagated. However, if the radius of the largest pore in the rock is smaller than the radius of the transition area, the wormhole will either not form or be insignificant.

2.2.2.2 Peclet Number

Peclet number (Pe) is defined as the ratio of convection transport rate to diffusive transport rate of acid. While many studies have been published on the effects of Peclet number on flow in porous media (Adewale et al. 2004), little research covered the impact of this number on acid flow in carbonates. Fredd and Miller (2000) analyzed how Peclet number controls shaping the wormhole and concluded that as Peclet number increases, a bigger wormhole is formed until reaching its optimum value, where a higher Peclet number results in a ramified wormhole. Depending on those

three factors described above, as shown in Figure 2.5, Hoefner and Fogler (1989) categorize wormholes in four main types as follows:

1- *Face Dissolution:* This happens at meager injection rates where the Peclet number is also very low and the Damkohler number is very high.

2- *Conical Channel:* A conical channel is formed when the injection rate is below the optimum rate, whereas Peclet and Damkohler numbers are at moderate values.

3- *Optimum Wormhole:* This situation is the target of any acid job. A perfect wormhole is created at the optimum acid injection rate where Peclet and Damkohler numbers are also at optimum values.

4- *Ramified Wormhole:* When the acid injection flow rate is high, Peclet number is also increased, and Damkohler number is low, a ramified wormhole is formed.

5- *Uniform Dissolution:* In this case, no wormhole is formed where the injection rate is very high.

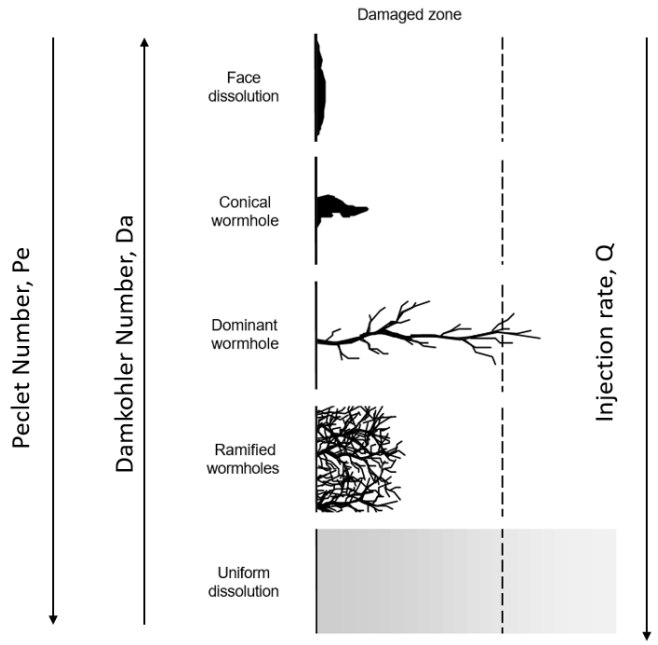

Figure 2.5: Factors affecting wormhole structure (after Freed 2000)

2.3 Wormhole Models

To give more details of the reaction between acid and rocks, in 1989, Daccord et al. were the first to introduce a kinetic parameter (P) that relates mass transfer to the surface reaction rates. By Daccord et al.'s definition, P is expressed as shown in Equation 2.8:

$$P = \frac{U_d}{U_s} \qquad (2.8)$$

Where:

U_d: Diffusive flux

U_s: Molecular flux caused by the surface reaction.

Equation. 2.8 is then modified to the following expression 2.9:

$$P = \frac{D}{E_f R C^{n-1}} \qquad (2.9)$$

Where:

D : Molecular diffusion coefficient

E_f: Surface reaction rate constant

R : Pore radius

C : Acid concentration

Based on this concept, Daccord et al. (1989) developed a wormhole propagation model by running experiments with plaster and water, assuming a linear flow of acid. The length of the wormhole is estimated using Equation 2.10:

$$L = \frac{aVN_{ac}}{A\emptyset} D^{-1.5} q^{-0.33} \qquad (2.10)$$

Where:

a: Experimental constant

V: Cumulative acid injected volume

N_{ac}: Acid capacity number

D : Molecular diffusion coefficient

A : Cross-sectional area

$\emptyset$: Porosity

q: Flow rate

Equation 2.10 implies that a longer wormhole is created at lower acid injection rates if the volume of acid injected is constant. Since q= v/t, taking the first derivative of Equation 2.10 with time results in Equation 2.11:

$$\frac{dL}{dt} = \frac{aN_{ac}}{A\emptyset} D^{-1.5} q^{-0.33} \qquad (2.11)$$

Daccord et al. (1989) were able to convert Equation 2.11 to the radial flow pattern to calculate the wormhole radius, leading to Equation 2.12:

$$r_{wh} = \left[\frac{bN_{Ac}V}{\pi h\emptyset} D^{-1.5} \left[\frac{q}{h}\right]^{-0.33}\right]^{\frac{1}{df}} \qquad (2.12)$$

Where:

r_{wh}: Wormhole radius

b : Constant = 1.5 * 10^{-5} SI units

d_f: Fractal dimension

h: Formation thickness

Another mechanistic model was developed by Hung et al. (1997), where an idealized cylindrical wormhole is assumed, as shown in Figure 2.6.

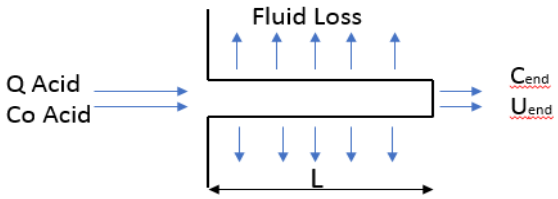

Figure 2.6: Wormhole idealization. (after Hung et al. 1997)

By applying a mass balance to the process of acid dissolving the rock, the change in wormhole length with time, termed wormhole velocity, is given by Equation 2.13. In this equation, the injection rate is assumed to be high, and acid reaches the wormhole's end as spent acid. A detailed illustration of the development of wormhole propagation models in the literature is presented in Appendix A.

$$\frac{dL}{dt} = \frac{\beta_{100}\rho_{acid}C_{end}U_{end}}{(1-\emptyset)\rho_{rock}} \qquad (2.13)$$

Where:

β_{100}: Dissolving power at 100% HCl

ρ_{acid}: Acid density

C_{end}: Acid concentration at the wormhole's tip

U_{end}: Acid flux at the wormhole's tip

ρ_{rock}: Rock density = 2.71 g/cm^3 for limestone

$\emptyset$: Porosity

3. Chapter 3: Critical Literature Review

This study investigates how the presence of crude oil in porous media around the wellbore affects the process of acidizing in carbonate formations. This chapter presents a detailed review of previous work that has been conducted in this domain. The presence of oil during acid injection raises several concerns, including the formation of acid-oil emulsions, the need to mitigate emulsions through de-emulsifiers, and the impact of crude oil on the efficiency of the acidizing process and the required acid injection rate and volume.

3.1 Acid-Oil Emulsion Characteristics and Stability

While acid stimulation aims to overcome formation damage, such operations run the risk of introducing additional damage, sometimes irreversibly. Formation damage associated with acid stimulation resulting from sludges or emulsions is well documented. These emulsions can be very viscous, even solid-like, and may plug the pores of the formation matrix (Rae and Di Lullo 2003). After acidizing wells in the Virginia Hill D-3 reef oil pool in Canada, several wells began producing what appeared to be a very thick emulsion (Moore 1965). A black precipitate was visible at the interface of the produced emulsion from the field. The precipitate proved to have a high percentage of asphaltic material. An acid-aromatic oil emulsion was successfully used to treat wells in this formation. Dunlap and Houchin (1990) performed a field study in which acid returns were examined via polarized microscopy for 32 wells in Alaska, California, and the Gulf of Mexico. Although precautions were used to prevent emulsions in each of the 32 studied wells, emulsions were evident, to varying degrees, in each case. Their study observed that solvent pre-flushes reduce the intensity of acid-crude emulsions in the formation and limit the severity of downstream emulsions. Knopp (2009) discussed the history of acidizing-induced formation damage in Canada from the 1970s to 2009. He claims that “bare-bones” acid stimulation in the

1970's often resulted in well productivity that was 10-30% of pre-stimulation drill stem test results, and sometimes even 0%. After a detailed study by an international oil company, it was determined that the formation damage at Swan Hills was caused by a combination of asphaltic sludge and spent acid emulsion. The solution to these problems has been the synthesis of de-emulsifiers to prevent or break up emulsions that tend to form between crude oil and live or spent acid fluids.

Although matrix acidizing is a long-established technique for application in carbonate reservoirs, it still does not perform to its full potential based on theoretical calculations. Recent studies by leaders in this field show that optimizing the most essential parameters to enhance the efficiency of wormhole propagation is still far from being an old topic (Fan et al. 2018; Shirley et al. 2017; Karale et al. 2016). Field operators still attempt different methods, including testing various chemicals and designing jobs with enormous volumes of acid injection to achieve enhancement in well productivity (Ga et al. 2019). In addition, extensive pre-and post-flush jobs are applied to obtain the most out of an acid injection (Panait et al. 2018). Most of these jobs are designed to minimize damage as a result of emulsion and sludge formation.

Emulsion flow in porous media is complex. In some cases, when dispersed emulsion droplets are much smaller than the pore throats, treating the emulsion as a continuous phase is adequate; characterizing a continuous phase (emulsion) viscosity and assuming Darcy flow can describe the flow behavior (Alvarado and Marsden 1979). A more complex model, deep-bed filtration theory, considers interactions between dispersed phase emulsion droplets and the pore structure (Soo and Radke 1984). Crude oil emulsions are generally classified as either macro-emulsions or micro-emulsions, where microemulsions can be identified as water in oil, oil in water, and multiple emulsions (Figures 3.1, 3.2, and 3.3 respectively), whereas macro-emulsions are classified as either single or double emulsions. If the droplets diameter size is less than 0.1 μm,

emulsions are categorized as micro-emulsion; otherwise, they are macroemulsions (Sharma and Shah 1985; Kokal 2006; Lake et al. 2006).

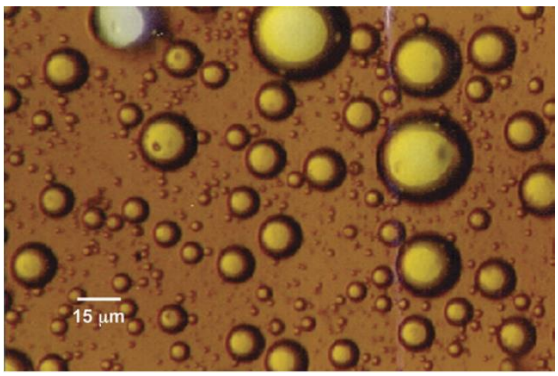

Figure 3.1: Water in oil emulsion (Kokal 2006)

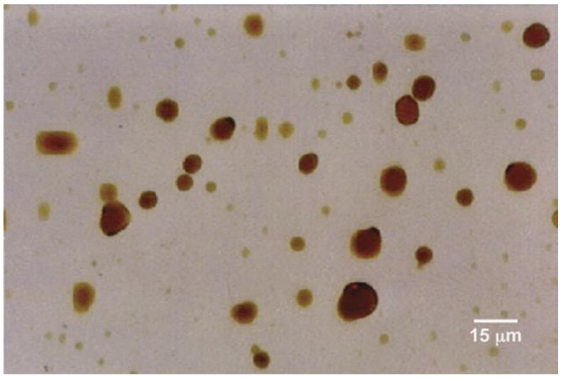

Figure 3.2: Oil in water emulsion (Kokal 2006)

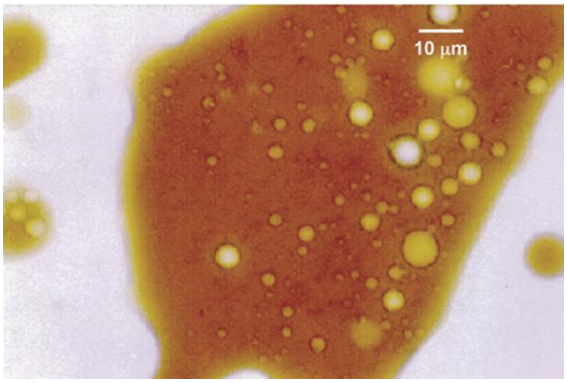

Figure 3.3: Multiple emulsion (Kokal 2006)

Under fixed temperature conditions, such emulsions' stability depends mainly on two factors: the water-oil interfacial tension and the time since mixing occurred (Czarnecki and Moran 2005, Liu et al. 2015, Jones et al. 1978). The stability and properties of water-crude emulsions

have been widely studied for decades. Water-in-crude emulsions are problematic mainly because of high emulsion viscosity, which can be substantially greater than the viscosity of either the oil or the water, causing severe flow assurance problems. Emulsion viscosity typically increases with increasing aqueous phase fraction until an inversion point is reached. The emulsion inversion point is where the continuous phase shifts to a dispersed phase which means emulsions become unstable, as shown in Figure 3.4. This point is controlled mainly by the system's water cut, temperature, and shear (Arirachakaran et al., 1989).

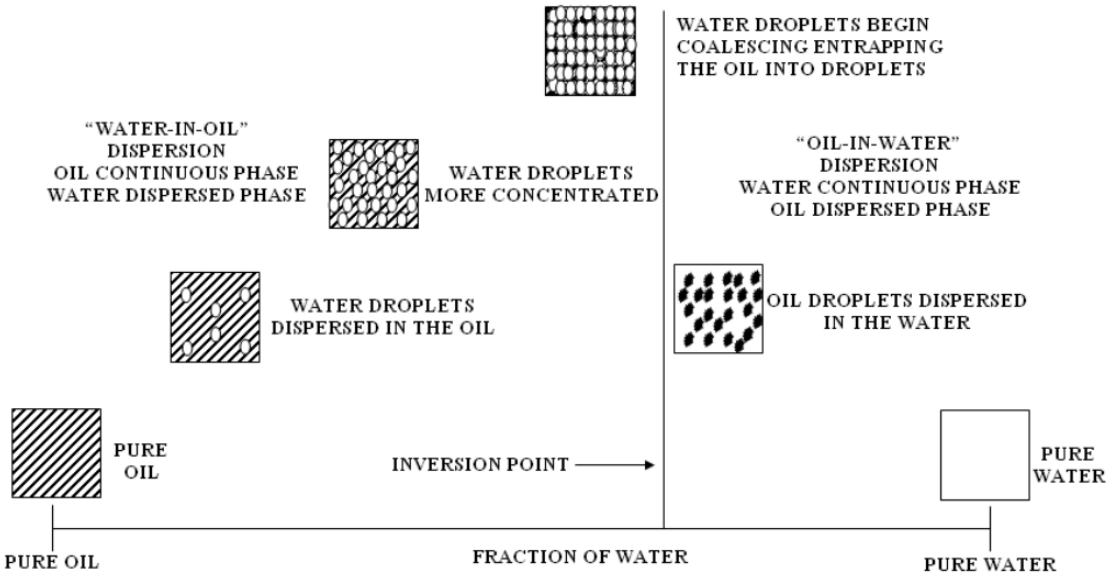

Figure 3.4: Emulsion inversion steps (Arirachakaran et al. 1989)

These emulsions are stabilized by films that form at the water-oil interface and inhibit the coalescence of dispersed water droplets. Evidence shows that heavy polar crude components, including asphaltenes, resins, waxes, and organic acids and bases, are the primary constituents of interfacial films in these emulsions (Kokal 2005). In some cases, natural surfactants are produced by reactions with alkali or acidic crude components (DeZabala and Radke 1986). Fine solids including clays, sand, corrosion products, mineral scales, and drilling muds may also be active at

the water-oil interface; often, fines are generated during acidizing operations, contributing to the acid-crude emulsion formation and stability (Kokal 2005, DeZabala and Radke 1986, Krueger 1988). Crude oil composition determines to a large extent its tendency to emulsify and the stability of emulsions formed. Aske et al. (2002) thoroughly characterized 21 different crude oils and condensates. Emulsion stability data was correlated with the collected physical and chemical data. Asphaltene content, aggregation state of asphaltenes, and interfacial elasticity were the most critical factors contributing to high emulsion stability. Another study identified asphaltene content and aromatic/alkane ratio in crude oil as factors controlling emulsion stability; with emulsification tendency decreasing with increasing aromatic content (Eley et al. 1988). Many other authors discuss the role of asphaltenes in stabilizing crude emulsions (Alvarado et al. 2011; Abdel-Raouf 2012; Mclean and Kilpatrick 1997; Sztukowski et al. 2002; yarranton et al. 2000). It was also observed that resins tend to solubilize asphaltenes in oil and remove it from the water-oil interface, thus lowering emulsion stability (Mclean and Kilpatrick 1997; Langevin et al. 2004; Yang et al. 2007). Waxes by themselves do not stabilize emulsions but work synergistically with asphaltenes by co-adsorbing at the interface, enhancing emulsion stability (Abdel-Raouf 2012). Organic acids such as naphthenic acid have also been shown to stabilize water-in-oil emulsions in some cases (Alvarado and Marsden 1979; Oluwatosin 2016). Solid particles such as metal oxides, silicas, and clays can enhance emulsions stability by adsorbing at the interface between the two fluids, forming what is called “Pickering emulsions” (Kilpatrick 2012).

Emulsion properties are affected by many factors. Increased contact time between oil and the aqueous phase generally results in greater resistance to interface compression and increased emulsion stability (Jones et al. 1978; Kimbler et al. 1966). Dunlap and Houchin (1990) made a similar observation in their microscopic evaluation of acid return samples; what appeared to be

increased stability of the emulsion phase with time. Temperature can also significantly affect emulsion, where the increase in temperature is associated with a decrease in emulsion viscosity and stability (Jones et al. 1978). Brine composition is also an important factor, where aqueous phase pH significantly impacts interfacial film stability. For most crude-brine systems, an optimum pH exists where emulsion separation most readily occurs. Outside of this optimum pH range, emulsion stability increases. Optimum pH for water separation changes from approximately 10 for distilled water to between 6 and 7 for the bicarbonate brine solution studied by Strassner (1968). In the case of acidizing in a low pH environment, asphaltenes may play a leading role in stabilizing emulsions as the rigid interfacial films formed by asphaltenes are strongest in acid PH (Strassner 1968; Omole and Falode 2005).

In addition to emulsion problems, while asphaltenes can associate with each other in favorable conditions, in unfavorable conditions, they can form larger clusters and precipitate out of the oil, forming a sludge (Dickie and Yen 1967; Hashmi and Firoozabadi 2011; Mullins 2011). Once formed in the reservoir, precipitated sludge can plug formation pores, coat the formation making it oil-wet, and stabilize emulsions (O'Niel et al. 2015). While it is generally assumed that the sludge is always asphaltic in nature, it is reported that crudes with little to no asphaltenes can also produce sludge; this is referred to as non-asphaltic sludge (Rietjens 1997). Asphaltic sludge is insoluble in most treating chemicals and is difficult to remove once present in the formation. Some of the primary factors favoring sludge formation in acidizing operations include the use of hydrochloric acid, increasing acid strength, iron-contaminated acid, the use of hydrochloric/ hydrofluoric acid, the use of low-surface-tension liquids such as diesel, and the use of some acid corrosion inhibitors (Jacobs 1989; Jacobs and Thorne 1986). Many design factors and fluid additives must be considered to minimize sludge and emulsions during acid jobs. The design

includes acid type, anti-sludging agents, de-emulsifiers, dispersants, mutual solvents, wetting agents, corrosion inhibitors, iron control additives, solvent pre-flushes, and organic solvents (Moore et al. 1965; Houchin et al. 1990; Krueger 1988; O'Niel et al. 2015; Jacobs 1989).

Most laboratory acidizing experiments are performed using brine-saturated cores since it is typical to inject a brine "pre-flush" before injecting acid in the field. However, the formation rock will never be completely brine saturated. Due to rock heterogeneity, relative permeability, wettability, capillary-trapping, and other factors, even with a brine pre-flush, there will be a complex saturation status in the near-wellbore area with brine, oil, and/or gas phases present. Field examples of produced water-in-oil emulsions following acid stimulation have been discussed, which shows that there will always be interaction, to some extent, between the injected acid and the resident hydrocarbons. Al-mutairi et al. (2012) performed core flood experiments in saturated cores using different grade oils. The oils they used included tar, intermediate oil (32°API), and condensate oil (45°API) using regular HCl and Emulsified HCl. Cores with heavier °API oil were found to have a low acid breakthrough volume. The authors theorize that the in-situ emulsification process and generation of stable acid-in-oil emulsion helped form deeper wormholes. They also note the benefit from emulsified acid diminished when rocks were saturated with oil; they attribute this to acid oil emulsification that provides a similar magnitude of retardation. Using regular acid created multiple wormholes when heavier oil was used but not in condensate-saturated cores; they again theorize regular HCl effectively emulsifies with the heavier oils but not the condensate. To the best of our knowledge, the publication by Al-mutairi et al. (2012) is the only available literature proposing in-situ acid/crude emulsification in the lab when explaining acidizing core flood results. Their proposal is logical but remains unsubstantiated by direct experimental evidence.

Although not the focus of this investigation, emulsion upsets to surface facilities have been described in some studies (Coppel 1975; Picou et al. 1992). These problems routinely involve commingled production as a risk factor. Partially spent acid may contain, in solution, material that could precipitate. As the pH of the produced acid becomes more basic after commingling with other production, fine solids capable of stabilizing extremely tight emulsions are precipitated. Although the emulsion problems in these cases may not affect well productivity, their resolution is often costly and may negate the profitability of the intended stimulation treatment.

3.2 The Use of De-Emulsifiers during Acid Stimulation

The concern about the negative effect of crude oil emulsions in the petroleum production system has been documented for decades (Moore et al. 1965; Kokal and Al-Juraid 1998; Kokal 2005; Kokal et al. 2001; Kokal et al. 2007) and is still being addressed in recent years (Abdulredha et al. 2020). Emulsions can cause many obstacles throughout the production system, including possible damage in the refining unit (Kokal 2005; Zolfaghari et al. 2016). When the emulsions form and settle in the formation, they can block the pores and block oil flow towards the wellbore resulting in lower productivity (Kokal et al. 2003). The formation and accumulation of emulsions in the production pipes or flowlines can cause an unwanted high-pressure drop (Kokal and Alvarez 2003). Besides, the high viscosity of these emulsions can cause the pumping system to fail or, at the least, increase the cost of maintenance. If emulsions are allowed to reach the final stage of the production system (refining and transportation), extracting the oil becomes more complex and costly (Kokal 2005; Zolfaghari et al. 2016; Atehortua et al. 2019).

Previous studies have shown that crude-water emulsions are dynamically stable, where their stability and viscosity decrease with time (Czarnecki and Moran 2005, Sjoblom et al. 1992, Bhardwaj and Hartland 1994, Mason et al. 1995, Wanli et al. 2000). However, our work shows

quantitatively that crude-acid emulsions' viscosity can increase with time (Scarborough et al. 2019). Previous research has shown the essential need for acid treatment additives such as corrosion inhibitors, solvents, dispersants, anti-sludging agents, and de-emulsifiers (Moore et al. 1965; Houchin et al. 1990; Krueger 1986; Oneil et al. 2015; Jacobs 1989). De-emulsifiers are typically used to mitigate the effect of crude oil emulsions on well deliverability. De-emulsifiers in the oil and gas industry are available in many categories, such as organic vs. inorganic matter, micro-molecules vs. macro-molecules, and ionic vs. nonionic types. A good de-emulsifier must have the following criteria (Opawale and Osisanya 2013; Paulis and Sharma 1997): (1) an ability to migrate quickly through the oil phase and successfully compete against considerable odds for its place at the water-oil interface, (2) the de-emulsifier's intense attraction to water should force different water droplets in the same condition to pound together as larger droplets of water, a mechanism called flocculation, and (3) de-emulsifiers should de-stabilize the films surrounding the large water droplets, allowing them to unite, a mechanism called coalescence.

Many studies show the advantages of using emulsified acids to reduce acid reaction rate and achieve deeper penetration (Nasr-El-Din et al. 2008; Sidaoui and Sultan 2016) or as diverting material to prevent acid from flowing to high permeability zones (Abdollahi et al. 2021), resulting in a more efficient wormhole propagation. However, the impact of emulsions on the backflow of oil into the wellbore has not been documented. Natural emulsifiers in some crude oils make them more prone to emulsifying with water or formation brine (Oluwatosin 2016; Gomez 2016). However, even oils that do not form stable emulsions with water can still form very stable emulsions with acid (Scarborough et al. 2019). The matrix acidizing technique, where acid is injected into the formation and mixes with crude oil, is proven to be a successful method of improving productivity. However, this mixing leads to very stable emulsions that can plug the

pores and adversely affect the oil flow efficiency into the wellbore post-acidizing (Scarborough et al. 2019; Salager and Forgiarini 2012; Umar et al. 2018). The emulsion problem during acidizing experiments is not commonly captured in laboratory studies because a vast majority of these experiments are conducted with water-saturated cores (Dong et al. 2017; Kumar et al. 2018). However, in reality, oil is still present in pores when acid is injected, even if a water pre-flush is applied. Shukla et al. (2006) highlighted the effect of oil or gas presence in the rock on acidizing optimization. They showed that the presence of an immiscible phase, whether oil or gas, affects wormhole propagation, resulting in less branching. Besides, oil saturation significantly impacts lowering the acid optimum injection rate and minimizing the volume of acid needed. The possible role of emulsions and the impact of de-emulsifiers in this process have not been addressed in the literature.

3.3 The Effect of Multi-Phase Flow, Permeability, Pressure, Core Dimensions, and Temperature on Matrix Acidizing in Oil-Bearing Carbonate Formations

To achieve the best stimulation results, an optimization of the acidizing process is essential. Optimization includes identifying the acid optimum injection rate and volume, which leads to the minimum amount of acid required to achieve efficient (longest) wormhole propagation (Wang et al. 1993). Acid optimum injection rate, by definition, is the rate at which minimum acid is injected, and the greatest wormhole propagation is achieved. In other words, as shown in Figure 3.5 and Figure 3.6, it is the rate that applies a compact dissolution, creates a dominant wormhole, minimizes the leak-off from the wormhole. Determination of this acid optimum rate has been the target of many studies over recent years (Glasbergen et al. 2009; Mahrous et al. 2017).

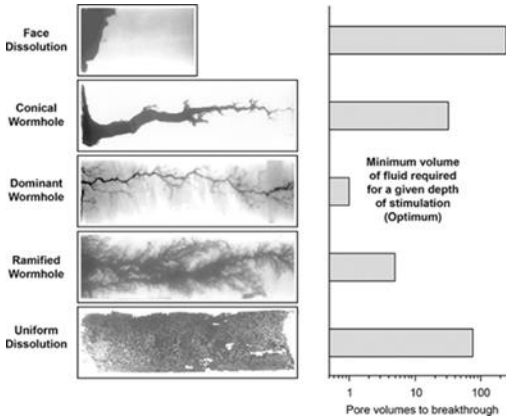

Figure 3.5: Wormhole shapes for different acid injection rate (Hoefner and Fogler 1988, Fredd and Fogler 1999)

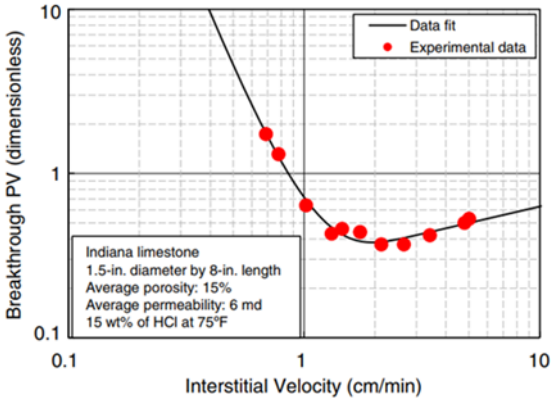

Figure 3.6: Acid optimum injection rate (Dong et al. 2016)

Many factors influence the optimum acid-injection conditions (Fredd and Fogler 1998; Fredd and Fogler 1999; Hoefner and Fogler 1989; Shukla et al. 2006; Wang 1993; Mostofizadeh and Economides 1994; Qiu et al. 2013; Xue et al. 2019). Previous laboratory studies have suggested that permeability, saturation, heterogeneity, core dimensions, temperature, and pressure can significantly impact the propagation of the wormholes and the optimum injection rate value. We cover the range and conclusions from these studies and highlight the limitations, gaps, as well as inconsistencies in the results.

3.3.1 The Effect of Saturation

Shukla et al. (2006) classified saturation conditions associated with matrix acidizing into four cases. The first case is when the acid job is performed after well completion, in which the saturation condition is either an irreducible water or a residual oil saturation, depending on whether the drilling mud used is oil- or water-based, respectively. The second case is when acidizing is done after producing for some time, in which the zone will be mainly oil-saturated with irreducible water. The third case is when a pre-flush is used, and this depends on the choice of fluid, in which

mostly a higher water saturation is achieved. The fourth case includes gas injection before or along with acid injection, which results in a high gas saturation to be established. With the justification that a water pre-flush can precede the acid job, many laboratory acid-stimulation studies are conducted using water-saturated cores. However, whether a pre-flush was implemented or not, oil will still be present in pores, to varying degrees, when acid is injected. In addition, introducing a pre-flush step is not always practical or efficient. This leaves the majority of studies on acidizing with a limited practical applicability of its findings.

The study by Shukla et al. (2006) was one of the earliest studies documenting the impact of an initial oil saturation on the acidizing process. They conducted the study using 6-in.- long/1-in.- diameter Indiana Limestone cores with a permeability of 6 mD. They used a backpressure of 1,000 psi when injecting 15 wt.% HCl to test the advantage of reducing fluid loss from the wormhole into the matrix by injecting gas or oil into the water-saturated cores before acidizing. They noted that the presence of gas or oil reduces the volume of acid needed by a factor of 3.0 and results in narrower (more efficient) wormholes. Kumar et al. (2018) investigated the effect of oil saturation on wormhole propagation and optimum acid-injection rate. Their range of injection rate was between 0.5 and 20 cm^3/min in 1.5-in.-diameter cores. A group of Indiana limestone and dolomite cores with 3- or 6-in. length were used. In these experiments, cores were saturated with either oil, water, or waterflood residual oil. All tests were conducted at a temperature of 200°F, a backpressure of 1,100 psi, and an acid concentration of 15 wt.% HCl. Their results show that the optimum acid injection rate for water-saturated cores was double the acid optimum injection rate for oil-saturated cores. In the case of residual oil cores, the results did not identify an optimum rate of acid injection. These results show that documenting factors impacting acidizing efficiency in oil-saturated cores is critical so that the conclusions are valid for a wider range of field applications.

With the scarcity of such experiments in the published literature, we next review the studies of acid-injection optimization in water-saturated cores.

3.3.2 The Effect of Permeability

The effect of rock permeability on the optimum acid-injection parameters in water-saturated cores has been studied extensively in the literature. Most of these studies reveal that formations with higher permeability require a larger acid-injection rate (Mostofizadeh et al. 1994); however, some do show inconsistent results, while others claim to find a clear proportional linear relation between permeability and the acid optimum rate. Bazin (2001) conducted his experimental work on 8-in.-long/2-in.-diameter limestone cores with two permeability values: high-permeability ones at 200 mD and low-permeability ones at 5 mD. These experiments were conducted at a temperature of 50°C and a backpressure of 2,610 psi using 7 wt.% HCl. Bazin concluded that higher permeability cores require higher optimum acid-injection rates and higher acid-injection volumes. Etten et al. (2015) conducted their experiment on 8-in.-long/1.5-in.-diameter Indiana limestone cores at room temperature and 1,500 psi backpressure, with permeability values ranging from 6 to 239 mD. Their correlation shows that higher-permeability cores indeed require higher volumes of acid injection, but very little variation in the optimum injection rate was observed, except for the lowest permeability case, which showed a lower rate needed, as shown in Figures 3.7.

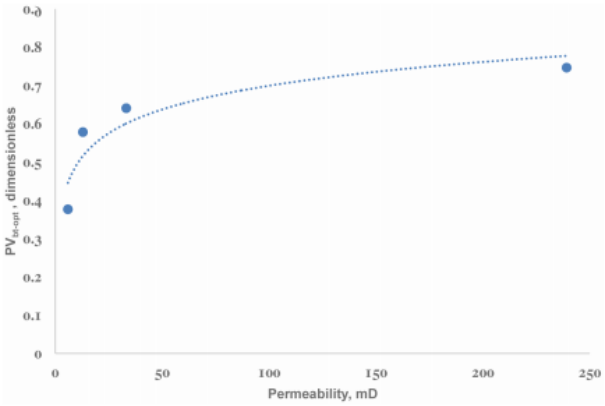

Figure 3.7: Relation between permeability and optimum acid volume (Etten et al. 2015)

Dubetz et al. (2016) found no direct correlation between changes in permeability and the acid optimum injection rate and volume within a limited permeability range (Figures 3.8 and 3.9); however, the large-picture trend of the results shows that high-permeability cores required a higher acid optimum injection rate and a larger acid volume.

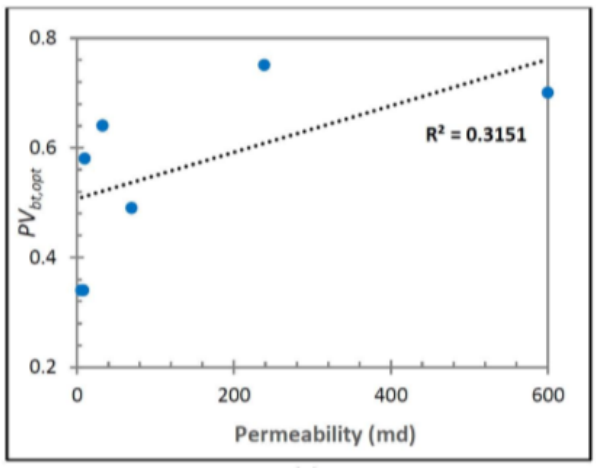

Figure 3.8: No good fit correlation between acid volume to breakthrough and permeability (Dubetz et al. 2016).

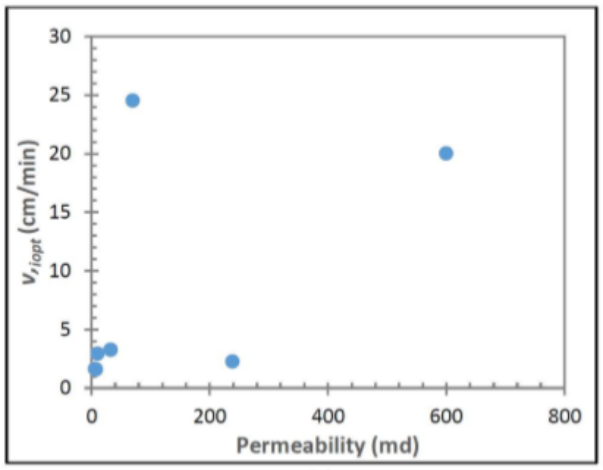

Figure 3.9: No correlation between acid optimum rate and permeability (Dubetz et al. 2016).

3.3.3 The Effect of Pressure

For a long time in the history of laboratory studies of carbonate acidizing, a backpressure of approximately 1,000 psi was considered good enough to keep CO_2 dissolved in solution after it is produced through the acid chemical reaction with the rock (Wang 1993; Bazin 2001). However, solubility at such a low pressure is very limited, especially in the presence of dissolved solids in the aqueous phase (Duan and Zhang 2006; Scarborough et al. 2019). Purtton and Savage (1945) found that the maximum solubility of CO_2 at 1,000 psi and 75^{o}F in a 10 wt.% calcium chloride solution is 0.75 mol%, which means that most of the produced CO_2 will not be dissolved in the aqueous phase (Cheng et al. 2016). The presence of CO_2 outside the aqueous solution results in changes in the fluid flow efficiency by introducing the complication of an additional phase and can contribute to the formation of stable emulsions that impact the acidizing processes (Elsafih et al. 2021). Qiu et al. (2014) investigated the effect of pressure on wormhole propagation in 12-in.-long/1.5-in.-diameter cores with 1- to 6-mD permeability. They concluded that a backpressure of 1,000 psi resulted in the presence of free CO_2. Their study claims that this free CO_2 led to lowering the efficiency of the acidizing process by increasing wormhole diameter and decreasing its propagation. The acid optimum injection rate at 1,000 psi was approximately 7 times that at 3,000 psi, and the acid volume needed was double. Cheng et al. (2016) conducted experiments with a range of pressure from 500 to 3,000 psi and at temperatures of 70°F and 150°F. They conclude that at the lower temperature, there was not much change in the acid optimum rate or volume between the lower- and higher-pressure experiments; however, at the higher temperature, a significant reduction in the optimum injection rate was noticed at higher pressure, with no change in the required acid volume to propagate the wormhole. The effect of temperature on optimum acid injection rate and volume in water-saturated carbonate cores has been consistently shown to increase the required rate and volume of acid injection (Bazin 2001; Dong et al. 2014). However,

a review of the published literature previously shared above reveals several gaps and contradictions regarding the impact of pressure conditions on the optimization process. Besides, the bulk of the work is limited to cores that are 100% saturated with water.

3.3.4 The Effect of Core Dimensions

Researchers began to look more at the effect of core geometry on the acid optimum injection rate. Buijse (2000) claimed that core dimensions could affect the wormhole structure and the way fluids are distributed. For example, the wormhole structure of an 8 cm diameter core is very different from a 2.5 cm diameter core wormhole, as shown in Figure 3.10. Bazin (2001) has approved that increasing in cores length would lead to an increase in acid optimum injection rate and optimum acid injected volume as shown in Figure 3.11, whereas optimum rate and volume for 20 cm cores are higher values 5 cm cores.

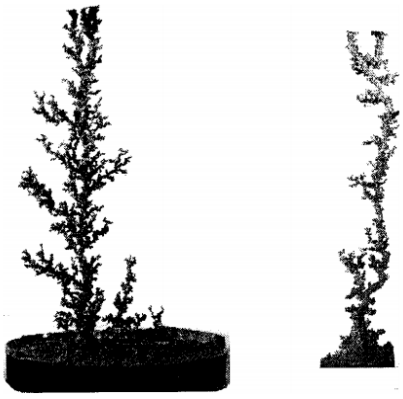

Figure 3.10: Effect of diameter on wormhole structure (Buijse 2001)

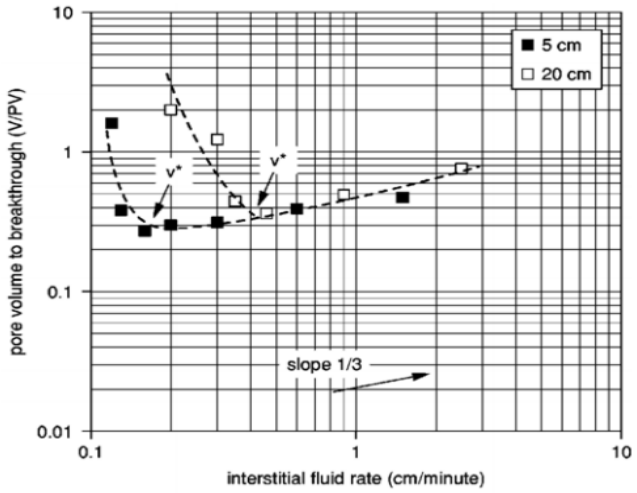

Figure 3.11: Effect of length on acid optimum injection rate and volume (Bazin 2001)

Dong et al. (2014) reached the same conclusion except assigning a length limit of which length does not affect optimum rate and volume. Their results showed that when core lengths increase at fixed core diameter, the optimum acid injection rate increases until the core length reaches 6-in., where the acid optimum injection rate becomes independent of core length (Figure 3.12). As for the diameter, the optimum acid injection rate decreases as the core diameter increases, as shown in Figure 3.13.

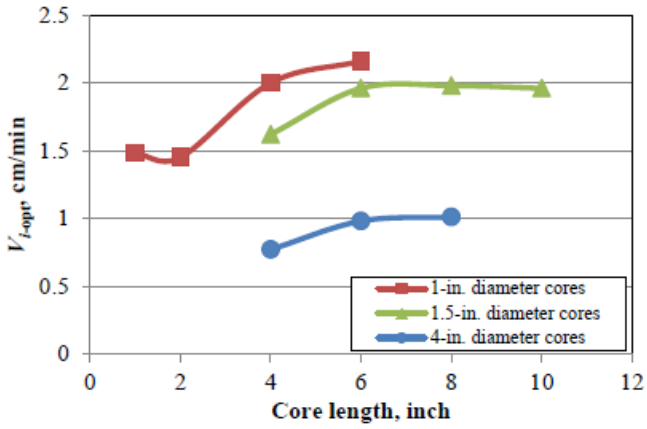

Figure 3.12: Relation of core length with acid optimum injection rate (Dong et al. 2014)

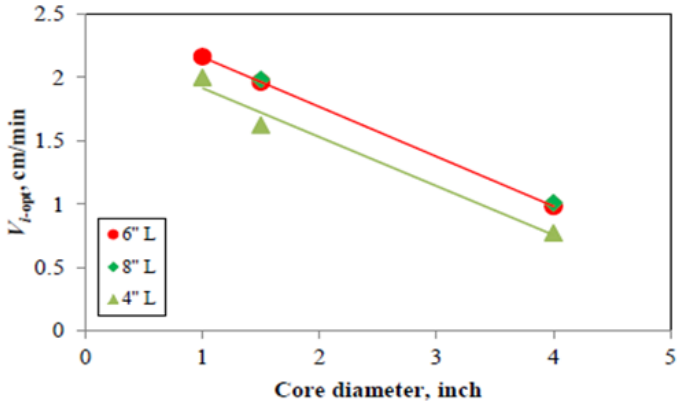

Figure 3.13: Relationship between core diameter and acid optimum injection rate (Dong et al. 2014)

The same relation took place between the optimum pore volume to breakthrough and core diameter. For higher core diameter, the optimum pore volume to breakthrough becomes less. Figure 3.14 shows this relation.

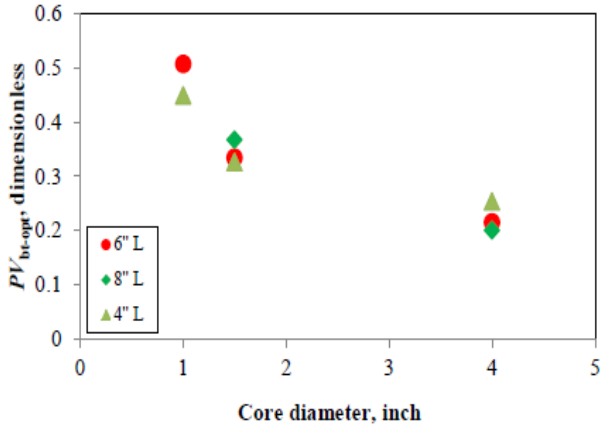

Figure 3.14: Relationship between optimum pore volume to breakthrough and core diameter (Dong et al. 2014)

3.3.5 The Effect of Temperature

Temperature has been approved to significantly affect optimizing the acidizing process, including optimum rate, acid type, and additives. (Kalia and Glasbergen 2009, Xue et al. 2019). Wang et al. (1993) and Bazin (2001) investigated how the optimum rate is affected by temperature. They showed higher temperature requires a higher optimum injection rate and lower acid volume for

Dolomite. As shown in Figures 3.15, while no optimum rate was found at 50 C, the optimum rate at 70˚ C was 60 ml/hr, and at 75˚ C, the optimum rate was 210 ml/hr. In contrast, acid volume dropped radically as temperature increased. As for limestone, both acid rate and volume increase as temperature increases, as shown in Figures 3.16, 3.17.

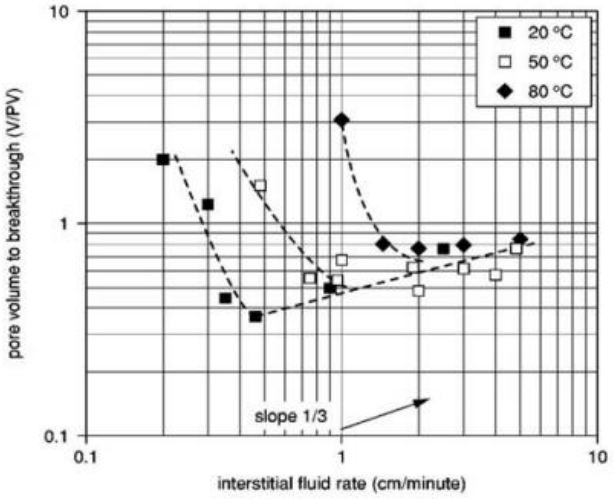

Figure 3.15: Optimum rate and volume increases as temperature increases (Bazin 2001)

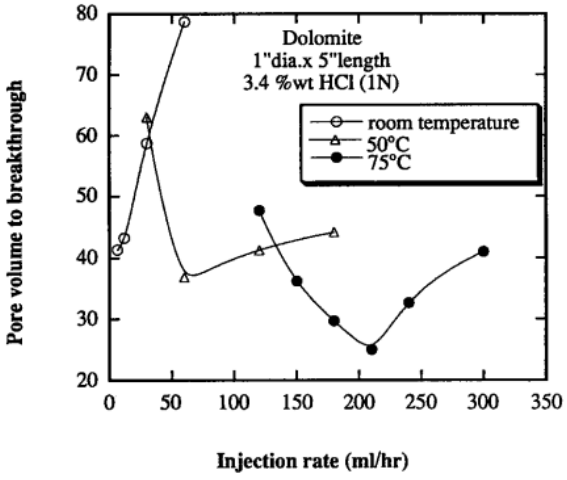

Figure 3.16: Effect of temperature on acid optimum rate and volume on Dolomite. Wang et al. 1993

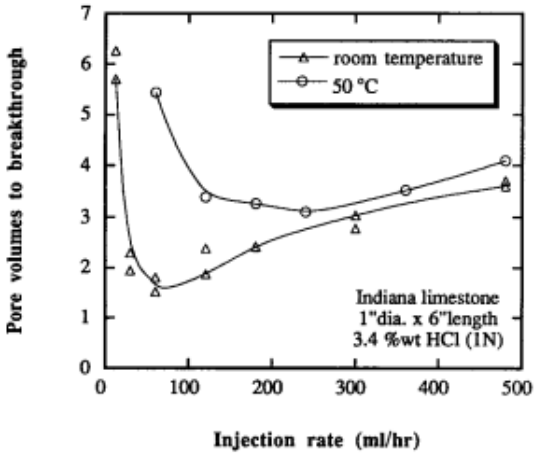

Figure 3.17: Effect of temperature on acid optimum rate and volume of limestone (Wang et al. 1993)

Xue et al. (2019) obtained the same conclusion regarding the acid injection rate; however, they claimed optimum acid volume is also increasing as temperature increases. Figure 3.18 shows these conclusions.

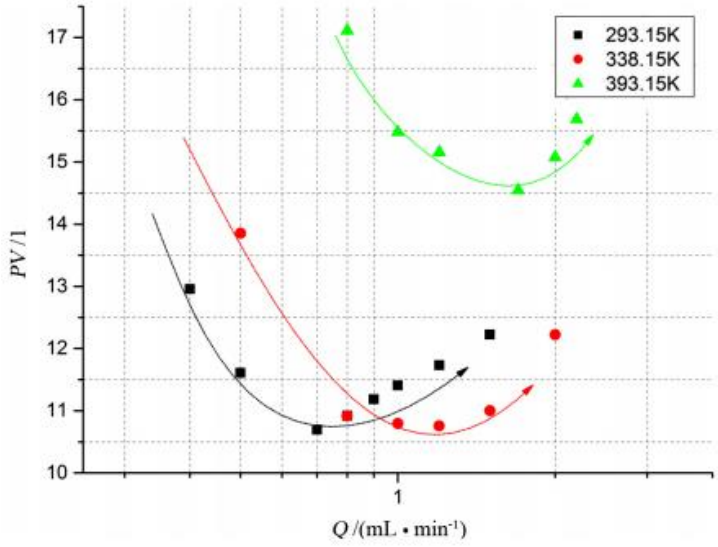

Figure 3.18: Effect of temperature on acid optimum rate and volume (Xue et al. 2019)

Dong et al. 2017 in their extensive study on optimizing acid injection rate, summarizes the relation between temperature and optimum rate as shown in Figure 3.19. Increasing temperature will always result in increasing in acid optimum injection rate. Literature shows that an alternative acid type is needed in a high-temperature situation. Although using other types of acid solves the issue of higher values of acid rate, the temperature still has a minor effect on acid optimum volume (Mahmoud et al. 2011). Figure 3.20 shows how the acid optimum rate of chelating agents was kept constant with different temperatures while acid volume slightly changed.

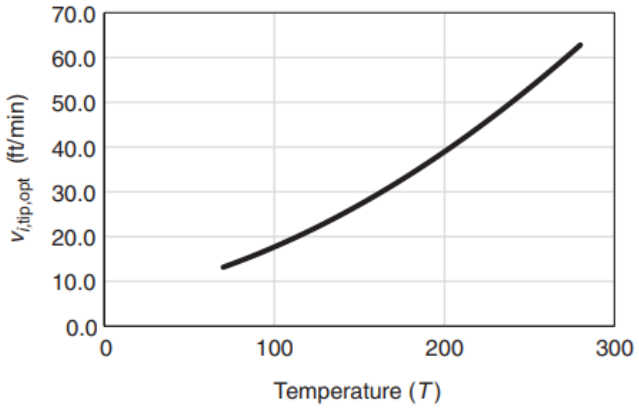

Figure 3.19: Relation between temperature and acid optimum rate (Dong et al. 2017)

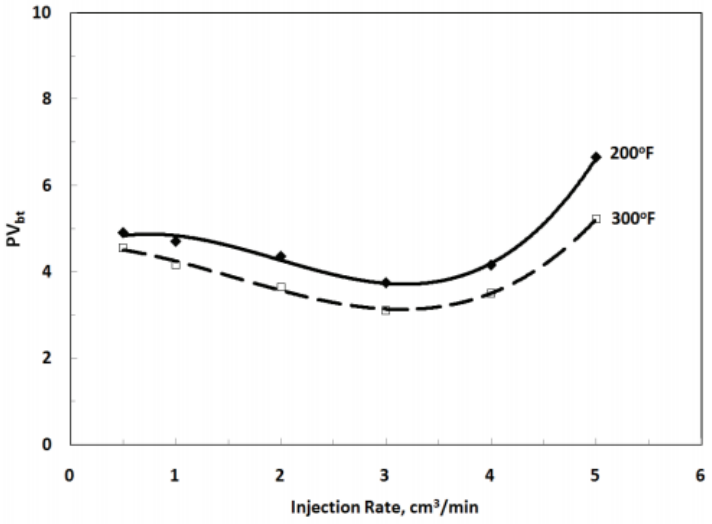

Figure 3.20: Effect of temperature on acid injection rate (Mahmoud et al. 2011)

3.4 Research Gaps

3.4.1 Formation of Acid-Oil Emulsions During Acidizing

Most laboratory studies have investigated and analyzed the acidizing process without considering the presence of oil in the formation. The direct contact between live acid and crude oil has been proven to produce a viscous and stable emulsion, which can be problematic and impact acidizing performance. Since not much attention has been paid to this matter, analyzing the effect of this

kind of emulsions would help better understand their role in the acidizing process and their impact on productivity.

3.4.2 Factors Affecting the Efficiency of the Acidizing Process in the Presence of Crude Oil

One of the most critical aspects of acidizing is optimizing the acid injection rate and the required optimum acid volume. To figure out an accurate acid optimum rate and volume, factors that affect them must be studied systematically. The following factors, which are not covered enough in the literature, are analyzed in this study:

3.4.2.1 Saturation Effect:

Many studies of acidizing have assumed water saturation as a normalized situation for experiments. However, the presence of oil can make a lot of difference in optimizing the acid injection rate.

3.4.2.2 Permeability:

Even though the effect of permeability is clarified in many studies, the majority were averaging the value of permeability for the whole block of cores which might result in misleading and contradictory conclusions. In this study, the permeability of each core is measured accurately using Nitrogen gas. In addition, the effect of saturation and backpressure is studied for the different ranges of permeability.

3.4.2.3 Backpressure:

As mentioned before, carbon dioxide forms as a result of an acid reaction with carbonate. For most studies, a pressure of 1,100 psi has been considered high enough to keep CO_2 soluble in solution. However, this is now proven not to be accurate. In this study, a pressure of 3,000 psi is applied, and results are compared to the 1,100-psi case.

4. Chapter 4: Experimental Work Part I-Characterizing Time-Dependent Stability and Viscosity of Acid-Crude Emulsions:

While aiming to enhance near-wellbore flow conditions, the process of matrix acidizing can damage effects when acid-oil emulsions form. Understanding the behavior of these emulsions, especially when it comes to their stability and viscosity, is an essential step in the design of acid jobs that can lead to successful well productivity enhancement. In this study, we investigate the time-dependent nature of these emulsions using bottle tests and core-flooding experiments. Some of this work includes results shared in Bryan Scarborough's master study (Scarborough 2016). The results of this work provide new insights into how a sludge, or a tight emulsion, forms over time, which directly impacts the design of acid jobs.

In this experimental work, acid-crude emulsions are investigated, documenting the changes in the viscosity and density of the sludge. Carbonate rock acidizing is performed on crude-saturated samples. A very viscous and stable emulsion is produced during the flooding process when the experiment is performed at low pressure, suggesting that the presence of a gaseous CO_2 phase helps with the shear mixing needed to create the emulsions. Additional evidence of that is provided using results from a simple dissolution experiment. This work was published in the journal of Fuels & Energy (Scarborough et al. 2019)

4.1 Materials

A crude oil from a reservoir in Texas with 25.6-cp viscosity and 0.88-g/cm^3 density was used in this study. Viscosity was measured using cannon capillary viscometers. Density was quantified using a pycnometer. The weakness of this way of measuring density is the small quantity used. The acid used was 15 wt.% HCl with a density of 1.07 g/cm^3. Toluene and acetone were used in the process of cleaning some of the instruments. Indiana limestone cores of 1.5-in.- diameter and

6-in.-length, with a 2 to 4-mD permeability and 15 to 17% porosity, were used in the core-flooding tests. Table.4.1 shows the sources of these materials and some of their specifications.

Table 4.1: List of materials providers and specifications

Product name	Provider	Specifications			
		purity	grade	color	density
Crude Oil	Texas Raw Crude	99%	NA	Dark Black	0.88 g/cm^3
Hydrochloric Acid	Sigma-Aldrich	>99%	ACS reagent	APHA	1.2 g/mL
Indiana Limestone	Kocurek Industries, Inc.	98.12 %	NA	Standard Gray	N/A

4.2 Experimental Setup and Procedures

Three main types of experiments were conducted. In the first set of experiments, emulsions were created, and then their stability and viscosity were studied using bottle tests. In the second, acid was injected into carbonate core samples, and then the pressure response and effluent fluids were analyzed. Finally, the effect of agitation caused by gaseous CO_2 was examined separately to support the analysis of the flooding tests.

In the first set of experiments, emulsions were prepared using a T18 homogenizer manufactured by IKA. 300 ml of fluid were mixed in each batch with varying oil to acid volume ratios of 8:2, 7:3, and 6:4. Mixing was performed at 5,000 rpm for 30 minutes. Oluwatosin (2016) optimized these parameters to ensure reproducible results and minimize heat effects resulting from mixing. This procedure of mixing includes the following:

- Calculate oil and acid target volumes for each emulsion, then convert the oil and acid volumes to mass based on densities. Add this weight amount of each fluid to a 500-ml beaker.
- Put the emulsion beaker under the homogenizer while it is centered, leaving 1 cm at the bottom of the beaker and ensuring that the holes of the homogenizer are submerged.
- Mix the fluids for 30 min at a speed of 5,000 rpm

Emulsion viscosity was measured using Cannon capillary viscometers, shown in Figure 4.1. Each viscometer has a range of viscosity for which it can provide accurate measurements of viscosity. The measurement of emulsion viscosity has been a challenge in the literature. If the measurement method interferes with the emulsion structure, it can lead to inaccurate measurements and impact the emulsion's stability. Our team did an extensive study to confirm the suitability of this method to characterize emulsion viscosity. The justification for this choice of method is included below:

- First, the diameter of the capillary viscometers was compared to the droplet size distribution of the emulsion. Our emulsions have aqueous phase droplets that range between 2 and 10 micrometers, with a mean value of 6 microns. The capillary viscometer #300 that measures viscosity between 50 and 200 cSt has an inner diameter of 1.27 mm, while capillary viscometer #400 that measures viscosity between 240 and 1,200 cSt has an inner diameter of 1.92 mm. These capillary diameters are over 200-times the average diameter of the aqueous phase droplets. Accordingly, for the case of 7:3 ratio, each cross-section of the capillary diameter is expected to hold over 10,000 dispersed droplets. This shows that the capillary viscometer does not interfere with the structure of this emulsion.
- The above calculations were confirmed by re-measuring the viscosity of the same fluid sample several times; where the sample was impacted, the same viscosity value is not expected to be reproduced. The results revealed the same value of viscosity measurement for the same sample when repeated (Oluwatosin 2016).
- The nature of these emulsions showed to be shear—thinning when viscosity was measured using a rotational viscometer, revealing a non-Newtonian nature (Helene

2019). However, repeated measurements with the rotational viscometer were shown to be reproducible for the same sample. This was also shown to be in-line with the viscosity measured by the capillary viscometer for the corresponding shear-value experienced during the measurement. It was also revealed to be in-line with the pressure drop experienced during flow in pipes (Helene 2019).

This background work gave us confidence in the ability of capillary viscometers to provide repeatable and reliable viscosity values for this system at a fixed shear value. The procedure to measure the viscosity of the sample is according to the following steps:

- Using a pipette, fill the viscometer bulb halfway with emulsion (around 10 ml).
- Draw the emulsion up to the above-marked line on the viscometer using the red suction.
- Take off the red suction, start timing when the emulsion passes the market line, and stop the timer when the emulsion reaches the bottom-marked line.
- Convert time to dynamic viscosity using the following equation 4.1:

$$Dynamic\ viscosity = time\ x\ viscometer\ constant\ x\ density \qquad (4.1)$$

Figure 4.1: Measuring viscosity using Cannon capillary viscometer (Scarborough 2016)

To ensure consistency of the collected viscosity data, all viscosity measurements were taken in the same place with the same room temperature, and only two sizes of viscometers were used. Size 300 viscometer for the range of (50 – 250 cSt) and size 400 viscometer for the range of (240 – 1200 cSt). In some cases, the heterogeneity of the emulsion layer was examined by measuring the density and viscosity for two samples per vial. Both samples were taken consecutively from the very bottom of the vial, as shown in Figure 4.2, and their properties were measured simultaneously. A constant volume of 10 cm^3 was collected each time to ensure that results are consistent. These viscometers were cleaned using toluene and then air-dried after each viscosity measurement. After the viscosity was measured, a few cubic centimeters of the sample were recovered from the viscometer, and density was evaluated using a graduated cylinder with a 2% random error associated with the volume evaluation (with less than a 0.3% random error in weight measurements).

Figure 4.2: Sample collection from the vial to study heterogeneity in the emulsion layer (Scarborough 2016)

In the second set of experiments, matrix acidizing was conducted on Indiana limestone core samples under varying conditions. When an initial liquid saturation was needed, the rock was saturated using the saturation setup shown in Figure 4.3 by placing it in a vacuum cell for two hours. Then, the liquid was transferred into the cell for an aging time between 1 and 14 days. The

flooding tests were conducted using an acidizing setup consisting of a 1.5-in.-diameter Hastelloy core-holder and a set of inlet and outlet piston-accumulators controlled by ISCO syringe pumps. A data acquisition setup allows for measuring inlet and outlet pressure throughout the experiment. Overburden pressure was kept at 500 psi higher than the inlet pressure during the experiment to avoid breaking the rock sample. A complete schematic of the setup is shown in Figure. 4.4. Dependent on the type of experiment being conducted, various components were disconnected. Some tests involved injecting the acid into the rock to propagate a wormhole throughout the whole length of the rock. Later tests involved injecting lower volumes of acid to target partial propagation of wormholes followed by backflow of oil mimicking production from a stimulated formation.

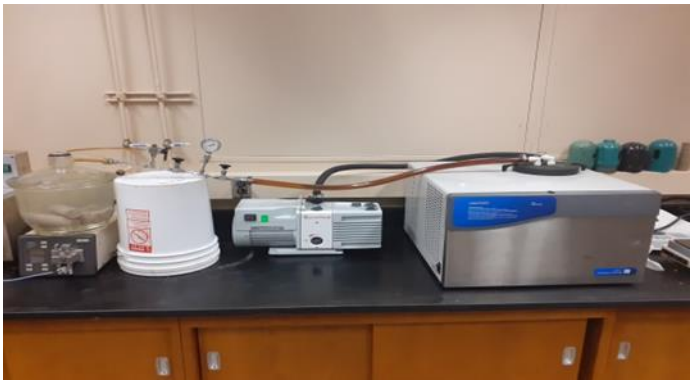

Figure 4.3: Core saturation unit

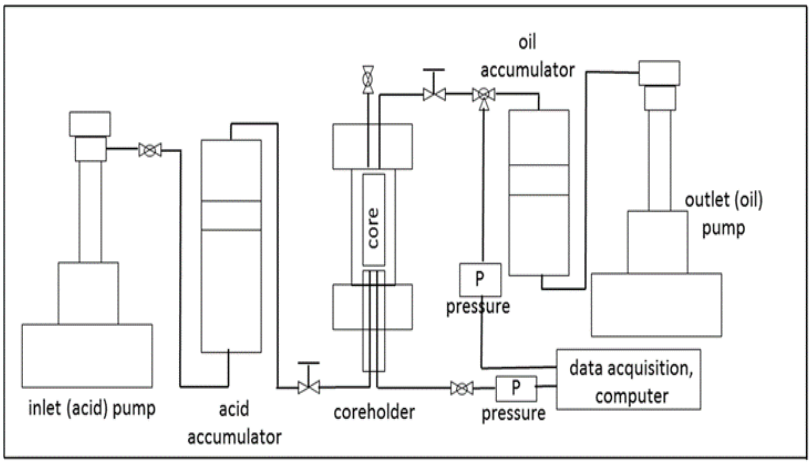

Figure 4.4: Schematic of the core-flooding setup used in acidizing experiments (Scarborough 2016)

The third type of experiment involves examining the effect of agitation caused by gaseous CO_2 on the creation of emulsions between the oil and the acid. Two scenarios were applied. In the first scenario, equal volumes of 15wt.% HCl and crude oil were placed in a beaker (Figure 4.5a). A dry piece of Indiana limestone was then placed in the mixture. Some of the turbulence caused by the reaction can be seen in Figure 4.5b. The fluid was then analyzed for signs and characteristics of emulsions. In the second scenario, an Indiana limestone core saturated with oil and aged for more than 2 years was placed in a beaker. 15wt.% HCl was then poured on the core, as shown in Figure 4.5c. The acid-rock reaction in this case was slower, and less agitation was observed. The resulting fluid was also analyzed for signs and characteristics of emulsions.

(a) **(b)** **(c)**

Figure 4.5: Images for testing the impact of agitation from gaseous CO_2 on the mixing of oil and acid: (a) crude oil on top of 15 % HCl and a carbonate, (b) reaction between carbonate and acid causing mixing, and (c) 15 % HCl poured on the core saturated with oil and aged for over two years

4.3 Results and Discussions

In this section, we present the results and analysis of the various experiments conducted in this study. We start with the bottle tests of live acid-crude oil emulsions. We then discuss the results of flooding tests and analyze the role of CO_2 in the emulsification process.

4.3.1 Impact of Time on Emulsion/Sludge Formation

The crude oil used in this study did not produce stable emulsions when mixed with distilled water unless emulsifiers were used (Oluwatosin 2016). However, when an oil sample was placed in a

vial with a 15 wt.% HCl solution, even a simple hand-shaking procedure for 3 minutes was enough to activate the process of emulsification and produce a very viscous sludge. An example of this is shown in Figure 4.6 for a 6:4 oil to acid ratio. The vial was stored in a vertical position but tilted for the picture at the various times shown. No signs of sludge can be seen after 5 hours, but the picture after 2 days shows a large sludge, which only increases in volume in the following days. The formation of the viscous sludge seemed to be occurring after 24 hours from mixing time. Since it was not possible to mix larger volumes and obtain reproducible results using this method, the homogenizer was used in later tests.

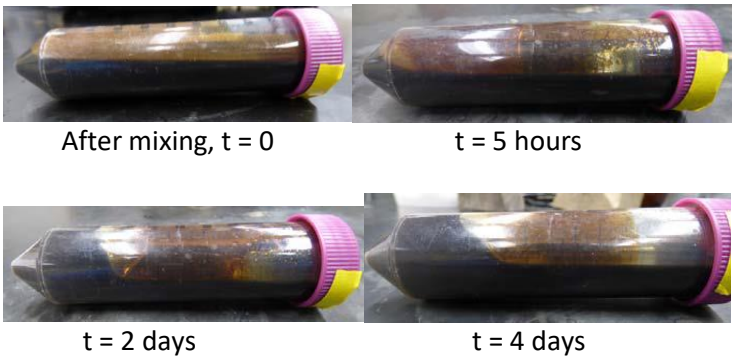

Figure 4.6: Effect of time on emulsion/sludge formation after hand-shaking the vial for 3 minutes; Example is for a 6:4 oil to acid ratio (Scarborough 2016)

To better characterize the effect of time on emulsion stability and properties, a 300-ml fluid mixture was prepared with three volume ratios of oil/acid: 8:2, 7:3, and 6:4. These were separated into nine vials of 32 ml each and then tested for viscosity over time. At each of the nine previously determined time stamps, one of the bottles is tested. The results of viscosity measurements, shown in Figure 4.7, taken at time zero for the first sample (very bottom) and second sample (next to bottom) from the three emulsions show the homogeneity of the emulsion created, the reproducibility of the viscosity measurements, and the significant impact the acid fraction has on emulsion viscosity. With the crude oil viscosity measured at 25.6 cp, the relative viscosity, defined

as the ratio of emulsion viscosity to crude oil viscosity immediately after mixing, is calculated to be 1.8 for a 20% acid content, 4.1 for a 30% acid content, and 5.7 for a 40% acid content.

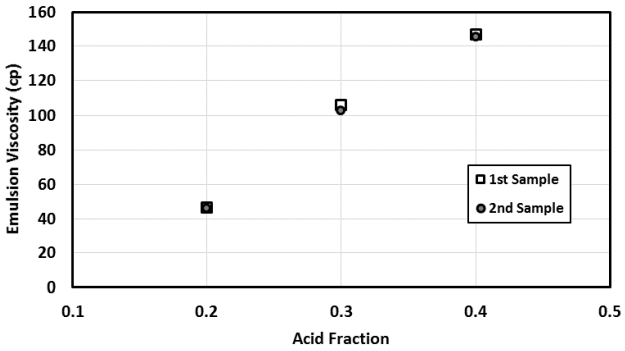

Figure 4.7: Impact of acid fraction on emulsion viscosity at time zero after mixing for the first sample (very bottom) and second sample (next to bottom)

The results for viscosity measurements for the first sample, which amounts to about a quarter of the total mixture, collected from the bottom of the vial over five days, are shown in Figure 4.8. For the emulsion with a 20% acid content, the relative viscosity increased to 8 after five hours and then to 14 after four days. The vials tested on days 1 to 3 revealed relative viscosities between 4 and 7, while the vial tested on day five recorded a relative viscosity of 3. These relative viscosity numbers indicate that sludge formation is not persistent in 20% acid content. It is possible that a continuous acid phase could have formed, creating an inverted emulsion with a lower viscosity, but this was not substantiated.

The viscosity values collected for the samples with a 30% acid content show similar behavior to that of the 20% content in the first 5 hours; however, relative viscosity increased to values between 15 and 34 for days 1 to 3, with the highest emulsion viscosity measured at 888 cp. The 24-hour mark is indicated as the onset of a sludge in this system with a 400-cp viscosity, which by day 4 had a viscosity beyond the limits of the instruments (over 3,200 cp). The emulsion created with 40% acid content resulted in a first sample relative viscosity ranging from 3 to 124, with the

highest emulsion viscosity measured on day five at 3,190 cp. The settling of acid droplets induced by gravity was identified as the reason for the formation of the sludge, which in most cases did not coalesce to form a continuous acid phase. The main finding is that while 20% acid emulsions are not highly susceptible to emulsions, 30% and 40% acid content can result in a highly viscous sludge.

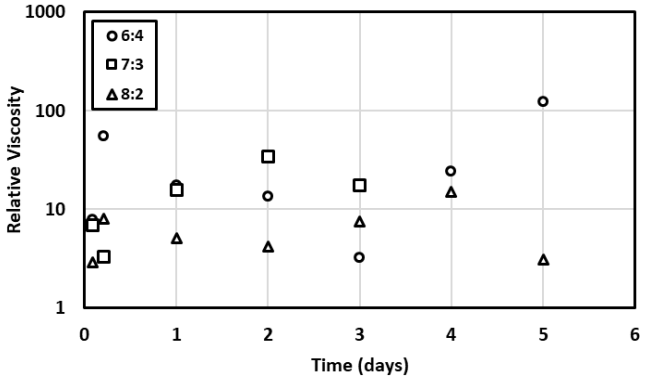

Figure 4.8: The change in the relative viscosity of the first (very bottom of vials) over time for each of the three emulsions of varying oil /acid ratios

To better understand these results, the density values of these samples were measured to quantify the acid content. This is plotted as viscosity versus acid fraction in Figure 4.9. The results show that higher viscosity values did correlate with higher values of acid content, as expected (Bullard et al. 2009; Das et al. 1992). In most cases, even after five days, acid droplets did not coalesce to form a continuous phase of lower viscosity. The first sample taken on day five from the 40% original acid content emulsion has a viscosity over 120 times the oil's viscosity. This emulsion had a density of 1.005 g/cm^3, indicating an acid content of 66%. The error in calculating the acid content resulting from the small volume collected is 10%, which explains the scatter of the data. However, the results confirm that settling acid droplets increases the acid content at the bottom of the vials. As the acid droplets sank to the lower parts of the vial, an oil layer was recognized at the top of the vial that potentially had no acid content, as indicated by its viscosity.

It was not possible for these emulsions to visually detect the oil and emulsion layers because the colors were indistinguishable. Oluwatosin (2016) reports observing up to four layers of different colors when studying emulsifier-stabilized emulsions for crude oil mixed with distilled water. A sample of these emulsions is shown in Figure 4.10.

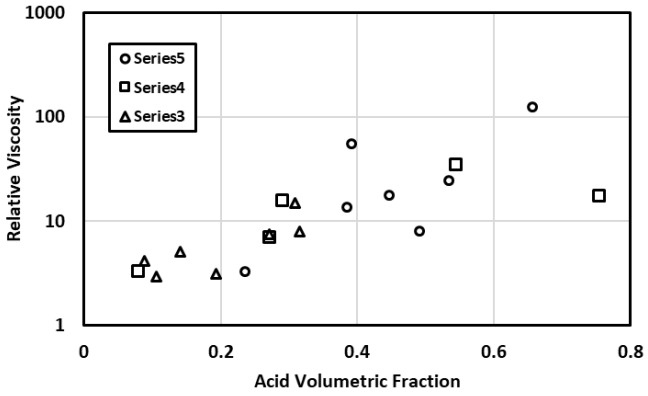

Figure 4.9: Relative viscosity plotted against acid fraction, measured for the first samples. The results show that the increase in viscosity is associated with an overall increase in acid content overtime for the samples taken from the bottom of the vials

Figure 4.10: Layers of varying colors were observed when an emulsion was created using a crude oil and distilled water with the help of an emulsifier. Four district layers can be observed, where if the top layer is oil and the bottom layer is water, the two middle layers indicate two different emulsion layers (Oluwatosin 2016)

In addition to studying the very bottom of each of the vials, labeled as the first sample, we collected a second sample representing the next-to-bottom layer. A constant volume was collected from the very bottom of the vial after removing the very bottom layer to ensure reproducibility. The main reason was to study how the emulsion became heterogeneous over time. Those second samples showed consistently lower viscosity values and lower density values than the first samples

for each emulsion. The viscosity data are presented for the three emulsions of 8:2, 7:3, and 6:4 oil to acid ratios over time in Figures 4.11a, 4.11b, 4.12a, 4.12b, 4.13a, and 4.13b, respectively. The plot showing the correlation between these viscosity values and acid content is presented in Figure 4.14 for both the first and second samples.

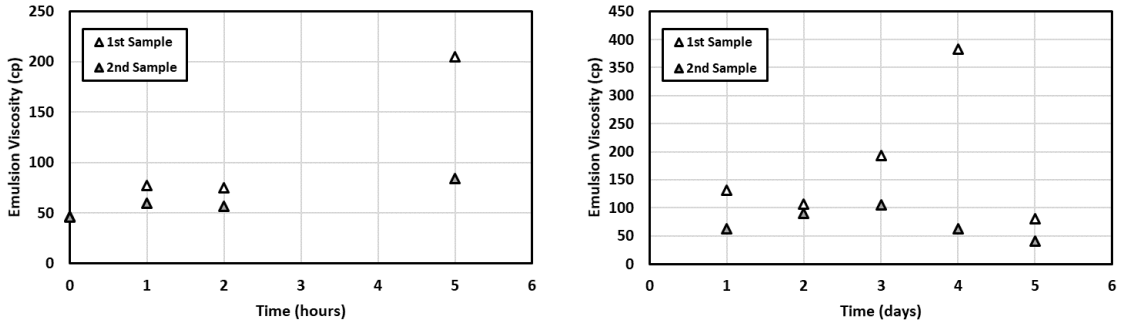

Figure 4.11: Viscosity for the first and second samples of the emulsion created with 20% acid content. (a) Over 5 hours. (b) Over 5 days

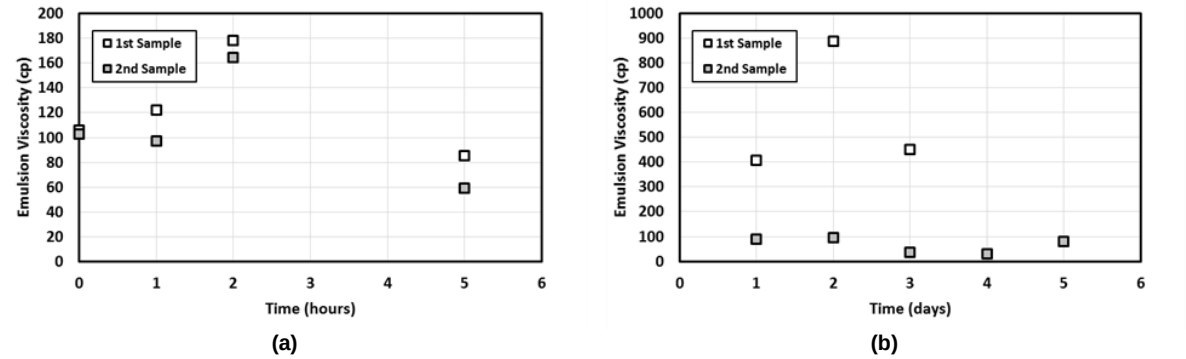

Figure 4.12: Viscosity for the first and second samples of the emulsion created with 30% acid content. (a) Over 5 hours. (b) Over 5 days

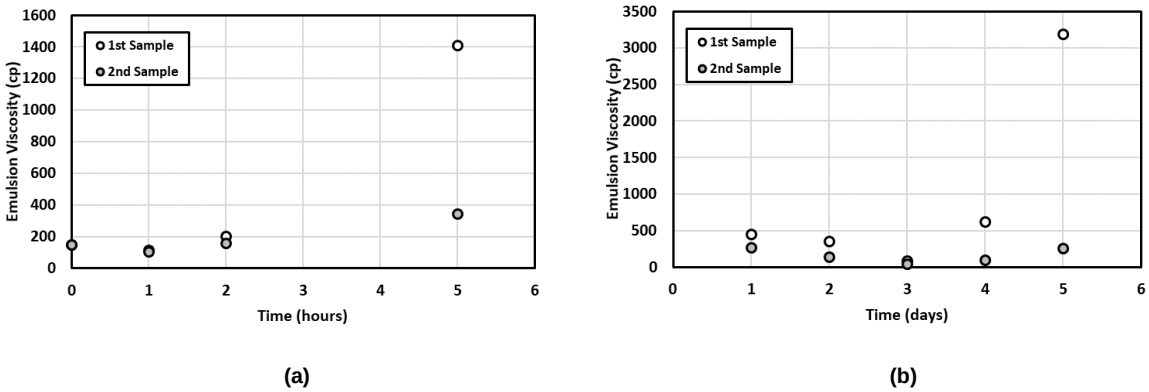

Figure 4.13: Viscosity for the first and second samples of the emulsion created with 40% acid content. (a) Over 5 hours. (b) Over 5 days

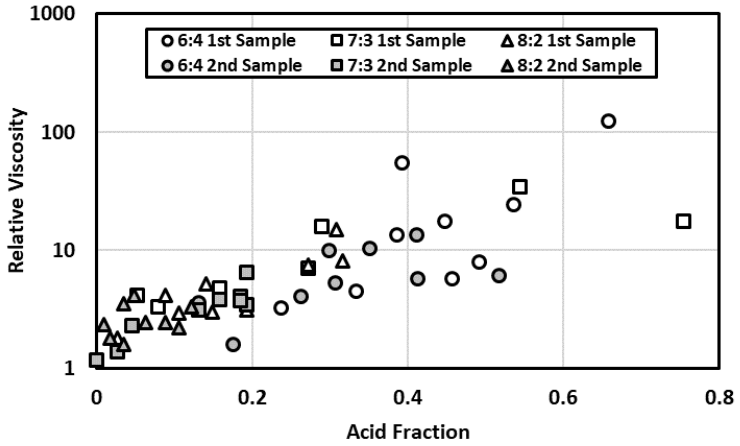

Figure 4.14: Emulsion viscosity plotted against emulsion density for the first and second samples shows that it follows the same trend. The grayed symbols appear closer to the lower left side of the plot, indicating lower viscosity and density values

The ratio of first sample to second sample viscosity is shared in Figure 4.15, showing different settling patterns depending on the original acid fraction. This is related to the different droplet size distribution, which depends on the volumetric ratio. An example of droplet size distributions from crude oil/brine emulsions created using the same crude and mixing method is shown in Figure 4.16. (Sergio 2018). The result shows a shift of emulsion Droplet Size Distribution (DSD) as the water cut in the emulsion increases. The 50% water cut has the widest range of DSD.

The second samples in some cases had a viscosity that is still 10 times higher than oil viscosity, as is the case for the 6:4 oil/acid ratio emulsion on day five. The density for that emulsion was recorded at 0.936, indicating a 30% acid content, which is lower than the original 40% acid content for that emulsion. However, its viscosity is 250 cp, which is larger than the original emulsion viscosity for that ratio of 145 cp. Given that we usually observe an increase in viscosity with the increase in acid content, these results indicate a change in the micro-structure of the emulsion resulting from the settling of larger acid droplets leaving behind a higher concentration of smaller acid droplets. The results observed in Figure 4.15 show that the second samples (filled markers) appear lower on the relative viscosity versus density graph.

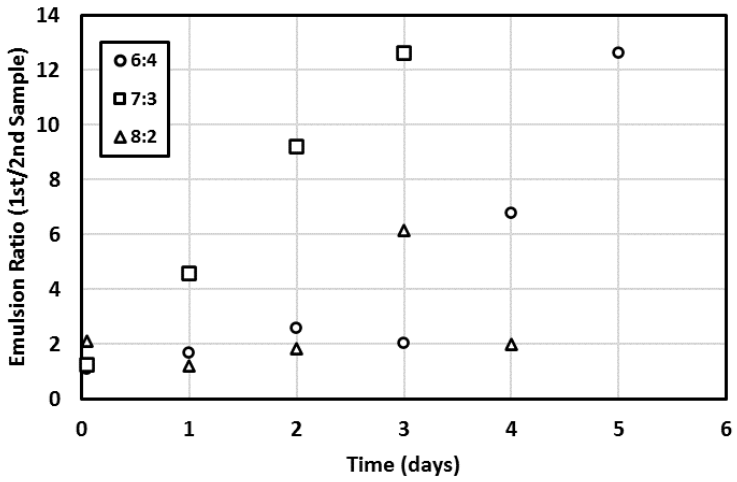

Figure 4.15: Ratio of first sample viscosity over second sample viscosity

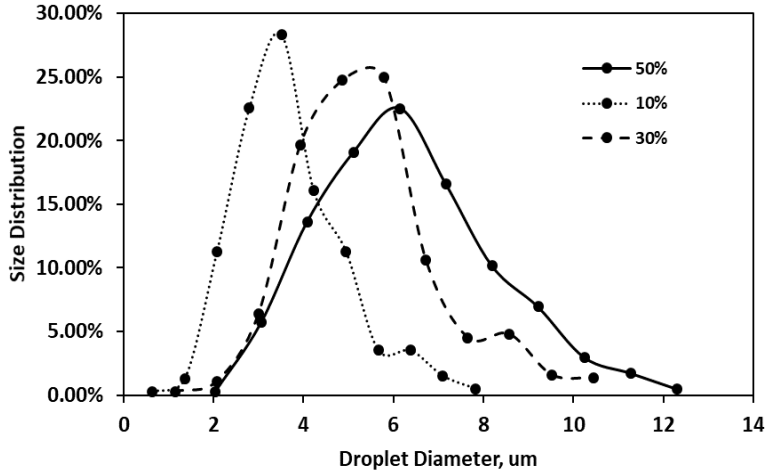

Figure 4.16: Change in droplet size distribution for three different water fractions emulsions mixed with $CaCl_2$ brine with a concentration of 8.55 mMol/L (Gomezm, 2018)

4.3.2 Acid Injection into Carbonate Core Samples

This set of experiments was conducted to examine the possible in-situ emulsification that could occur when acid is injected into the rock matrix that contains crude oil. The experiments are listed in Table 4.2, showing the properties of the core samples, their saturation state before acid injection, and the type of experiment performed.

Table 4.2: List of core samples along with their properties and the type of experiment conducted.

Core Designation	Length (cm)	Diameter (cm)	Porosity (%)	Initial Saturation (Aging time)	Type of Experiment
LS-2	15.44	3.79	15.8	98% Crude (60 days)	Full wormhole propagation, no backpressure
LS-3	15.29	3.76	15.7	Air	Full wormhole propagation, no backpressure
LS-4	15.31	3.76	15.7	97% Crude (2 days)	Full wormhole propagation, 1,200 psi backpressure
LS-5	15.37	3.76	16.0	Air	Full wormhole propagation, 1,200 psi backpressure
LS-8	15.32	3.78	16.9	95% Water	Full wormhole propagation, 1,200 psi backpressure
LS-9	15.41	3.78	16.8	97% Crude (4 days)	Partial wormhole, 1,200 psi backpressure
LS-12	15.16	3.78	17.0	98% Crude (14 days)	Partial wormhole, 1,200 psi backpressure (24 hr soak)
LS-13	15.26	3.78	16.9	97% Crude (14 days)	Partial wormhole, 1,200 psi back pressure

In acidizing experiments, acid is injected into a core packed in a core holder. Usually, six to ten of such experiments are conducted at varying acid injection rates to detect the optimum rate that minimizes the pore-volume-to-breakthrough, PV_{bt}, required to propagate a wormhole through the whole length of the core. PV_{bt} represents the fraction of the volume of acid injected until wormhole breakthrough to the total pore volume of the core. In our experiments, we injected acid at a fixed rate of 3.5 cm^3/min, which was reported to be the optimum injection rate for these rock samples by Scarborough (2016). This optimum rate can vary for cores saturated with different fluids, but we decided to keep the injection rate at a constant value for the purpose of this work.

The first two experiments were conducted with the goal of propagating a full wormhole throughout the length of the rocks without applying any backpressure. LS-2 was saturated with crude oil and aged for 60 days, while LS-3 was air saturated without exposure to oil. Inlet pressure was recorded throughout the experiment. Acid injection was halted when the differential pressure decreased to zero, indicating a wormhole traverses the rock. The results for differential pressure across the rocks in these two cases are presented in Figure 4.17a. It shows that the rock which was saturated with crude oil recorded higher injection pressure but had a 0.35 PV_{bt} while the rock that was air-saturated had a 1.32 PV_{bt}; it takes more acid injection to propagate a wormhole through an air-saturated core than it takes for a crude-saturated core. Since the outlet of the setup was open to atmospheric pressure, it was easy in this case to collect an effluent sample for the crude-saturated

core injection. The sample collected had a viscosity of 860 cp and a density of 1.045 g/cm^3 when measured directly after the injection test. The density indicates an 86% acid content, and the viscosity is equivalent to a relative viscosity of 33. These numbers are in-line with the properties of emulsions collected from bottle tests, as shown in Figure 4.17b. A picture of the emulsion residue taken after a few days of the experiment, presented in Figure 4.18, shows the accumulation of a solid-like emulsion similar to that observed in bottle tests reported earlier. To the best of our knowledge, this is the first time an in-situ generated emulsion is reported with direct evidence of its formation in a core-flood experiment. According to the drop size distribution shown in Figure 4.17, this emulsion is a macro-emulsion whose droplets diameter size is between 0.1 µm to 100 µm. One explanation for the formation of this emulsion is the presence of CO_2, a bi-product of the reaction between hydrochloric acid and calcium carbonate, in the gaseous phase due to the low-pressure conditions. This free CO_2 would have aided in mixing the acid and the oil, resulting in the formation of an emulsion similar to that created in bottle tests. This hypothesis is further examined in the last part of this chapter.

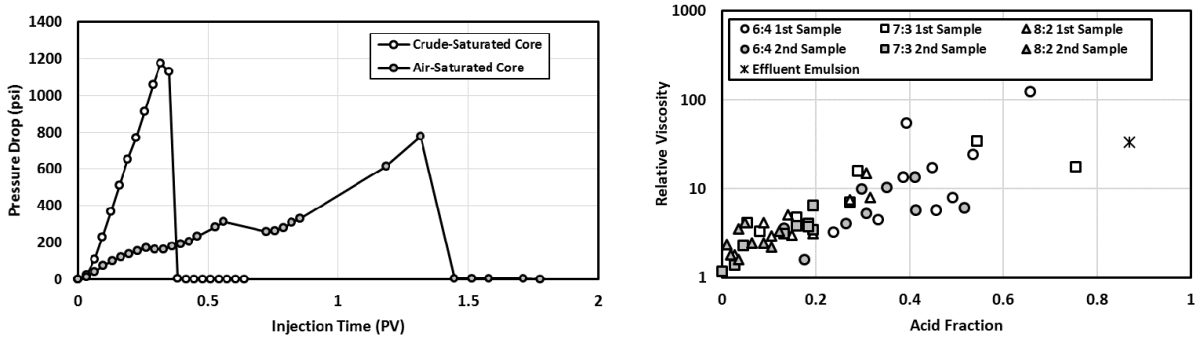

(a) **(b)**

Figure 4.17: Pressure drop during acid injection at a rate of 3.5 cm^3/min into LS-2 (crude-saturated core) and LS-3 (air-saturated core) with the outlet open to atmospheric pressure

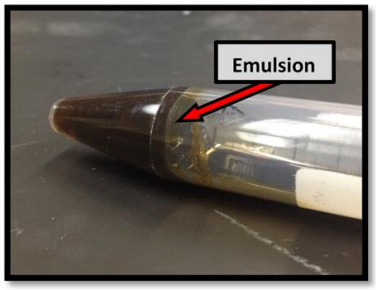

Figure 4.18: A picture of the effluent emulsion taken after a few days of the injection test for LS-2, a crude-saturated core, where acid was injected into the core at 3.5 cm^3/min with the outlet open to atmospheric pressure (Scarborough 2016)

The same acid injection experiments were repeated for cores LS-4, LS-5, and LS-8, this time with a backpressure of 1,200 psi applied to the outlet of the cores using an outlet accumulator filled with nitrogen and controlled by an ISCO pump at constant pressure. LS-4 was crude-saturated, LS-5 was air saturated, while LS-8 was saturated with deionized water. The results for the pressure drop across the cores are shown in Figure 4.19. The efficiency of wormhole propagation at this injection rate was highest in the crude-saturated core, which recorded the lowest PV_{bt} value under 0.28. The water-saturated core had a PV_{bt} value of 0.31, while the air-saturated core had a PV_{bt} value of 0.51. Note that the pressure drop across the air-saturated core, in this case, was very low and did not exceed 35 psi, while the pressure drops across the crude-saturated core reached over 800 psi; the pressure data missing between 0.22 and 0.29 pore volumes of acid injection is due to transducer limitation. Due to the high backpressure of 1,200 psi and the presence of an outlet accumulator, it was not possible in the case of LS-4 injection to collect a large enough sample of emulsion to analyze. A picture of the effluent mixture from this experiment is shown in Figure 4.20. Presented next, in Figure 4.21, are pictures of the inlet and outlet faces of these core samples after acid injection. It shows the entrance and exit locations of the wormholes for cores LS-4, LS-5, and LS-8. No significant difference is observed in the wormhole's size for these cores, irrespective of the saturation state. The only difference was the amount of acid needed to propagate

that wormhole through the core, which was lowest in the case of crude-saturated cores and almost doubled in the case of air saturated cores.

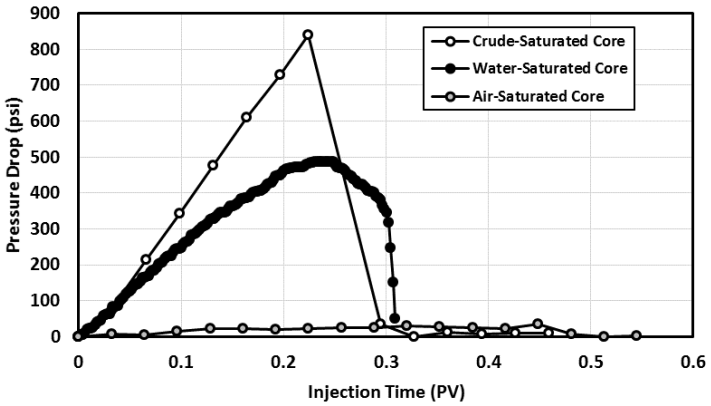

Figure 4.19: Pressure drop during acid injection at a rate of 3.5 cm^3/min into LS-4 (crude-saturated core), LS-5 (air-saturated core), LS-8 (water-saturated core) with an outlet pressure maintained at 1,200 psi

Figure 4.20: A picture of the effluent emulsion taken directly after acid injection into LS-4, a crude-saturated core, where acid was injected into the core at 3.5 cm^3/min with the outlet pressure kept constant at 1,200 psi (Scarborough 2016)

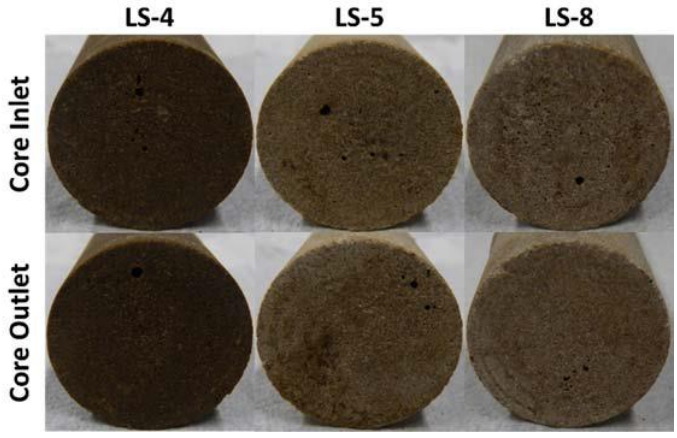

Figure 4.21: Pictures of the inlet and outlet faces of LS-4, LS-5 and LS-8 that were subjected to acid injection at 3.5 cm^3/min with an outlet pressure of 1,200 psi (Scarborough 2016)

In the next phase of the experiments, the work targeted injecting a small volume of acid to propagate a partial wormhole through the rock for cores saturated with crude oil. In these experiments, the outlet accumulator was filled with oil. Oil was injected at the outlet side of the core at a rate of 0.3 cm^3/min to record the initial pressure response from oil flow. A small volume of acid was then injected at the inlet for about half the time it takes to propagate a full wormhole while backpressure was maintained at 1,200 psi. The acid injection was then followed by oil backflow injection from the core outlet at 0.3 cm^3/min. In some cases, a 24-hour soaking time was introduced between the acid injection stage and the oil backflow stage. This was performed to investigate whether the increase in emulsion viscosity with time could introduce problems during the oil backflow process.

We first observe the pressure response during the acid injection period for cores LS-9, LS-12, and LS-13. The results are shown in Figure 4.22**.** Those cores went through a similar process of crude oil saturation. Core LS-9 was aged for 4 days in oil and did not undergo oil injection before acid injection. Cores LS-12 and LS-13 were aged for 14 days each, and acid injection was preceded by oil injection from the outlet sides. The process of acid injection for partial wormhole propagation for all three cores was similar, and the results of pressure response compared to LS-4 (a case of full propagation) show that the experiment is reproducible. The amount of acid injected in all three cores was the same, and it was about half the amount needed to propagate a full wormhole. The difference between the experiments for LS-12 and LS-13 was for the post-acid injection procedure, where LS-12 was left to soak for 24 hours after acid injection before oil backflow, while LS-13 was subjected to oil backflow immediately after acid injection.

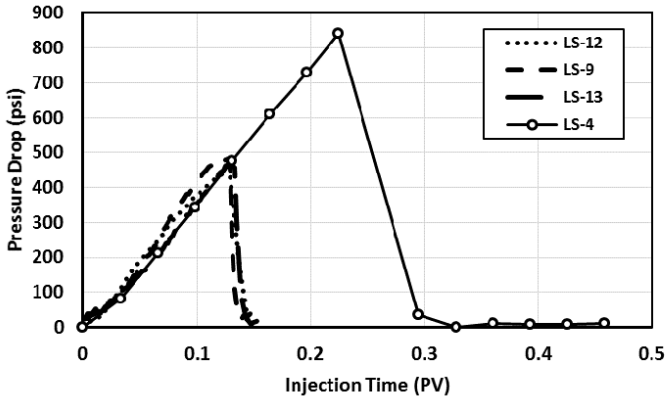

Figure 4.22: Pressure drop during acid injection at a rate of 3.5 cm^3/min into LS-9, LS-12 and LS-13 targeting partial wormhole propagation. All three cores were crude-saturated. The result is compared to that of LS-4 reported earlier

We next observe the pressure response from oil injection. The results of pressure drop during oil injection for core LS-13 before and after acidizing are shown in Figure 4.23, while the results for LS-12 are shown in Figure 4.24. The main observation from these experiments is that oil injection after acidizing required a higher pressure drop than oil injection before acidizing. This pressure difference could be affected by several factors, including relative permeability effects and the possible plugging due to emulsions. One interesting observation is that the pressure response for post-acid oil injection seems to be less severe in the case where the core was left to soak for 24 hours. The comparison is presented in Figure 4.25 along with the post-acid pressure response for LS-9, showing the reproducibility of the LS-13 data set. This is contrary to the expectation that the time factor might work against you in the presence of emulsions, given that the settling of a sludge during the static conditions of soaking is expected. One possible explanation is that soaking time allowed further dissolution of the rock matrix. We recommend future investigation to study the effect of longer soaking times.

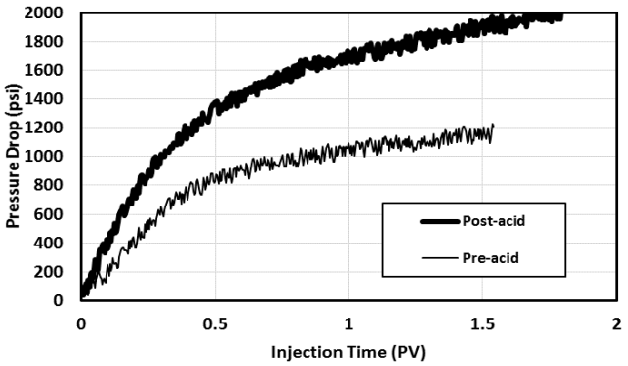

Figure 4.23: Pressure drop oil injection at 0.3 cm^3/min before and after the acidizing process for core LS-13, crude-saturated, was not subjected to any soaking time after acid injection

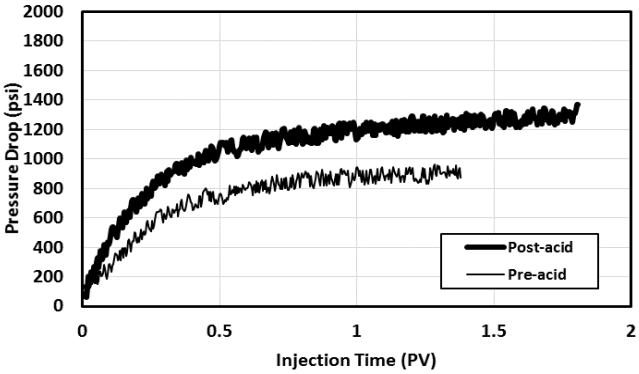

Figure 4.24: Pressure drop oil injection at 0.3 cm^3/min before and after the acidizing process for core LS-12, crude-saturated, was subjected to 24-hour soaking time after acid injection before oil backflow

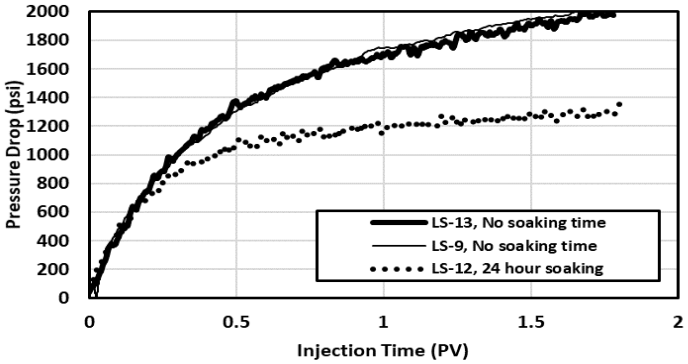

Figure 4.25: Pressure drop oil injection after the acidizing process for cores LS-13 and LS-9 showing overlapping pressure profile, both were not subjected to soaking after acid injection, compared to the pressure response for LS-12 after acidizing and following a 24-hour soaking time

Out results outline one workflow that can be used to examine post-stimulation flow conditions towards optimizing the acid injection process. Examining the inlet faces of the core samples that were used in partial wormhole propagation experiments did not show evidence of a major wormhole presence. This observation is in-line with previous observations that several small

wormholes might get initiated at the beginning of acid injection before a major wormhole takes over. Pictures from these rock samples are shown in Figure 4.26.

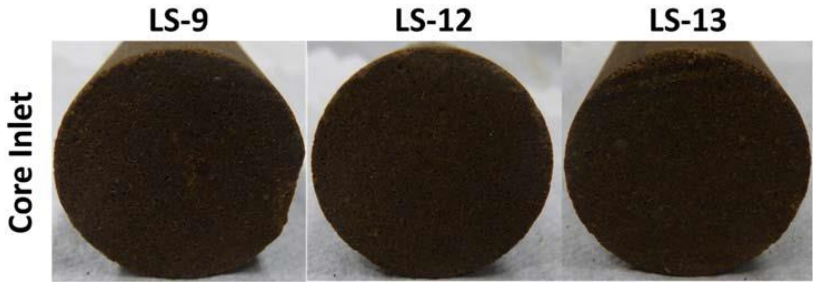

Figure 4.26: Pressure drop during acid injection at a rate of 3.5 cm^3/min into LS-9, LS-12 and LS-13 targeting partial wormhole propagation. All three cores were crude-saturated. The result is compared to that of LS-4 reported earlier for full wormhole propagation (Scarborough 2016)

4.3.3 Effect of Agitation Resulting from Gaseous CO_2

The third set of experiments was conducted to test the effect of the presence of insoluble CO_2 on the formation of an acid−oil emulsion and its characteristics. When the acid−oil emulsion formed after a dry carbonate rock was placed in a mixture of oil and acid (Figure 4.27a), its density and viscosity were higher than those of the crude oil. The density recorded was 0.98 g/ cm^3, which, if converted to an acid fraction, results in a value of 52%. However, the presence of CO_2 in crude also results in an increase of over 2% in the crude density (Mehana et al. 2018). The increase in viscosity toward a relative viscosity of 3.5 indicates that both acid and CO_2 influenced the value of density observed; if corrected by 2% in the density value to account for CO_2, the resulting acid content is 42%. When 15wt.% HCl was poured on the oil-saturated core, the acid−oil emulsion formed was by far higher in density, and its viscosity was unmeasurable because it took the form of a sludge (Figure 4.27b and 4.27c). The density of this sludge was recorded at 3.2 g/cm^3, indicating the presence of solids. This set of measurements provides evidence that agitation resulting from gaseous CO_2 plays a part in the formation of emulsions.

(a) **(b)** **(c)**

Figure 4.27: Images documenting the impact of the acid−rock reaction on the mixing of oil and acid: (a) acid−oil emulsion from the dry core, (b) acid−oil emulsion from the saturated core, and (c) sludge-like acid−oil emulsion from the saturated core.

Table 4.3: Density and viscosity of oil and acid-oil emulsions resulted from the third experiment

#	Crude Oil	Acid-oil Emulsion /Dry Indiana Limestone Rock	Acid-oil Emulsion/ Oil Saturated Core
Density, g/cm^3	0.8725	0.9797	3.2
Viscosity, cp	65.75	90.301	NA

4.4 Conclusions

The following conclusions are drawn from the results of the experiments reported in this study:

- The viscosity of the emulsion created by mixing acid and oil increases with time as the oil separates out of the emulsion, and a higher acid fraction is entrapped in the remaining emulsion layer.
- The emulsion layer is heterogeneous, showing an increase in emulsion viscosity and density with depth due to gravity segregation. There are indications of changes in the microstructure of these emulsions, reflected in the variation in emulsion viscosity for a given emulsion density.
- Injecting acid at a pressure that allows CO_2 to be in a gaseous phase could aid in the formation of stable emulsions in the rock.

- The process of creating wormholes during acid injection is more efficient in crude-saturated cores than it is in a water-saturated or air-saturated cores.
- Contrary to our expectation from bottle test results, preliminary core experiments showed that a soaking time of 24 hours after acid injection could aid the backflow process by reducing the resistance to flow. This observation lays the ground for further experiments in this area.

5. Chapter 5: Experimental Work Part II- Quantifying the Effect of De-emulsifiers on Acid Treatment in Carbonate Formations:

In this work, we performed a stacked study where bottle tests and core-flooding tests were conducted to show that (1) emulsion-risk in the pore space is real, and (2) the addition of de-emulsifiers to the acid is essential to enhance well performance. A light crude oil (25.6-cp viscosity) from a field in Texas is used in this study. Indiana Limestone cores are used in the flooding tests. Although this oil doesn't emulsify with water, it creates a stable emulsion when mixed with a 15 wt.% HCl solution. Ten different de-emulsifiers were investigated to identify the most effective one in eliminating the emulsion. A core flooding experiment is designed to simulate the process of well stimulation and oil backflow production. The analysis of pressure and rate data was performed in the case of emulsion-prone fluid systems and emulsion-free fluid systems.

Our results showed a significant improvement in oil flow rate efficiency when the selected de-emulsifier was added to the acid. A 50% reduction in pressure is recorded when emulsion-free fluid systems are used as compared to emulsion-prone systems. This significant pressure difference reflects the damage to well productivity resulting from emulsions when de-emulsifiers are not utilized. The results show that this pressure response is not just apparent in the transient phase of acid recovery and two-phase flow but is sustained over the oil production phase. Given that many small operators elect to inject straight 15 wt.% HCl solutions into the wells without regard to de-emulsifiers, the results show the critical need to invest in such additives after identifying the suitable type and amount of emulsifier for a given formation. This work was published in the Energies journal (Elsafih et al. 2021).

5.1 Materials

5.1.1 Indiana Limestone Core

A 6-in.-length and 1.5-in.-diameter sample of an Indiana Limestone was cored using water-based drilling and then dried. Its porosity was measured using a helium porosimeter as 16 % and absolute permeability using nitrogen gas as 55 mD. The method of measuring absolute permeability includes injecting the nitrogen gas through the core and measuring the change in outcome volume of gas as we manually change the inlet pressure while outlet pressure is kept constant at 100 psi. The inlet pressure is adjusted from 50.8 psi to 97.6 psi with an increment of 5 psi. Data shown in Table 5.1 is then plotted as in Figure 5.1, where permeability is calculated from the Darcy slope of the generated line.

Table 5.1: Permeability worksheet

Inlet Pressure	Outlet Pressure	Vol Initial	Vol. Final	Volume	Time	Flow Rate	Inlet Pressure	Outlet Pressure	(P1^2-P2^2)/2L	q/A
psig	psig	cc	cc	cc	sec	cc/sec	P1 (atm)	P2 (atm)		
100.3	50.8	400	1000	600	12.7	47.24	7.82	4.46	1.32	4.17
99.8	57.1	400	1000	600	13.9	43.17	7.79	4.89	1.18	3.81
100	64.4	400	1000	600	16.7	35.93	7.80	5.38	1.02	3.17
99.9	71.9	400	1000	600	19.8	30.30	7.80	5.89	0.83	2.68
99.9	79.3	400	1000	600	25.5	23.53	7.80	6.40	0.64	2.08
100	87.5	400	1000	600	41.5	14.46	7.80	6.95	0.40	1.28
99.8	93.2	400	1000	600	71.9	8.34	7.79	7.34	0.22	0.74
100.5	97.6	400	1000	600	165.3	3.63	7.84	7.64	0.10	0.32

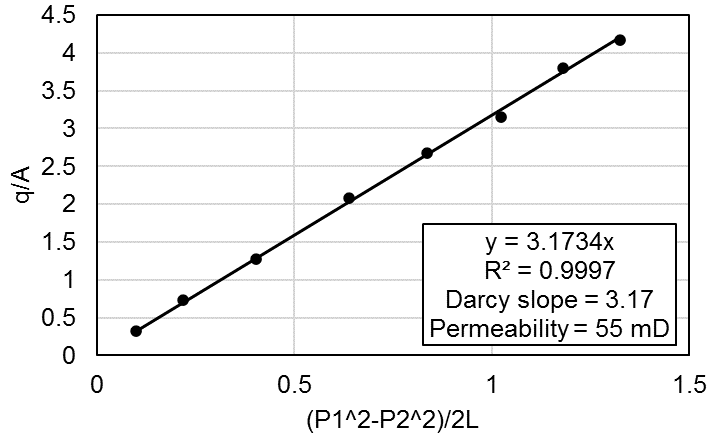

Figure 5.1: Permeability graph

5.1.2 Crude Oil and HCl Spent -Acid

A crude oil sample was purchased from Texas Raw Crude to be used in this study. The dynamic viscosity was measured using a cannon capillary viscometer to be 25.6 cp. The density was measured using a pycnometer to be 0.88 g/cm^3. Live-acid was used to prepare a spent-acid solution for use in this work. 37 wt.% HCl solution obtained from Sigma Aldrich was first diluted to a 15 wt.% acid, which is typical for carbonate acidizing. Chunks of Indiana Limestone (>99% calcium carbonate) were used to fully spend the acid, as shown in Figure 5.2a, so that it does not have any more dissolving power. As shown in Figure 5.2b, the spent-acid was then filtered to remove impurities and obtain the final spent-acid used in the bottle and flow tests. The pH of the spent-acid was measured to be 5, which is close to the 4.5 pH value typically measured for spent-acid during backflow in the field (Saneifar et al. 2010).

5.1.3 De-Emulsifiers

A set of nine de-emulsifiers were tested using a simple bottle test to examine their effectiveness in limiting the formation of an emulsion between acid and crude oil. These de-emulsifiers were obtained from a vendor without identifying the content. Live acid was used in these tests, given that the emulsion between crude oil and live-acid is the more viscous and stable emulsion.

5.1.4 Surfactant

In some of the experiments, there was a need to add a surfactant into the oil to act as an emulsifier instead of naturally occurring surfactants. The surfactant used for this purpose was Span-85.

(**a**) (**b**)

Figure 5.2: Spent-acid preparation. (a) live-acid is reacting with Indiana Limestone chunks; (b) filtering the resulted spent-acid

5.2 Experimental Setup and Procedures

In this section, we describe the experimental setup and procedures used in this work. The bottle tests used to evaluate the de-emulsifier's effectiveness are first described, followed by the procedure used to quantify the effect of a de-emulsifier on the stability and viscosity of emulsions. After that, the core preparation method and the flooding experiments are presented.

5.2.1 Bottle Tests for Screening De-Emulsifiers

Bottle tests were used to screen the de-emulsifiers and identify the effective ones in inhibiting emulsification between live acid and crude oil. A total of 5 cm^3 of fluids was placed in a vial with a 3:7 volumetric ratio of live-acid to crude oil. 1 wt.% of de-emulsifier was added to the acid before mixing. The small vial was then vigorously hand-shaken for five minutes then placed on a counter. The separation of an oil or an acid phase was then observed. While the concentration of emulsifier can impact its effectiveness, the goal of this step was not to identify the best or optimum concentration but to quickly screen for an effective de-emulsifier. This goal was achieved, and thus there was no need to test variations in concentration.

5.2.2 Bottle Tests for Emulsion Viscosity and Stability

Bottle tests were also used to study the emulsification behavior of three fluid systems that are used in this study. These tests included creating a total of 150 cm^3 of mixture for each fluid system using an emulsion study protocol developed by our team that proved to result in reproducible emulsions to allow for consistent experiments (Oluwatosin 2016). A homogenizer was used to mix the emulsion for 30 minutes at 5000 rpm. The 150 cm^3 of emulsion were then divided into five different vials. The first vial was used to capture the viscosity of the emulsion after mixing. The other four vials were observed at time intervals of 5 hrs, 24 hrs, 3 days, and 5 days. At each time interval, the separation was observed, and then a sample was recovered from the top of the emulsion to collect viscosity information.

The three fluid systems that were studied were: (1) Spent-acid + Oil (a system not prone to emulsions), (2) Spent-acid + Oil, and 1 wt.% Surfactant (a system prone to emulsions), and (3) Spent-acid and 1 wt.% de-emulsifier + Oil and 1 wt.% surfactant (where the effectiveness of the de-emulsifier in eliminating emulsions is documented).

5.2.3 Core Preparation Procedure

The goal of the core flooding work is to quantify the effect of the emulsion on the backflow of oil after acidizing. This requires the propagation of a wormhole only part of the way through the rock and then injecting oil from the other side of the core. In previous work (Scarborough et al. 2019), an attempt to inject live acid into the core to generate a partial wormhole was challenging as no visible wormhole entry was observed. Accordingly, we designed a simple experiment to allow the study of the backflow process of spent-acid and oil without having to go through live-acid injection. A small hole was drilled into the core to represent a wormhole. To use the smallest of the drill bits, we cut two 1-inch length pieces from the inlet of the core, as shown in Figure 5.3a,

and used a 1/16-in.-drilling bit to drill a hole in the two inlet pieces. The image shown in Figure 5.3b shows the width of the drilled hole as compared to a wormhole casted in a different core after live-acid injection. To limit the number of factors that can influence the experiment's reproducibility and simplify the analysis process, it was determined that the work be performed with no initial water saturation and at room temperature. With this being the first study of its kind, the impact of variable initiation saturation and temperature can be deferred to future studies.

(**a**) (**b**)

Figure 5.3: Core preparation. (a) Core is cut and drilled; (b) the 1/16-in.-drill bit used to simulate a wormhole

5.2.4 Core Flooding Tests

After the core was prepared, it was saturated with crude oil using a vacuum cell. The procedure for core-flooding involved packing the three pieces of the core in series with the two drilled pieces placed at the inlet of the core. Three phases of injection were then conducted using the setup shown in Figure 5.4. The setup consists of an injection pump, an acid accumulator, an oil accumulator, a core holder, pressure gauges, and a confinement pressure pump. The following procedure is followed for each case on injection:

- The core is saturated, injected with oil.
- The tubing line is filled with acid using the injection pump, while the oil tube line is closed by closing V-3, V-6, V-8, and V-11.
- The core is packed and desired confining pressure is applied.

- Spent-acid is injected, and inlet pressure is recorded.
- After injecting spent-acid is finished, valves V-4, V-5, and V-9 are closed, and V-3, V-6, V-8, and V-11 are opened.
- Oil is injected from the backside of the core, and inlet pressure is recorded.
- After the oil injection is finished, the core is unpacked and cleaned by multicycles injection of toluene and methanol to be ready for the next injection.
- Previous steps are then repeated for each fluid of the three fluids systems studied.

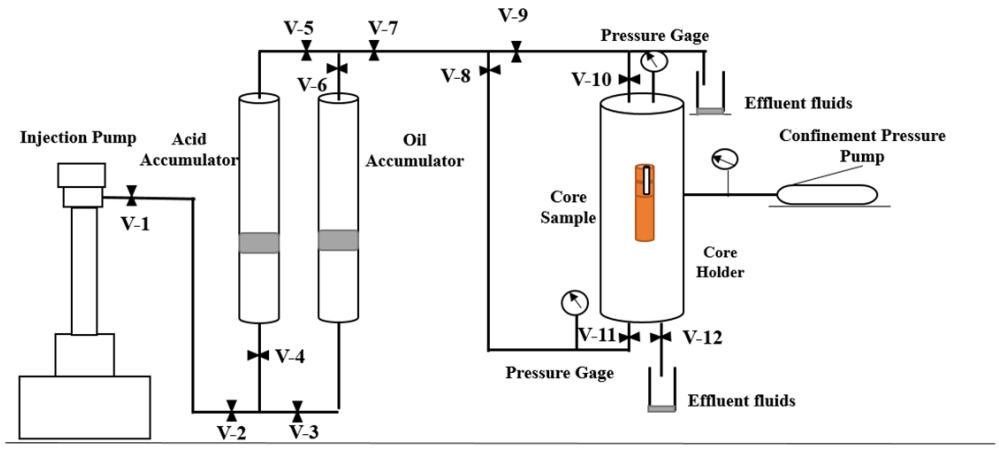

Figure 5.4: Core flooding setup schematic

Oil was injected from the inlet of the core at a constant rate of 1 cm^3/min to establish a pressure profile and oil mobility after the initial vacuum-saturation process. The oil injection was followed by spent-acid injection at the inlet of the core at the same rate of 1 cm^3/min. The last phase was oil injection from the back of the core, also at 1 cm^3/min. Three such flooding tests were conducted along the same lines as the bottle test experiments: (1) Spent-acid + Oil, (2) Spent-acid + Oil and Surfactant, and (3) Spent-acid and de-emulsifier + Oil and surfactant. At the end of each test, the core was exposed to a cleaning process using cycles of toluene and methanol to extract the fluids in preparation for re-saturating with crude oil to conduct the next experiment. The data

collected are the profiles of pressure build-up during injection, which document the resistance to the flow of the injected phase. The pressure gauge used in this flooding setup had a maximum pressure rating of 314.7 psi; accordingly, the injection was halted when that pressure was reached.

5.3 Results and Discussion

5.3.1 Bottle Tests for Screening De-Emulsifiers

These tests' goal was to identify an effective de-emulsifier to use in the rest of this study. The formation of emulsions was observed over 24 hours. Various amounts of thick emulsion were observed for each of the various de-emulsifiers, as shown for select samples in Figures 5.5a, 5.5b, and 5.5c, except for de-emulsifier # 7, in Figure 5.5d. Accordingly, de-emulsifier # 7 was used in the remainder of the study and is referred to as merely "de-emulsifier" henceforth in this study.

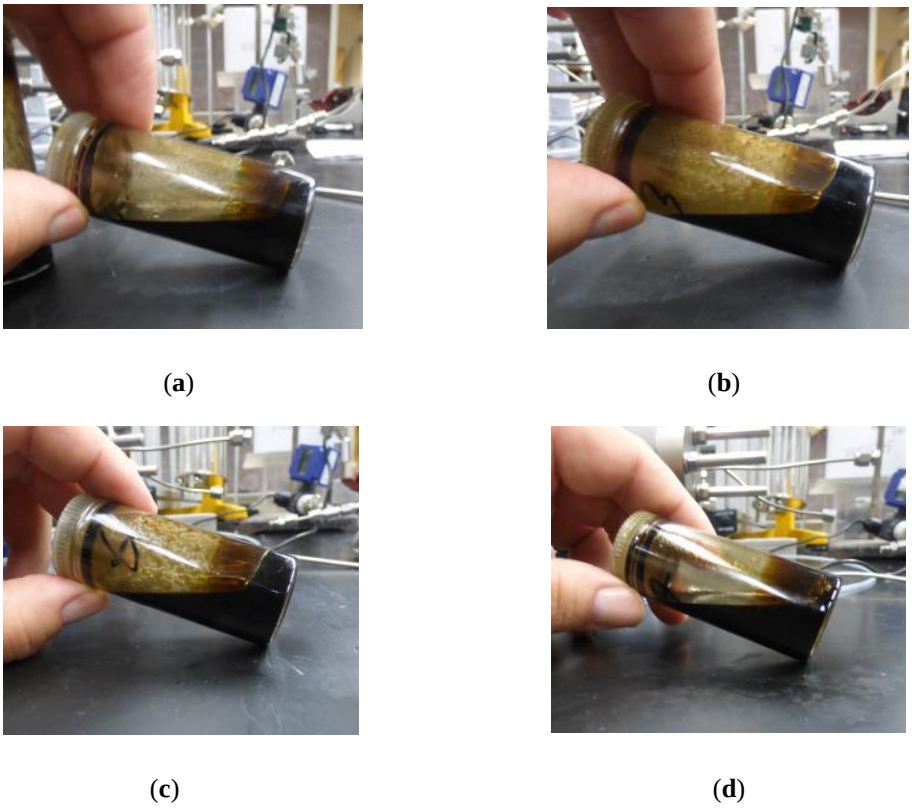

(**a**) (**b**)

(**c**) (**d**)

Figure 5.5: Images taken after 24 hours of mixing, showing the presence of a thick emulsion (sludge) at the bottom of the vial for (a) de-emulsifier 1, (b) de-emulsifier 3, and (c) de-emulsifier 6, and the absence of a thick emulsion in (d) de-emulsifier # 7

5.3.2 Bottle Tests for Emulsion Stability and Viscosity

This set of bottle tests was designed to answer two questions: (1) while this oil emulsifies with live-acid, does it actually emulsify with spent-acid to allow us to use this experimental design for studying backflow behavior after acidizing? And (2) Does the de-emulsifier work in breaking these emulsions between the oil and spent-acid?

The first set of experiments between the oil and spent-acid showed that although an emulsion does form, it was not a stable emulsion. Acid separation can be seen at the bottom of the vial in Figure 5.6a. This separation was expected since this oil does not emulsify with water. A surfactant that had been proven in our previous work to result in stable water-in-oil emulsions (Gomez 2018) was added to the oil sample. The result of mixing spent-acid with the "oil and surfactant" is shared in Figure 5.6b. It shows that there was no separation observed even after 5 days from the time of mixing. The last image, shown in Figure 5.6c, shows the separation resulting from using the de-emulsifier in the spent-acid and mixing it with the "oil and surfactant." These results established for us three scenarios: (1) A case of spent-acid and oil that is not prone to emulsions, (2) A case of spent-acid and oil that is prone to emulsions (presence of surfactant and absence of de-emulsifier), and (3) A case of spent-acid and oil that is typically prone to emulsions, but where a de-emulsifier is added to control for these emulsions.

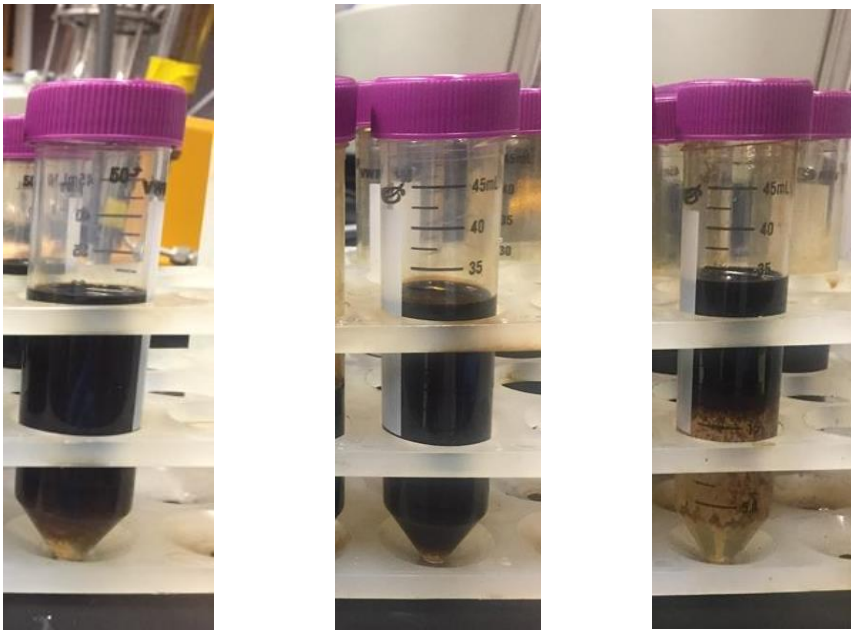

(**a**) (**b**) (**c**)

Figure 5.6: Separation of spent-acid oil emulsion after 5 days whereas (a) spent-acid is mixed with crude oil; (b) spent-acid is mixed with oil and surfactant; and (c) Spent-acid and de-emulsifier is mixed with oil and surfactant

These three systems were further analyzed by measuring the viscosity of the emulsion over time. The results over 5 days are shown in Table 5.2 and Figure 5.7 right after mixing, after 5 hrs., 1 day, 3 days, and 5 days. It shows that the presence of the surfactant in the oil, when mixed with spent-acid, results in a viscous emulsion that is almost 10 times more viscous than the oil. The viscosity value drops to around 140 cp after 24 hrs.; however, it is still more than 5.4 times the oil's viscosity. The oil itself also produces a stable emulsion when mixed with the spent-acid. However, the viscosity starts at around 130 cp then drops to approximately 60 cp, a little over 2 times the oil's viscosity. The addition of the de-emulsifier to the spent-acid shows that it effectively limits the stability and viscosity of the emulsion in the presence of the surfactant; the complete separation between the spent-acid and the oil is observed by day 5; as confirmed in the image

shared in Figure 5.6c. These results ensure that using these three systems in flooding tests can provide insight into the possible role of emulsions during the process of oil backflow.

Table 5.2: Viscosity values for the three fluid systems over time

Scenario #	(1) Oil&Acid, cp	(2) Oil+Surfactant&Acid, cp	(3) Oil+Surfactant &Acid +De-emulsifier, cp
Emulsion viscosity	132.95	221.59	94.96
Emulsion viscosity 5hrs	96.86	161.44	88.13
Emulsion viscosity 1day	82.30	141.82	79.02
Emulsion viscosity 3days	72.81	141.18	66.86
Emulsion viscosity 5days	63.31	141.18	27.35

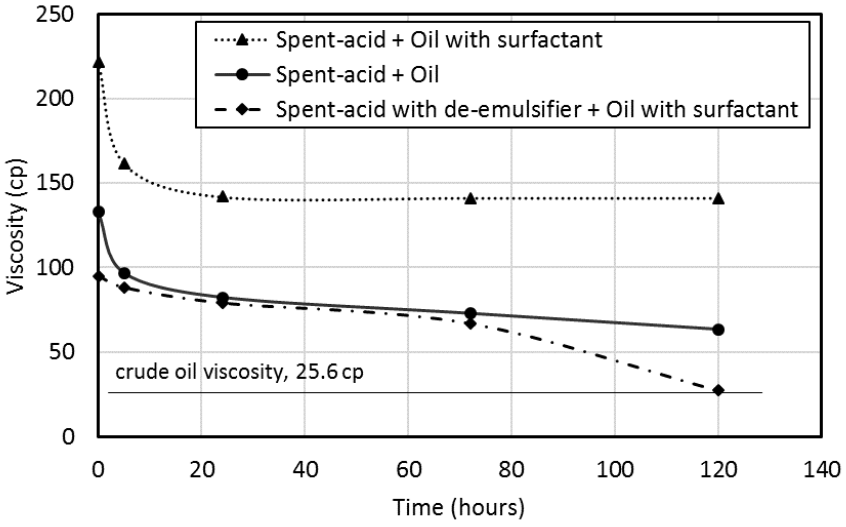

Figure 5.7: Spent-acid + oil emulsion viscosity vs. time for the three scenarios

5.3.3 Core Flooding Tests

The three fluid systems were utilized in the flooding experiments. This section compares and analyzes the pressure response from these scenarios during the three stages of injection. The first graph, shared in Figure 5.8, shows the pressure response when spent-acid is injected for the three scenarios. The lowest pressure was observed when the de-emulsifier was added to spent-acid, which was associated with the case of a surfactant added to the oil. The pressure profile for the case of the two emulsion-prone systems shows a slope of pressure build-up that is double that of the emulsion-free system. Given that the only difference between the fluid systems is their

susceptibility to emulsions, this could reveal that the injection of acid results in mixing, leading to the formation of emulsions and resulting in higher resistance to flow. While it is not the only mechanism that explains these results, it is evident that emulsion-prone systems have a very different flow behavior than emulsion-free systems.

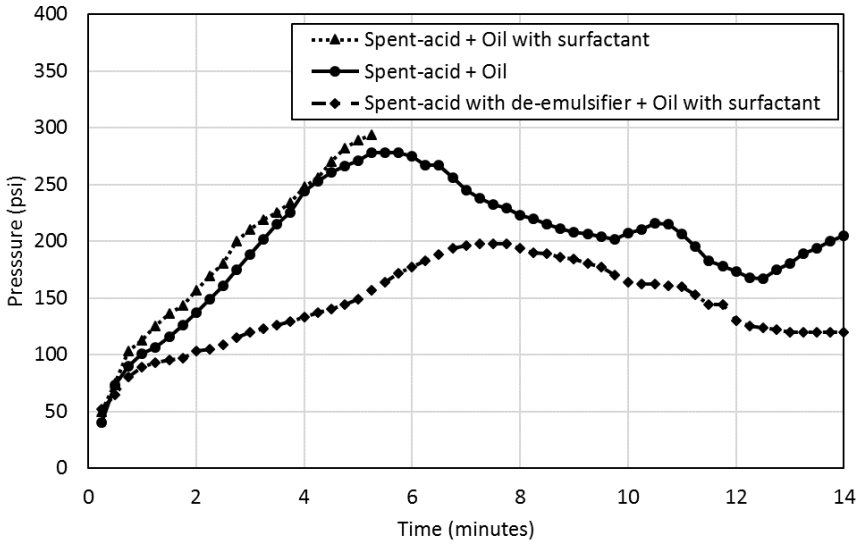

Figure 5.8: Pressure responses when spent-acid was injected for the three scenarios

The result of pressure build-up when injecting oil from the outlet of the core following spent-acid injection is captured in Figure 5.9. In all three scenarios, the two-phase immiscible flow resulted in pressure values beyond the pressure transducer's limits. However, when a de-emulsifier is used, a slow pressure build-up was observed in the case of oil flow. Both cases of oil injection without the use of a de-emulsifier recorded the fastest pressure build-up, indicating that oil is experiencing a higher resistance to flow. The presence of the surfactant in the oil results in a more accelerated pressure build-up as it intensifies the emulsion problem. The drop in the slope of pressure build-up by less than half when a de-emulsifier is used indicates that the effective permeability to oil has been doubled in the emulsion-free fluid system compared to emulsion-prone systems. Oil b represents a cleanup mechanism that removes the spent acid and reaction

products from the acidized region. The mechanism of acid-oil interactions that result in viscous emulsions negatively impacts the flow capacity for oil, reflecting the damage to well productivity resulting from emulsions when de-emulsifiers are not utilized. Given that many small operators elect to inject straight 15wt.% HCl solutions into the wells without regard to additives such as de-emulsifiers, the results show the critical need to invest in such additives after identifying the suitable type and amount of de-emulsifier for the relevant fluid system.

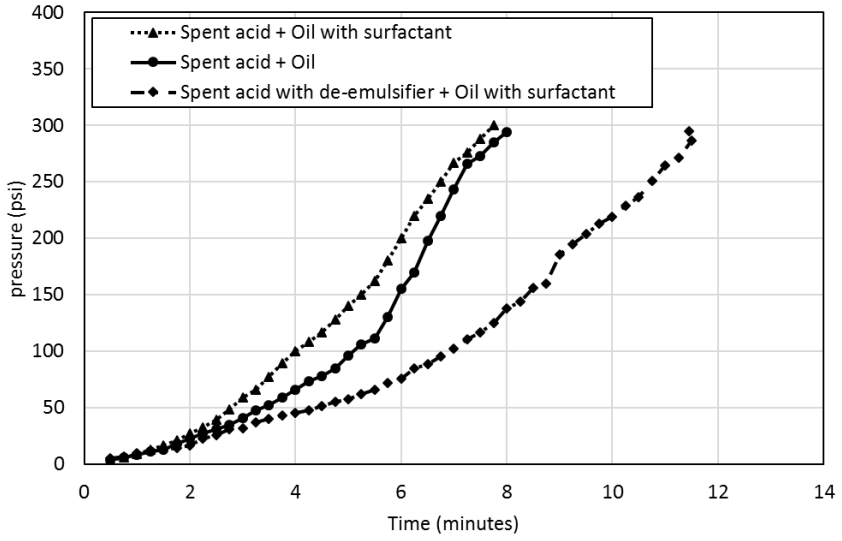

Figure 5.9: Pressure responses for the three scenarios when oil was injected from the outlet end of the core after spent-acid injection from the inlet side was completed

Since the same core was used in these three flooding scenarios and had to undergo multiple rounds of cleaning in between the various stages, we compared the pressure building during oil injection before spent-acid was injected into the core to confirm that the core did not change and that the initial condition was reproduced in each experiment. In addition, absolute permeability was measured after each cleaning which was maintained to 55 mD. The results shared in Figure 5.10 show that the pressure profiles follow the same trend in all three cases. This shows that the

alteration to the core properties was minimal during these rounds of injection and that the cleaning protocol was successful in establishing reproducibility.

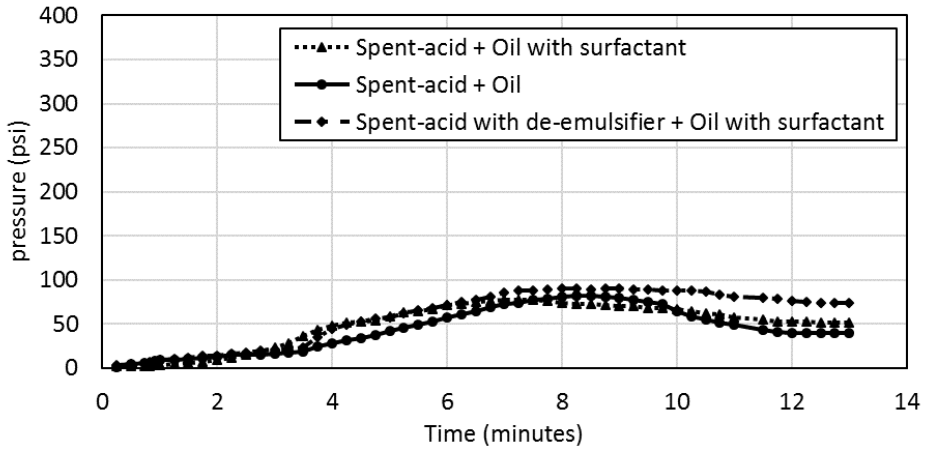

Figure 5.10: Pressure responses from the three scenarios when oil was injected at the inlet of the oil-saturated core before spent-acid was injected

5.5 Assumptions and Limitations

There were some assumptions and limitations that the authors want to layout for consideration. The first is that the work assesses the transitional pressure build-up and not the steady-state flow in the displacement process. While this is a critical stage of the acidizing and the acid cleanup process, this limits the conclusion to that unsteady-state displacement phase. The work was performed at room temperature to simply the experimental workflow and limit the variables investigated in this study. When this workflow is being used to quantify the de-emulsifier's impact on a particular rock-fluid system for field application, it is vital to perform these experiments at reservoir temperature and injection pressure conditions (Kokal et al. 2008). One assumption that was made was that the drilled hole represents a wormhole. This is a valid assumption given that the diameter of the hole is similar to that of an actual wormhole generated during optimum acid

injection conditions. One expects the wormhole generated in oil-saturated cores not to have branches, and that supports the validity of the assumption.

5.6 Conclusions

While many studies exist that study the process of matrix acidizing in laboratory settings, very few of the studies are relevant to the field conditions where the presence of oil results in conditions that can impact well productivity after stimulation. The following conclusions can be drawn from the results shared in this study:

- Emulsion-prone systems result in higher resistance to flow during both the acid injection phase and the oil production phase indicating reduced flow capacity in the pore space, which can be explained by the presence of emulsions resulting from spent-acid and oil mixing.
- De-emulsifiers that successfully control the formation of emulsions result in doubling the flow capacity for both spent-acid and oil. This improvement in flow capacity has the potential to improve the performance of the matrix acidizing treatment in carbonate formations.
- The experimental protocol followed in this study proved to be effective in documenting the effect of de-emulsifiers on flow properties in acidizing treatments.

6. Chapter 6: Experimental Work Part III- Quantifying the Effect of Multi-Phase Flow on Matrix Acidizing in Oil-Bearing Carbonate Formations

It is common to inject acidic stimulation fluids into oil-bearing carbonate formations to enhance well productivity. This process of matrix acidizing is designed to maximize the propagation of wormholes into the formation by optimizing the injection parameters, including acid-injection rate and volume. Previous studies have suggested that saturation conditions, permeability, heterogeneity, temperature, and pressure can significantly affect the design of matrix-acidizing treatments. However, laboratory studies' results are inconsistent in their conclusions and are mostly limited to water-saturated cores. In this work, we designed a systematic experimental study to evaluate the impact of multiphase flow on the acidizing process when injecting 15 wt.% hydrochloric acid (HCl) into crude-oil-saturated Indiana Limestone cores. The results reveal the following: Contrary to published literature for water-saturated cores, acidizing in partially oil-saturated high-permeability cores at high pressure requires less acid volume than in low-permeability cores; lower pressure acid injection results in more efficient wormhole propagation in low-permeability cores compared to high-pressure acid injection; acidizing in low- and high-permeability cores at low pressure leads to similar efficiency; and wormholing is more effective in partially oil-saturated cores, resulting in multiple parallel branches as compared to inefficient leakoff in water-saturated cores. This section explains the experimental work, including the rocks and fluids used in the study, the experimental setup's design, and the procedures used to conduct these experiments. This work was published in the SPE production & Operations journal (Elsafih and Fahes, 2021).

6.1 Materials

6.1.1 Rock Samples

A block of Indiana Limestone with average permeability of 50mD was cored using a 1.5-in.-diameter bit into the 32 cores, 6-in.-length as showing in Figures 6.1a and 6.1b. Another group of higher permeability average of 200mD was cored any dried. The choice of these dimensions is based on the study by Dong et al. (2014), which confirmed these to be suitable core dimensions to eliminate the length effect. X-ray fluorescence scans show that these cores are 97% Calcite, with less than 1% clay content, approximately 0.4% iron content, and a calcium/magnesium ratio of 39:1. The coring was done parallel to the visible bedding lines.

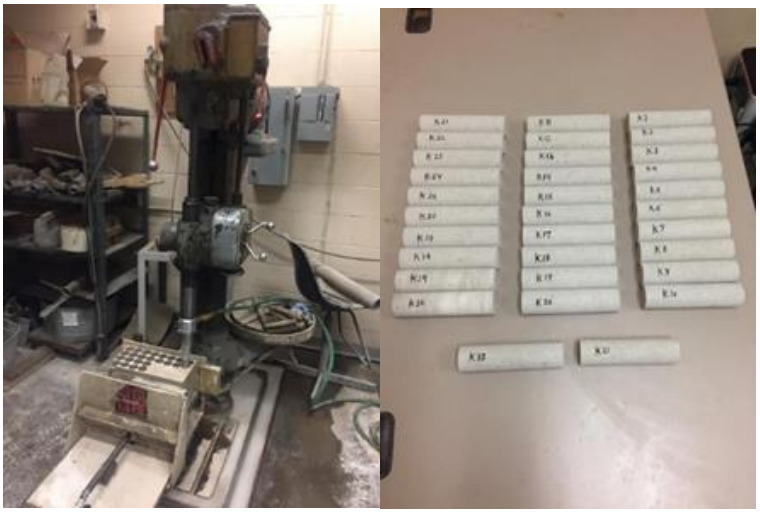

(a) **(b)**

Figure 6.1: (a) Coring an Indiana Limestone block (b) 32 cores used for experiments

The porosity and the absolute gas-permeability values for each of the cores were measured using helium. Although the block was indicated to have a permeability of 50 mD, the permeability values ranged between 27 and 93 mD. Sixteen of these cores were used in this study under five experimental conditions (Groups A through E); their relevant properties are shared in Table 6.1. To document the effect of permeability, three cores of approximately 200-mD permeability were

used (Group F). The spread of permeability and porosity for these six groups is shown in Figure 6.2. Two cores (Group G) with a permeability of approximately 2 mD were used in a previous study (Scarborough 2016), and some of their results are compared in this work. We were careful to group the cores used in each experimental condition so that the permeability has very little variation within each group, as shown in Figure 6.2. This strategy resulted in graphs that show very little scatter, as evident in the results section. The initial water-saturation condition for the six main comparison groups is shared in Figure 6.3. The range of water saturation for groups C, D, and F, was mostly between 40 and 60%, eliminating that as a factor causing variability in the results. Group B had a lower water saturation, between 20 and 30%; however, that experimental condition was reproduced using Group C. The oil relative permeability under these saturation conditions was 0.15 to 0.18 in Group B, 0.11 to 0.15 in Groups C and D, and 0.34 to 0.38 in Group F.

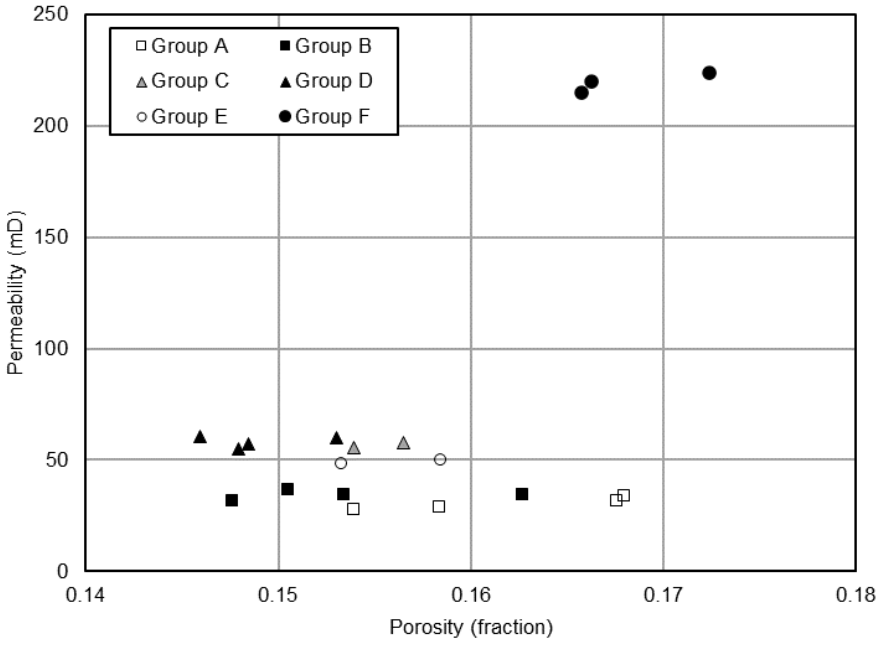

Figure 6.2: Grouping of cores into the various experimental conditions, showing the spread of porosity and permeability

Table 6.1: Physical properties of cores, with information on the experimental condition for each group

Group	#	Length, in	Permeability, mD	Porosity, %	Experiment condition
A	Core 26	6.04	27.7	15.3	Water-saturated; 3,000-psi backpressure
	Core 30	5.98	33.8	16.8	
	Core 7	6.00	29.0	15.8	
	Core 29	6.03	31.7	16.7	
B	Core 9	6.02	34.4	15.3	Partial oil-saturation; 3,000-psi backpressure
	Core 17	6.00	34.2	16.2	
	Core 6	6.01	36.4	15.0	
	Core 8	6.02	31.5	14.7	
C	Core 16	6.01	57.5	15.6	Partial oil-saturation; 3,000 psi-backpressure
	Core 27	6.03	55.5	15.4	
D	Core 11	6.05	57.0	14.8	Partial oil-saturation; 1,100 psi-backpressure
	Core 2	6.04	55.0	14.7	
	Core 1	6.03	60.7	14.6	
	Core 4	6.04	59.9	15.2	
E	Core 23	6.01	49.7	15.8	Water-saturated; 3,000 psi-backpressure
	Core 25	6.03	48.4	15.3	Water-saturated; 1,100 psi-backpressure
F	Core 44	6.19	220	16.6	Partial oil-saturation; 3,000 psi-backpressure
	Core 45	6.10	224	17.2	
	Core 42	6.16	215	16.5	Partial oil-saturation; 1,100 psi backpressure
G	Core 4-b	6.03	2-4	~15.7*	Full oil-saturation; 1,200 psi-backpressure
	Core 7-b	6.06	2-4	~16.6*	

*For these two cores, porosity is calculated and not directly measured

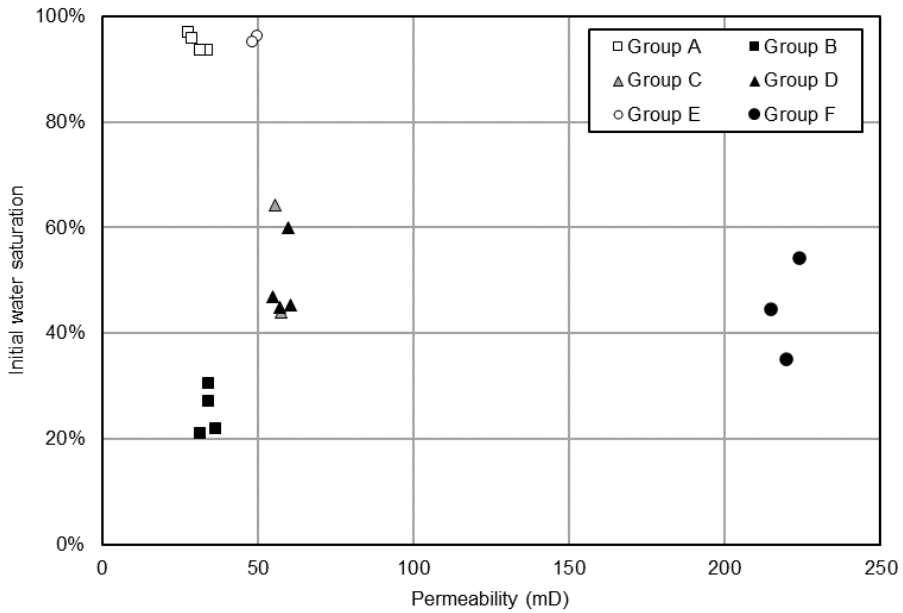

Figure 6.3: Grouping of cores into the various experimental conditions, documenting the initial water saturation before acid injection

6.1.2 Fluids

Texas crude oil was used in this study. The measured density and viscosity of the oil are reported in Table 6.2. Asphaltene content was measured using pentane/oil ratio of 40:1 and was found to be low at 0.7 mg/g of oil. Live HCl with a concentration of 37 wt.% was diluted with deionized water to 15 wt.% for use in the experiments. Helium cylinders were used for measuring porosity and permeability of the core samples.

Table 6.2: Relevant physical properties of fluids used in this work

Material/property	Provider	Color	Density, sc (g/cm^3)	Viscosity (cp)
Crude Oil	Texas Raw Oil	Black	0.88	25.6
HCl, 15 wt.%	Sigma-Aldrich	White	1.07	1
Helium, 99% purity	Air Gas	NA	0.000178	0.02
Water	University Facilities	NA	1	1

6.2 Experiment Setup

The acid-flooding apparatus schematic that was used to run all acid-injection experiments is shown in Figure 6.4. The setup consisted of positive displacement pumps (ISCO pumps) that are used to inject oil, water, and acid into the cores; accumulators for oil, water, and acid; a core holder where

the core is packed; confining pressure pump to apply enough pressure around the cores during injection; pressure transducers to record inlet and outlet pressures; a backpressure regulator to control pressure; and a data acquisition system in which pressure responses are recorded. The properties and capabilities of each part of the apparatus are detailed in the following:

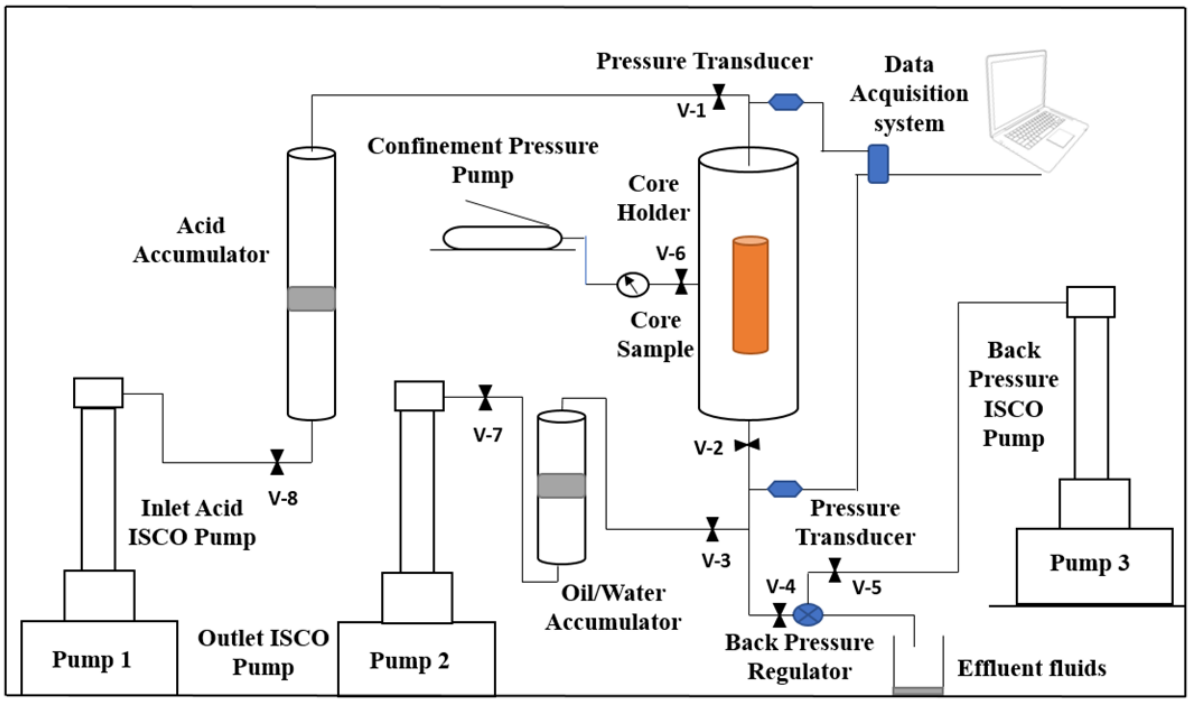

Figure 6.4: Acid flooding apparatus

6.2.1 ISCO Pumps

In matrix acidizing experiments, a high-efficiency pump is needed. Therefore, an ISCO pump shown in Figure 6.5 is used to deliver the desired injection rate for different experiment scenarios. This pump is highly capable with the following specifications (Table 6.3) according to its manual:

Figure 6.5: ISCO pump used to inject fluids

Table 6.3: ISCO pump specifications

Property	Range	Unit
Flow rate	0.001 to 200	mL/cm^3
accuracy	0.5 max error	%
Pressure	0 to 10,000	Psi
Capacity	500	mL/cm^3
Pressure accuracy	0.5	%
Displacement Resolution	31.7	mL

6.2.2 Fluid accumulators and core holder

One accumulator for acid and another one for oil (Figure 6.6a) were used to hold fluids during the injection. Each accumulator is attached to an ISCO pump that is filled with water. When the desired rate is set on the pump, it injects water under the accumulator piston, and therefore, the piston push fluids toward the core. The capacity of each accumulator is 5,000 ml. The core holder shown in Figure 6.6b is designed to handle the high pressure required to prevent any leak inflow around the core during the fluid injection process. The core can be packed inside a rubber sleeve coated with a metal tube where a confining pressure is applied around it using a pump.

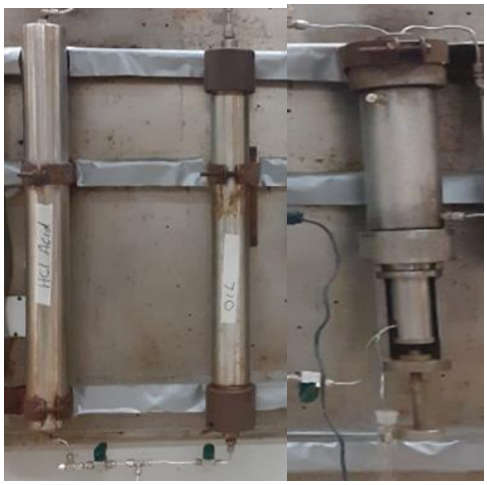

(a) **(b)**

Figure 6.6: (a) Acid and oil accumulators (b) Core holder

6.2.3 Confining Pressure Pump

The confining pressure pump functions: First is to simulate the reservoir pressure by implementing a surrounding pressure around the core. The pump injects a mineral oil into the core holder right behind the rubber sleeve that surrounds the core. The second purpose of the confining pump is to prevent the injected fluid from escaping around the core; instead, it forces fluid to flow through the core by keeping the difference between injection pressure and confining pressure at least 500 psi. The pump, shown in Figure 6.7, is used manually to apply desired confining pressure that would be read on the pressure gauge attached to the pump.

Figure 6.7: Confining pressure pump

6.2.4 Backpressure Regulator

The purpose of the backpressure regulator is to apply backpressure at the core outlet to keep the resulting carbon dioxide in solution. In this study, backpressure was set either at 1,100 psi or at 3,000 psi. The backpressure regulator shown in Figure 6.8a is attached from the top to an ISCO pump filled with water where the desired pressure can be set. The water coming from the pump and fluid sections coming out of the core are separated by a diaphragm, preventing any physical contact between the two fluids, as shown in Figure 6.8b.

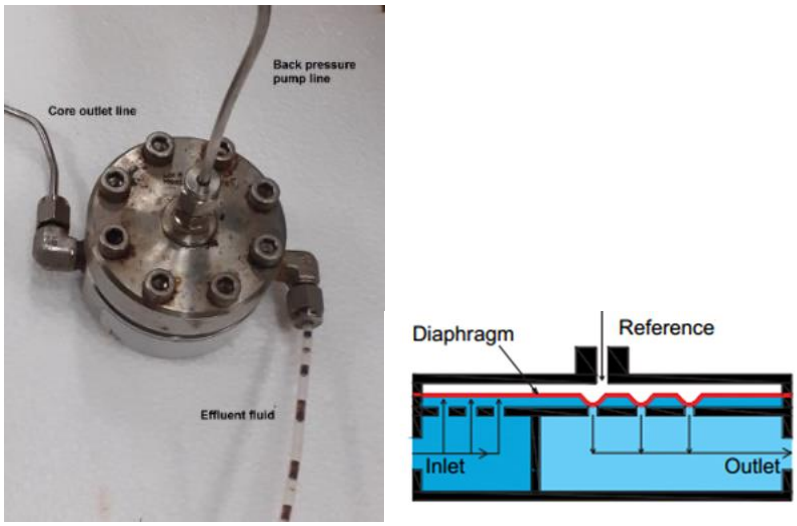

(a) **(b)**

Figure 6.8: (a) Backpressure regulator used (b) Mechanism of the backpressure regulator (Abhishek 2014)

6.2.5 Pressure Transducers

As shown in Figure 6.9, two pressure transducers with a range of 0 to 5,000 psi are connected at the core inlet and outlet from one side and attached to the DI-1100 USB Data Acquisition starter kit channels on the other side.

Figure 6.9: Pressure transducers used

6.2.6 Data Acquisition System

Pressure responses for each core flooding with water, oil, and acid are collected using DI-1100 USB Data Acquisition starter kit (Figure 6.10) with Windaq software. It can feature four differential analog input channels, 12-bit measurement resolution, and a full-scale range of ±10V. Figure 6.11 shows an example as a screenshot of the Windaq software after recording pressure while acid injection.

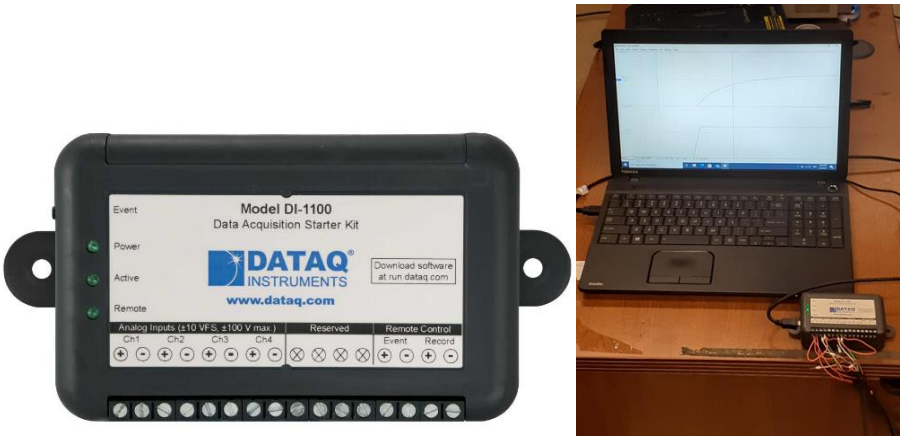

Figure 6.10: Data acquisition system used to record pressure responses

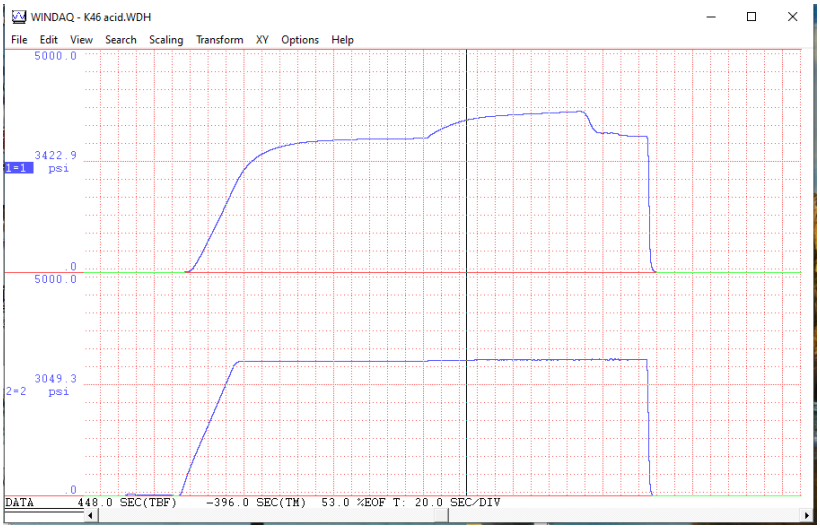

Figure 6.11: An example of pressure responses while injecting acid

6.3 Experimental Procedure

After the cores were grouped into the specific experimental condition, the initial saturation was established. All cores were initially water saturated using a vacuum system. The water saturation obtained through this process was between 93 and 99%. Those with a water-saturated experimental condition were then subjected to water injection from the outlet direction to establish the appropriate backpressure value of 1,100 or 3,000 psi for the experiment. Then acid was injected at the constant assigned rate from the inlet of the core. Cores with an oil-saturation experimental condition were subjected to water injection after vacuum saturation, followed by oil injection to establish an initial oil saturation and then were left to age for approximately 3 weeks. Effluent fluids resulted from oil injection in some cores are showing in Figure 6.12. An example of pressure responses to water and oil injection is documented in Appendix B. The cores were then subjected to oil injection from the core's outlet to establish the backpressure condition of 1,100 or 3,000 psi before acid was injected at a constant rate at the inlet side. The saturation data for water and oil are summarized in Table 6.4. and Table 6.5, respectively. Cores are carefully saturated with water and/or injected with oil with high consistency, as shown in Figure 6.13.

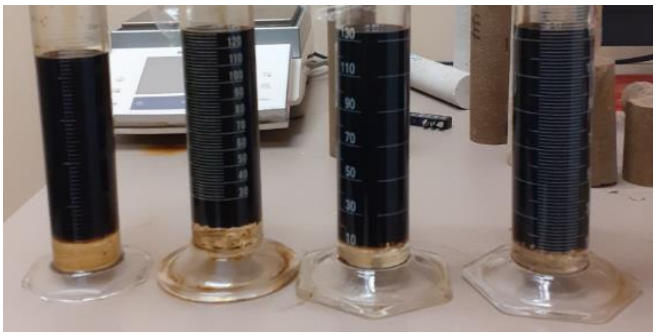

Figure 6.12: Effluent fluids resulted from cores' oil injection

Table 6.4: Water/oil saturation data

Group #	Core #	Por. %	Perm. mD	Dry weight g	Matrix density gm/cc	Weight after water saturation and injection g	Water saturation After water injection %	Weight after oil injection g	Water saturation after oil injection %
Group A	26	15.39	27.7	394.38	2.673	420.38	96.85	NA	NA
	30	16.79	33.8	387.50	2.696	414.60	93.42	NA	NA
	7	15.83	29.0	419.20	2.693	419.20	95.84	NA	NA
	29	16.75	31.7	415.70	2.681	415.70	93.46	NA	NA
Group B	9	15.34	34.4	394.70	2.680	420.38	96.21	418.24	30.55
	17	16.27	34.4	390.91	2.691	417.08	92.72	414.79	27.07
	6	15.04	36.4	394.96	2.678	420.04	96.03	417.69	21.91
	8	14.76	31.5	396.07	2.671	421.59	99.41	419.17	20.97
Group C	16	15.65	57.5	392.39	2.681	417.97	94.15	416.25	43.9
	27	15.39	55.5	393.05	2.660	418.90	96.42	417.79	64.0
Group D	11	14.84	57.0	396.16	2.667	420.62	94.26	419	44.8
	2	14.79	55.0	396.17	2.665	420.82	95.55	419.25	46.92
	1	14.59	60.7	396.9	2.670	420.84	94.27	419.27	45.34
	4	15.30	59.9	394.17	2.668	419.61	95.33	418.39	60.0
Group E	23	15.84	49.7	391.46	2.679	417.9	96.13	NA	NA
	25	15.32	48.4	394.45	2.674	419.81	95.21	NA	NA
Group F	44	16.62	219.6	392.95	2.700	420.57	95.21	418.42	35.13
	45	17.24	224.0	384.59	2.702	412.75	94.98	411.2	54.13
	42	16.57	214.9	391.55	2.702	419.51	97.13	417.65	44.56

Table 6.5: Partial oil saturation data

Group #	Core #	Partial oil saturation %
Group B	9	65.66
	17	65.65
	6	74.11
	8	78.44
Group C	16	50.19
	27	32.21
Group D	11	49.46
	2	48.63
	1	48.92
	4	35.30
Group F	44	60.08
	45	40.85
	42	52.57

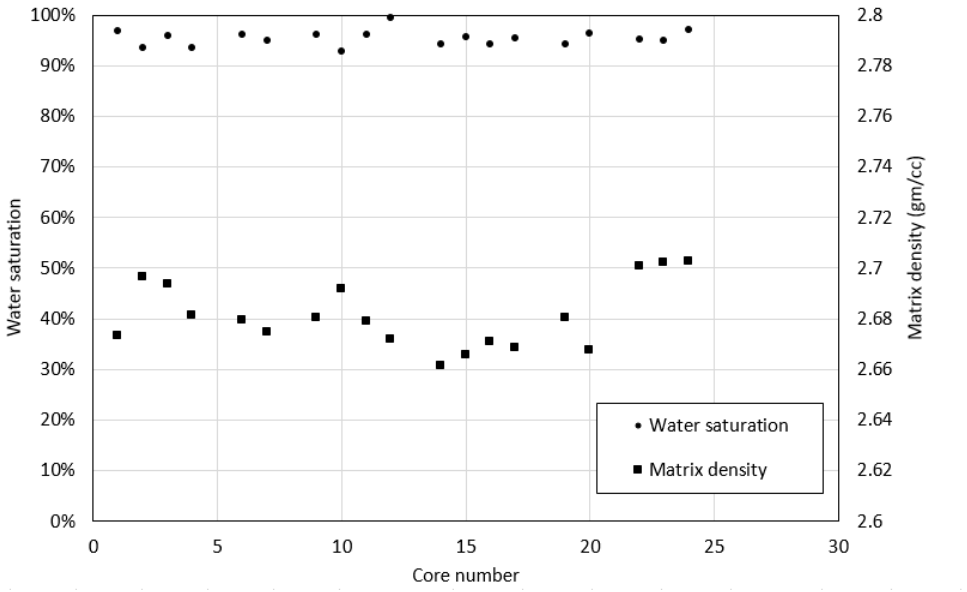

Figure 6.13: Water saturation and matrix density distribution of cores

The experiments were performed at room temperature, where the following steps are followed in each injection of cores (as shown in Figure 6.4):

- Fill the lines with fluids by running pump 1 for acid, pump 2 for oil and pump 3 for water. Close end valves (V-1, V-2, V-4, and V-5).
- Pack the core, apply desired confining pressure, and close the valve (V-6).
- Open valve V-5, apply desired backpressure using pump3.
- Open valves v-7, V-3, V-4, V-2, and V-1. Run oil pump 3 at constant backpressure (When pressure is reached, close valve V-3)
- When the pressure stabilizes, run acid pump 1 at the desired rate.
- While pressure is being recorded, Stop pump 1 when the pressure difference is zero.
- Close valves, unpack the core, dry it, and cast it.

In all cases, the acid injection was terminated when the pressure drop across the core became zero, indicating that the wormhole has penetrated the core. This Acid-Volume-to-

Breakthrough (AV_{bt}) is then converted to a dimensionless number noted as Pore-Volume-to-Breakthrough (PV_{bt}) using equation 6.1. Most of the results are reported as PV_{bt} as a function of acid-injection rate. The following flow diagram (Figure 6.14) summarizes the experiment procedure.

$$(PV_{bt}) = \frac{Acid-Volume-to-Breakthrough(AV_{bt}),\ CC}{Core\ pore\ volume,\ CC} \qquad (6.1)$$

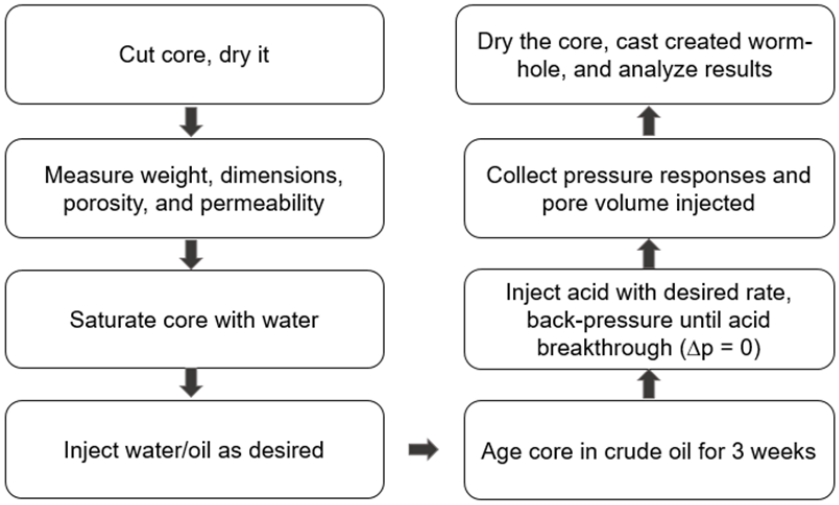

Figure 6.14: Experiments flow diagram

The choice to eliminate the temperature as a factor in this study was made to reduce the complexity of the experimental design and be able to adequately assess the impact of each of the studied parameters. The literature seems to be consistent in that the effect of temperature in water-saturated cores results in higher rates and volumes of acid needed, leading to the industry practice of injecting acid at the highest rate possible. However, the effect of temperature on acidizing in oil-saturated cores has not been consistently documented and will require further study.

6.4 Results and Discussions

In this section, we analyze and discuss results from the experimental work to see how the three factors—saturation, pressure, and permeability—affect the efficiency of the acidizing process.

6.4.1 Effect of Oil Saturation

The first group of cores, group A, which includes cores 26, 30, 7, and 29 with a low permeability of 27.8 to 33.8 mD, were saturated with water, and then acid was injected at four different rates using a backpressure of 3,000 psi. The relevant data is shared in Table 6.6. The plot of PV_{bt} vs. injection rate is shown in Figure 6.15. The results show that the optimum injection rate to propagate an efficient wormhole through the core's length with the minimum amount of acid is approximately 4 cc/min, with a PV_{bt} of roughly 0.7.

Table 6.6: Acid injection parameters for group A: water-saturated cores; 3,000-psi backpressure

Core	Perm., mD	Inj. rate, cm^3/min	AV_{bt}, cm^3	PV, cm^3	PV_{bt}
Core 26	27.8	1	32.00	26.85	1.19
Core 30	33.8	2.5	22.33	29.00	0.77
Core 7	29.0	5	19.66	27.45	0.72
Core 29	31.7	10	27.80	29.17	0.95

Table 6.7: Acid injection parameters for group B: oil-saturated cores; 3,000-psi backpressure

Core	Perm., mD	Inj. rate, cm^3/min	AV_{bt}, cm^3	PV, cm^3	PV_{bt}
Core 9	34.4	0.1	16.50	26.69	0.62
Core 17	34.2	0.5	13.21	28.22	0.47
Core 6	36.4	1	14.00	26.12	0.54
Core 8	31.5	5	19.00	25.67	0.74

The second group of cores, group B, which includes cores 9, 17, 6, and 8 with a low permeability of 31.0 to 36.0 mD (Table 6.7), were subjected to oil injection and aging. The value of water saturation at the end of oil injection was measured to be between 20 and 30%, with a

corresponding oil relative permeability of 0.15 to 0.18. Note that the gas permeability was used as the reference in calculating the relative permeability because the water saturation achieved after vacuum-saturating the cores was not at 100%. Thus, water permeability noted during water injection does not represent the rock's absolute permeability (it varied between 50% and 95% of the gas-measured permeability). The water permeability of cores has been correlated in the literature to air-measured permeability (Swanson 1981); however, for the purpose of consistency in this study, the absolute permeability measured using helium was elected as the baseline for absolute permeability. Acid was injected into the cores at four different rates at the same condition of backpressure as group A at 3,000 psi. The plot of the data, shared in Figure 6.15, shows a shift in the curve as compared to group A. The acid optimum injection rate decreased to approximately 0.5 cm^3/min, and the acid PV_{bt} also decreased to 0.47. This result is consistent with the literature findings (Shukla et al. 2006; Kumar et al. 2018), in which the presence of oil gave an advantage of reducing the volume of acid required to propagate a wormhole as well as reducing the acid-injection rate required for efficient wormhole propagation as shown in Figures 6.16 and 6.17. In other words, the presence of oil, which introduced multiphase flow, resulted in acid progressing more efficiently through the core. This can be achieved by reducing the relative permeability to the acid in the matrix surrounding the wormhole, where the presence of an immiscible phase (oil) can reduce the fluid loss from the main wormhole, thus allowing for deeper penetration and less leak-off. To give more confidence in this concluded observation, error analysis is performed in section 6.5 in this chapter. As the error bars show in Figure 6.15, an experimental error for group A was calculated as 3.33 %, while the error for group B was 3.28 %. Thus, with the error range mentioned, even when the experimental error happens, the conclusion about the shift between water-saturated and oil-saturated cores does not change.

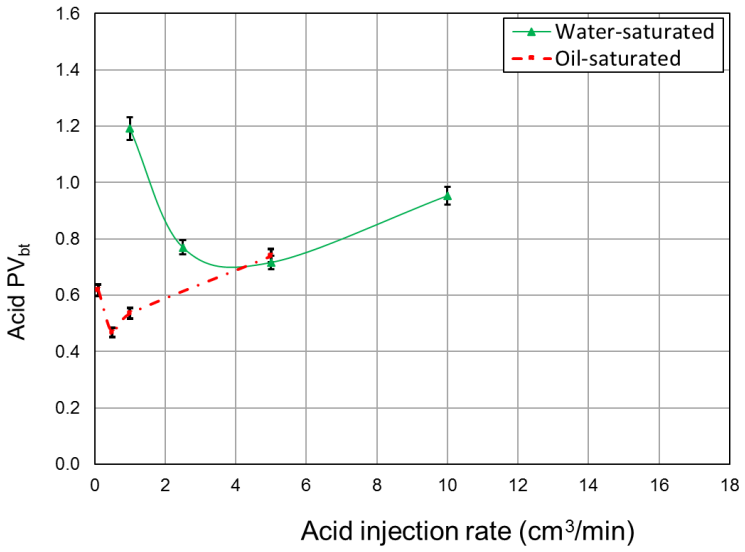

Figure 6.15: Effect of initial saturation on acid injection data for low permeability groups A and B at a 3,000 psi-backpressure

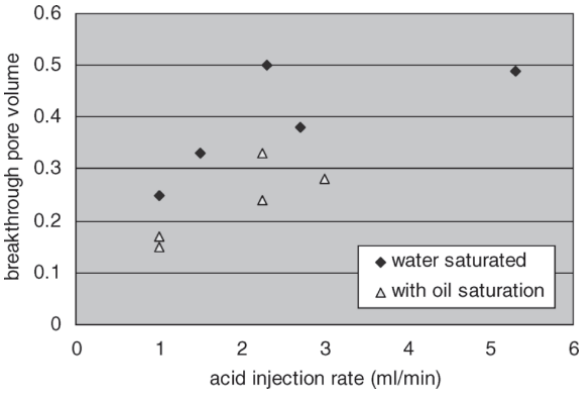

Figure 6.16: Comparison between acid volume needed to breakthrough for water-saturated and oil-saturated cases (Shukla et al. 2006)

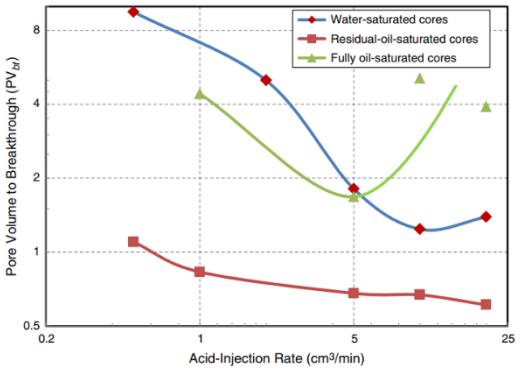

Figure 6.17: Comparison between water-saturated, oil-saturated, and residual-oil-saturated cores (Kumar et al.2012)

To compare our results to previously published data, Figure 6.18 shows data for water-saturated cores from literature by Zakaria et al. 2015 and Dong et al. 2014. Their optimum acid volume and rate are different from ours because the conditions are not precisely the same, but the trend of curves and optimum conditions are comparative. We also added core 25 (Table. 6.10), a water-saturated core with a permeability of 48.4 mD, injected at backpressure of 1,100 psi to compare it with the published data for a similar condition of backpressure. Note that 48.4 mD is

the nitrogen permeability of the core. The water permeability for core 25 measured under similar conditions to Zakaria et al. (2015) and Dong et al. (2014) is 37 mD. The value we measured for PV_{bt} for core 25 lies between the Zakaria et al. (2015) curve for 60-mD cores and the Dong et al. (2014) curve of 6-mD. This reveals the consistency between our results for water-saturated cores and those published in the literature under similar conditions of temperature, pressure, and core dimensions. The trend of change in PV_{bt} in Fig. 6.18 shows that the amount of acid needed increases with the increase in core permeability for water-saturated cores. This is in-line with the literature findings and common industry practice but is the opposite trend from what our work shows for the first time in oil-saturated cores.

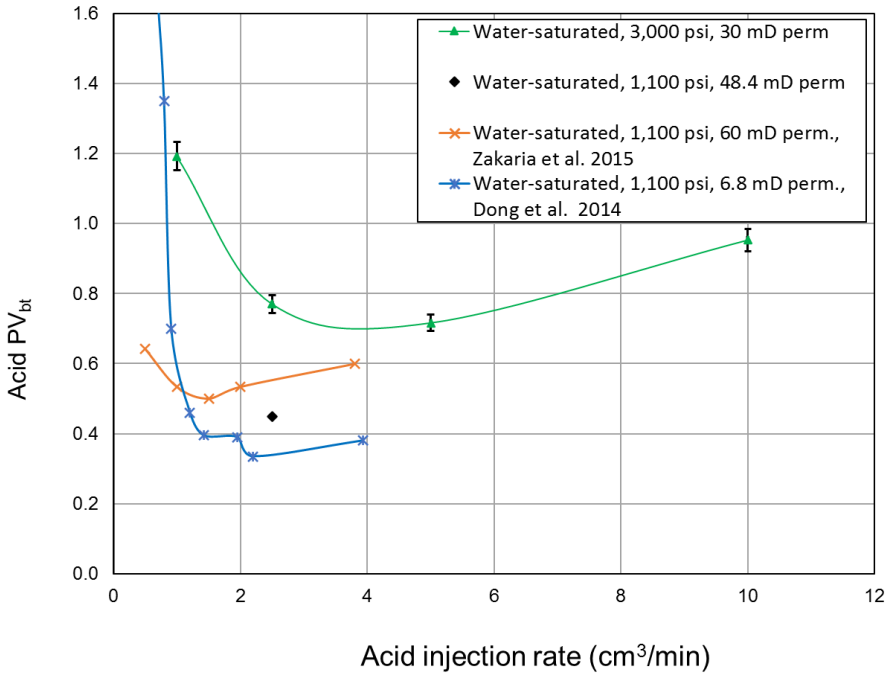

Figure 6.18: Comparison of our results to previous work

Our results are further confirmed by visually examining the entry and exit locations of the wormhole in the cores that exhibited the minimum PV_{bt} in each of the groups. The images, shared in Figures 6.19a and 6.19c for the inlet of the cores and Figures 6.19b and 6.19d for the outlet of

the cores, show that the wormhole in the water-saturated core had a larger diameter and a clearly visible exit location, indicating a larger amount of rock dissolution (requiring a larger volume of acid) even at the optimum injection conditions. This observation was further examined through the use of wood's metal casting (described in detail in Appendix D) for cores 26 (water saturated) and 6 (74% oil saturation) that were subjected to acid injection at 1 cm^3/min. The results, shown in Figures 6.20a and 6.20b, reveal a very different wormhole geometry. The water-saturated core has a thicker wormhole and evidence of acid leak-off at the sides of the wormhole, while the core that has an oil saturation of approximately 74% shows a thinner wormhole that branches at times to create parallel wormholes rather than showing a leak-off of acid. These differences in wormhole diameter and branches explain the difference in the acid volume needed to propagate the wormhole. The wormhole diameter of the water-saturated core is roughly double the partial oil-saturated one; thus, the volume of required acid is reduced to half for the partial oil-saturated core. This observation of wormhole branching was visible in all oil-saturated cores that were selected for casting, as shared in the remainder of this study. Note that the metal casting for core 6 did not propagate to the second half of the core, and thus only the first half of the wormhole is observed in the figure.

Core 17: oil-sat, 3000 psi: front (a) and back (b) **Core 7: water-sat, 3000 psi: front (c) and back (d)**

Figure 6.19: Images of the inlet and outlet faces of the cores subjected to the optimum injection rate for the oil-saturated and water-saturated cases. The wormhole in the water-saturated core is clearly more visible with a larger diameter, reflecting the need to inject a larger acid volume into water-saturated cores compared to oil-saturated cores.

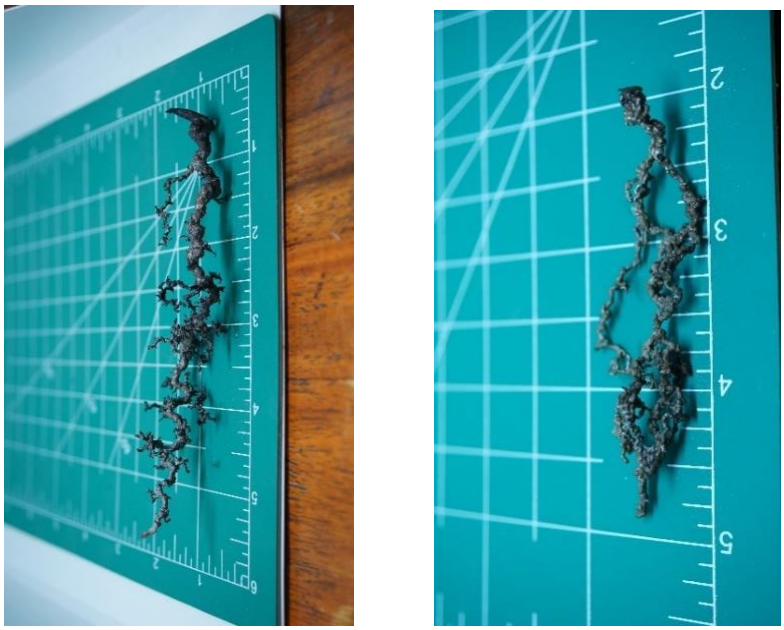

(a) Core 26: water-saturated, 3,000 psi, 1.19 PV_{bt} **(b) Core 6: 70% oil saturation, 3,000 psi, 0.57 PV_{bt}**

Figure 6.20: Images of the casted wormholes in core 26 (left) and in core 6 (right) subjected to acid injection at 1 cc/min. Acid leak-off is visible in the water-saturated core compared to wormhole branching in the oil-saturated core.

These results are consistent with previous research results reported by Shukla et al. (2006), illustrated in Figure 6.21. The wormhole created in the presence of immiscible fluid (oil or gas) is less branched and thinner in diameter.

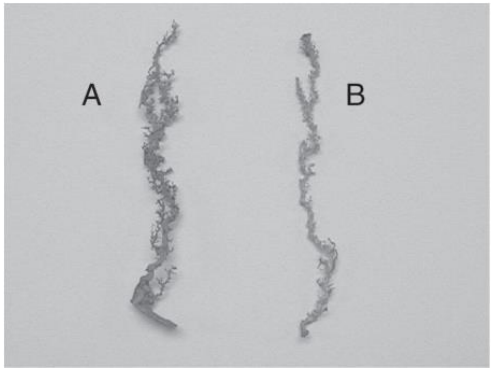

Figure 6.21: Difference in created wormhole between water-saturated case (A) and when immiscible fluid is present (B) (Shukla et al. 2006)

6.4.2 Effect of backpressure and permeability

In this section, the impact of backpressure on wormhole propagation is documented. The results reveal that the effect of backpressure varies with rock permeability, and accordingly, the effect of both parameters is shared in the same section. This includes the results from Group B (partial oil saturation, low permeability of 30 mD, 3,000 psi) shared in the previous section, along with Group C (partial oil saturation, low permeability of 55 mD, 3,000 psi), Group D (partial oil saturation, low permeability of 55 mD, 1,100 psi), Group E (fully water saturated, low permeability of 55 mD, 3,000/1,100 psi), Group F (partial oil saturation, high permeability of 220 mD, 3,000/1,100 psi), and Group G (full oil saturated, very low permeability of 2 to 4 mD, 1,200 psi). The data for Groups C, D, E, F, and G are shared in Tables 6.8 – 6.12, respectively.

Table 6.8: Acid injection parameters for group C: oil-saturated cores; 3,000-psi backpressure.

Core	Perm., mD	Inj. rate, cm^3/min	AV_{bt}, cm^3	PV, cm^3	PV_{bt}
Core 16	57.5	0.5	11.74	27.17	0.43
Core 27	55.5	1	15.28	26.80	0.57

Table 6.9: Acid injection parameters for group D: oil-saturated cores; 1,100-psi backpressure.

Core	Perm., mD	Inj. rate, cm^3/min	AV_{bt}, cm^3	PV, cm^3	PV_{bt}
Core 11	57.0	0.5	7.53	25.95	0.29
Core 2	55.0	1	6.97	25.80	0.27
Core 1	60.7	5	13.72	25.40	0.54
Core 4	59.9	15	23.49	26.69	0.88

Table 6.10: Acid injection parameters for group E: water-saturated cores; *at 3,000-psi and ^at 1,100-psi backpressure

Core	Perm., mD	Inj. rate, cm^3/min	AV_{bt}, cm^3	PV, cm^3	PV_{bt}
Core 23*	49.7	2.5	20.35	27.50	0.74
Core 25^	48.4	2.5	12.02	26.70	0.45

Table 6.11: Acid injection parameters for group F: oil-saturated cores; *at 3,000-psi and ^at 1,100-psi backpressure

Core	Perm., mD	Inj. rate, cm^3/min	AV_{bt}, cm^3	PV, cm^3	PV_{bt}
Core 44*	220.0	0.1	10.73	29.01	0.37
Core 45*	224.0	1	7.12	29.65	0.24
Core 42^	215.0	1	8.35	28.78	0.29

Table 6.12: Acid injection parameters for group G: oil-saturated cores; 1,200-psi backpressure

Core	Perm., mD	Inj. rate, cm^3/min	AV_{bt}, cm^3	PV, cm^3	PV_{bt}
Core 4-b	2-4	3.5	7.48	26.70	0.28
Core 7-b	2-4	3.5	6.01	28.61	0.21

We start by analyzing the impact of backpressure on acidizing in low-permeability cores, which includes comparing the results from Group B (oil-saturated, 3,000-psi backpressure) and Group D (oil-saturated, 1,100-psi backpressure). The results are shared in Figure 6.22. It shows that acidizing in these cores is more efficient in the low-pressure case. Almost half the value of the acid volume is needed at the optimum injection rate, represented as a lower value of PV_{bt}. The error bars indicate that error for group D is 3.32 %, compared to 3.28 % for group B. This minimizes the uncertainty of our conclusion. Low pressure introduces a new phase inside the pore space; that is, CO_2, which is immiscible in the spent acid at this low pressure. These results are in line with the earlier observation that the presence of an additional phase reduces the pore space available for the acid leading to more efficient forward propagation of the wormhole. Another factor that could also contribute to these observations is that the evolution of CO_2 from the aqueous phase can make some of it available for dissolution in the oil, allowing for oil swelling and reducing oil viscosity (Qiu et al. 2014; Cheng et al. 2016). This evolution generates lower resistance to flow because the aqueous phase has to displace the oil to propagate.

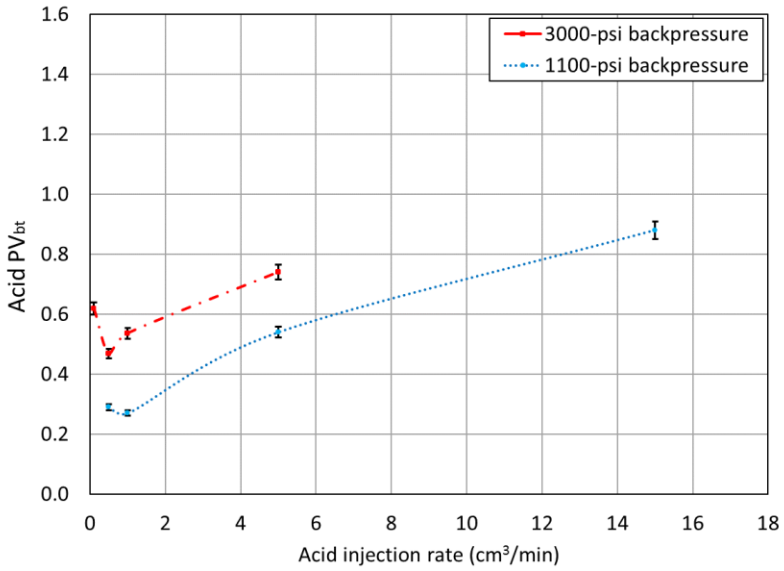

Figure 6.22: Effect of pressure on acid injection data for partially oil-saturated low-permeability cores; groups B and D

To confirm that the small difference in permeability (30 mD for Group B vs. 55 mD for Group D) did not influence these results, we repeated the 3000-psi injection (Group B experimental condition) for Group C that has a permeability of 55 mD (similar to Group D). The results, shown in Figure 6.23, reveal that this small difference in permeability does not affect the results. The error value of group C is 3.34 % which keeps the values of PV_{bt} still close to group B values. The differences in acid performance observed in Figure 6.22 are solely due to the difference in the imposed backpressure.

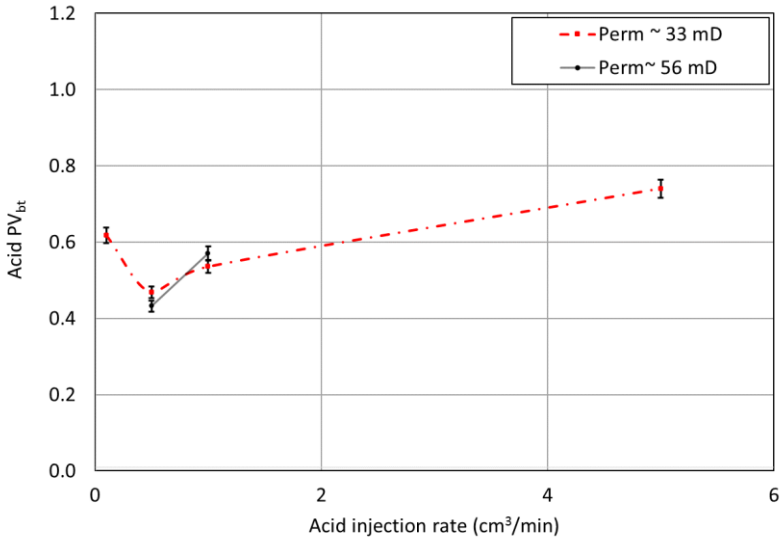

Figure 6.23: Acid injection data for partially oil-saturated cores groups B and C at a 3000-psi backpressure

To further diagnose the impact of pressure on wormhole propagation in these low-permeability cores, metal casting was created for the wormholes of two cores, core 2 from Group D (acidized at 1,100 psi, with 0.27 PV_{bt}) and core 27 from Group C (acidized at 3,000 psi, with 0.57 PV_{bt}), both subjected to acid injection at 1 cm^3/min. The results are shared in Figures 6.24a and 6.24b. The metal casting for core 27 also propagated just halfway through the core. The results show that no leak-off is observed in both cores, and the wormhole branches into parallel wormholes instead. Focusing on these branches, one would observe that those created at low pressure (with the additional CO_2 phase), except for one main entry branch observed in Figure 6.20a, are thinner wormholes compared to those created at high pressure. These thinner branches at low pressure reduce the volume of acid needed by almost half the volume. In addition to phase competition impacting the propagation of the acid, we theorize that the evolution of CO_2 out of solution at low pressure could be further contributing to plugging the sides of the wormhole by causing the acid and the oil to mix, limiting the ability of the wormhole to widen further.

The observations on the impact of pressure in high-permeability cores were different. Two oil-saturated cores with a permeability of around 220 mD were subjected to acid injection at 1 cm^3/min (Group F), with core 42 acidized at 1,100 psi and core 45 acidized at 3000 psi. The value of acid PV_{bt} was 0.29 for low-pressure injection and 0.24 for high-pressure injection. This reveals that the presence of CO_2 as a separate phase in this high-permeability core contributed to making wormhole propagation slightly less efficient in these high-permeability cores. The casting of these wormholes reveals a similar pattern of branching where a multitude of much thinner wormholes is observed towards the end of the core, as shown in Figures 6.25a and 6.25b. The very similarity of both wormholes in diameter and branches results in the almost same volume of acid needed.

(a) Core 2: oil-saturated, 1,100 psi, 0.27 PV_{bt} **(b) Core 27: oil-saturation, 3,000 psi, 0.57 PV_{bt}**

Figure 6.24: Images of the casted wormholes in the low-permeability cores, core 2 (left) and in core 27 (right) subjected to acid injection at 1 cm^3/min. Wormhole branching is visible in both cores, however, the one at low pressure has visibly thinner branches reflecting the increased efficiency of acid forward propagation with limited further dissolution that widens the wormhole

(a) Core 42: oil-saturated, 1,100 psi, 0.29 PV_{bt} **(b) Core 45: oil-saturation, 3,000 psi, 0.24 PV_{bt}**

Figure 6.25: Images of the casted wormholes in the high-permeability cores, core 42 (left) and in core 45 (right) subjected to acid injection at 1 cm^3/min. Wormhole branching is visible in both cores, and pressure does not seem to contribute to significant variation in wormhole propagation

The plot of PV_{bt} as a function of injection rate, shared in Figure 6.26, shows that acidizing performance in these high-permeability cores at 3,000 psi is more efficient than that in the low-permeability cores at the same pressure, and is almost identical to the efficiency in the low-permeability cores at 1,100 psi. This result is very different from the results reported in the literature of acidizing in water-saturated cores. It has been established that higher-permeability cores require larger volumes of acid injected at higher rates to propagate wormholes (Bazin 2001; Etten et al. 2015; Dubetz et al. 2016), as shown in Figure 6.27. Our results show that the optimum rates do not vary much by permeability or pressure, but the volume of acid needed in oil-saturated, high-permeability cores at high pressure ranges between 55 and 66% of that required in oil-saturated, low-permeability cores. Error-values for Group F are 3.34 % which would not alter the data points much and would not change our conclusion.

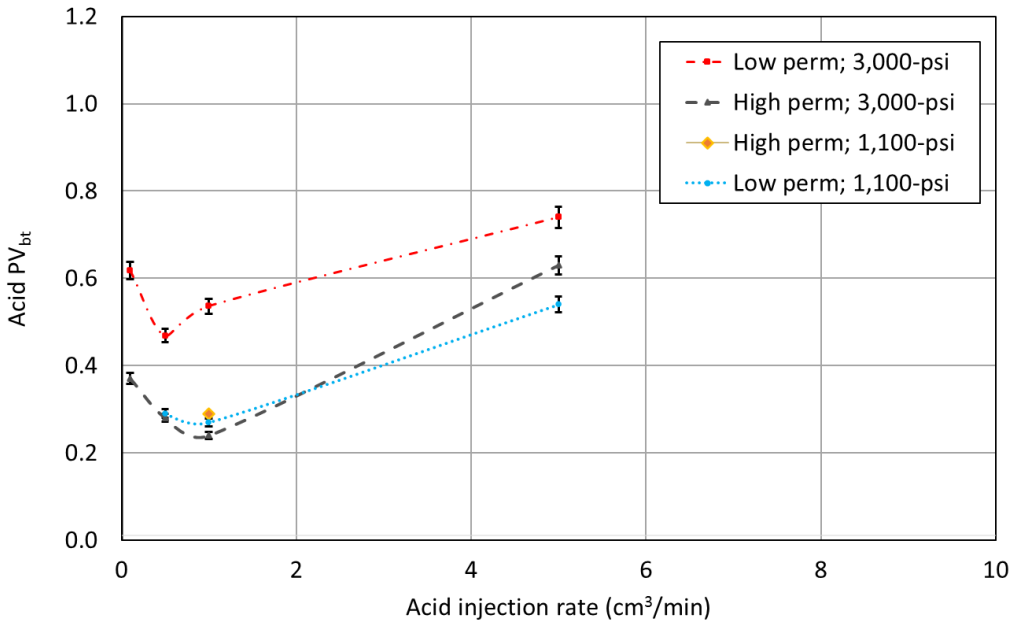

Figure 6.26: Acid injection data for oil-saturated cores, Groups B, D, and F

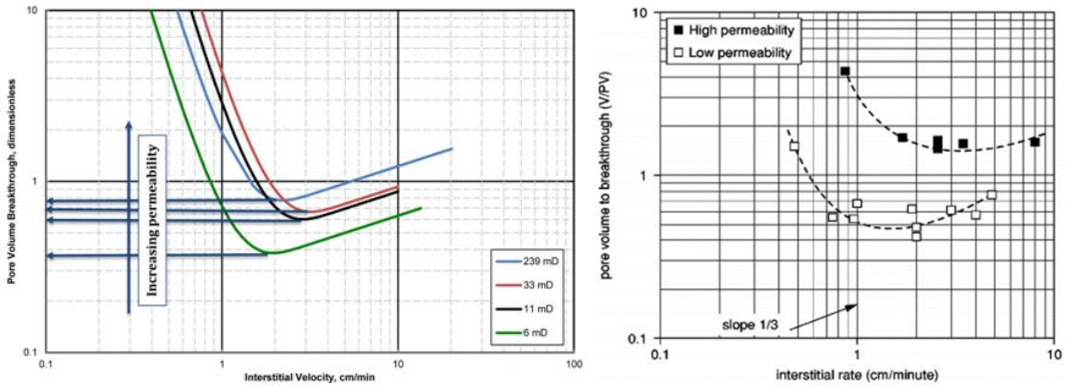

Figure 6.27: Effect of permeability on acid optimum volume and rate, left (Etten et al. 2015), and right (Bazin 2001)

These results are further clarified in Figure 6.28, showing the effect of pressure, permeability, and saturation condition on the value of PV_{bt}. The results reveal that at high pressure, higher permeability cores require a lower volume of acid injection, while at low pressure, the volume of acid needed does not seem to vary significantly with permeability value. On the other hand, within the same low-permeability range, both water- and oil-saturated cores (Groups E, C,

and D) require less acid volume at low pressure, while this is not the case for oil-saturated high-permeability cores (Group F). The water-saturated core that was subjected to lower backpressure had a PV_{bt} value that is 61% the PV_{bt} value at the higher backpressure, while the oil-saturated core subjected to lower backpressure had a PV_{bt} value that is 47% the PV_{bt} value at the higher backpressure. This difference in PV_{bt} is likely because less CO_2 is generated in oil-saturated cores (compared to water-saturated cores) because of the lower volume of rock dissolved, allowing the impact of low-pressure to be more pronounced in water-saturated cores.

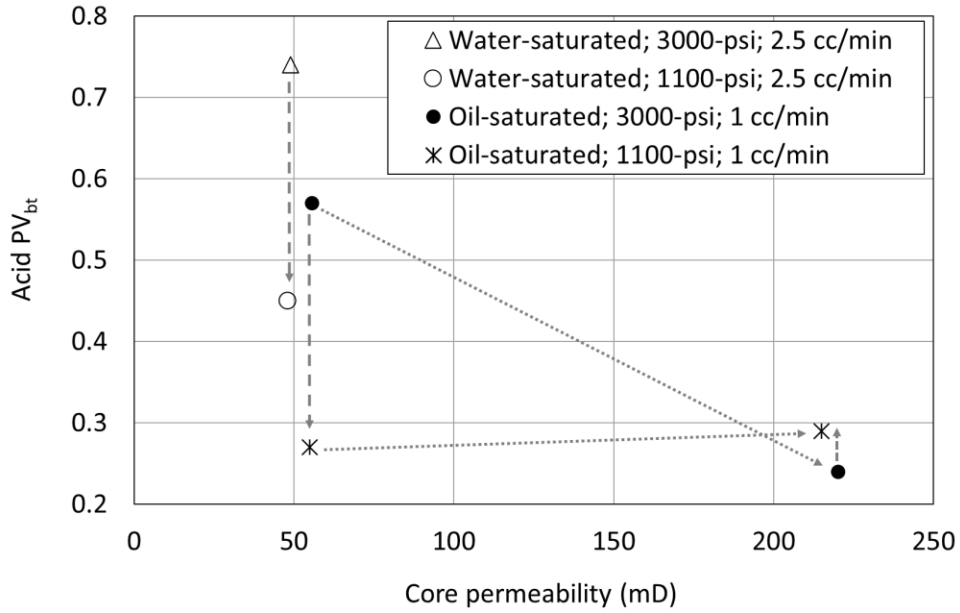

Figure 6.28: Effect of pressure, permeability, and saturation on acid PV_{bt}. Vertical arrows indicate impact of change in backpressure, and inclined arrows indicate impact of permeability within the same pressure condition

The last experimental condition, Group G in Table 6.1 and 6.10, concerned two cores with permeability in the range of 2-4 mD and were fully saturated with oil without prior water saturation. Core 4-b was aged for only 2 days while core 7-b was aged for 19 days, then both were subjected to acid injection at a rate of 3.5 cm^3/min with a backpressure of 1,200 psi (Scarborough 2016). Metal casting was performed to assess the wormhole geometry, and the resulting shape of

the wormhole is shown in Figures 6.29a for core 4-b and 6.29b for core 7-b. There is neither branching nor leak-off visible in these cases, except for minor branching towards the last third of core 4-b. This reveals a very different mechanism of acid propagation. Clearly, the absence of water limits acid access to the matrix in these tight cores and allows acid to propagate more efficiently, with PV_{bt} values of 0.28 for core 4-b and 0.21 for core 7-b. This results in a much lower volume of acid needed. The result also reveals that longer aging (core 7-b) allowed oil to form a more substantial barrier to acid, further lowering the PV_{bt} value. The presence of an initial water saturation for cores in Groups B, C, D, and F resulted in blocking leak-off of acid but allowing acid to propagate in parallel wormholes. On the other hand, the absence of oil invites inefficient acid propagation with thicker wormholes and highly branched leak-off.

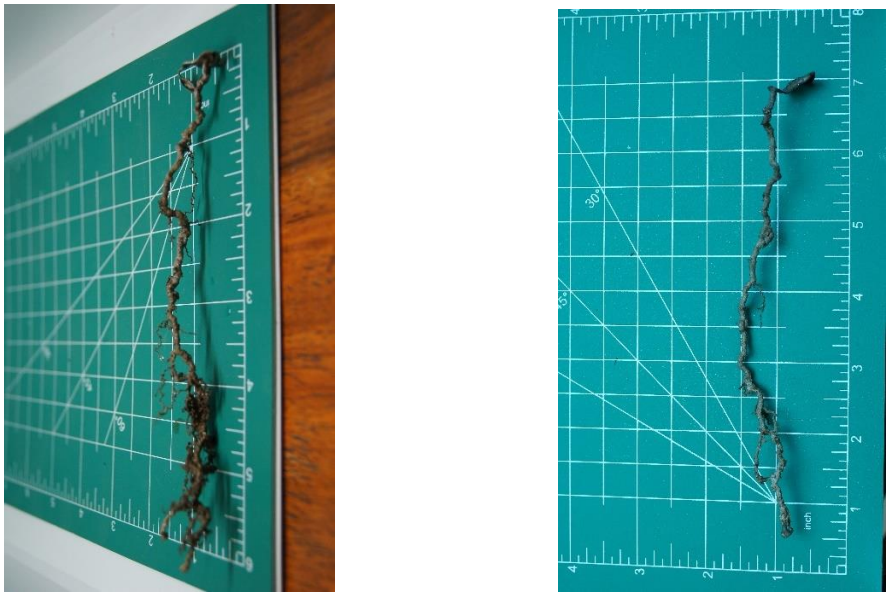

(a) Core 4-b, 1,100 psi, aged 2 days, 0.28 PV_{bt} **(b) Core 7-b, 1,100 psi, aged 19 days, 0.21 PV_{bt}**

Figure 6.29: Images of the casted wormholes in the tight cores, 2-4 mD, fully saturated with oil and aged for several weeks before acid injection. No significant branching or leak-off behavior is observed

Additional diagnostic plots are shared in Figures 6.30 and 6.31 for the pressure drop across the cores during acid injection for Group B and Group D. The results for injection at high pressure (Figure 6.30) show that the optimum acid injection rate, resulting in the minimum volume of acid injection, required a significant build-up of pressure. On the other hand, the results for injection at low pressure (Figure 6.31) show that pressure build-up at the optimum injection rate was very low. This reveals a significant difference in the rate optimization process and very different mechanisms at play within the cores at the different pressure conditions. Investigating that is outside the scope of this paper and is deferred for a future study.

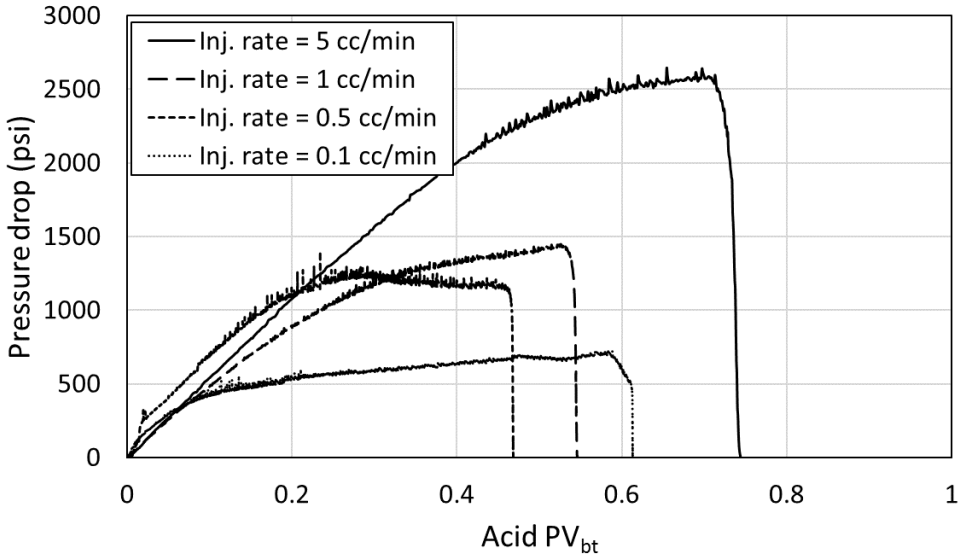

Figure 6.30: Pressure drop across the cores from Group B, oil-saturated, low-permeability cores subjected to acid injection with a backpressure of 3,000 psi

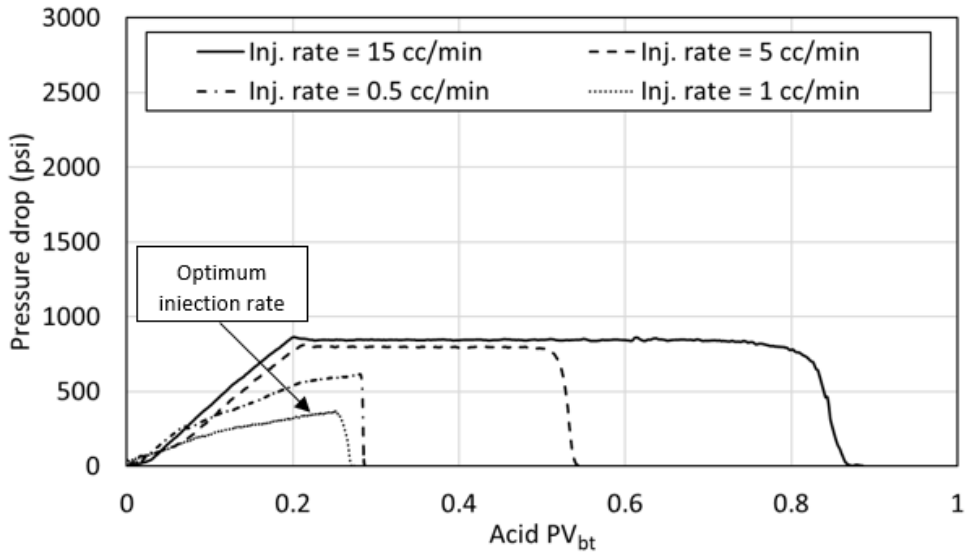

Figure 6.31: Pressure drop across the cores from Group D, oil-saturated, high-permeability cores subjected to acid injection with a backpressure of 1,100 psi

One observation in the diagnostic plots is that pressure build-up is consistently higher for experiments performed at high pressure. This observation is apparent in Figures 6.32 and 6.33 for the rates of 1 and 0.5 cm^3/min, respectively. The experimental pressure condition has a more significant effect on pressure build-up in low-permeability cores than in high-permeability cores; while for high-permeability cores, the pressure drop at 3,000 psi is only around 20% higher than the pressure drop at 1,100 psi, it is more than double in the low-permeability cores. Comparing across permeability in Figure 6.32, it is noticed that acid injection at high pressure results in pressure build-up that is 4 times higher in the low-permeability core than in the high-permeability core. On the other hand, acid injection at low pressure results in pressure build-up that is only 40% higher in the low-permeability core than in the high-permeability core. This reveals that the presence of oil in the core at low pressure minimizes the impact of permeability on acid propagation. This is understandable as other mechanisms of a multi-phase flow activated by CO_2 evolving out of solution start to dominate the flow. These results can have implications on

acidizing layered formations where the current practice results in high-permeability layers receiving a large proportion of the injected acid given the more efficient propagation of wormholes in these layers at high pressure. Designing acidizing jobs that allow for similar efficiency of acid propagation in low- and high-permeability layers through simply designing for additional multi-phase flow controls can be another simple method of acid diversion.

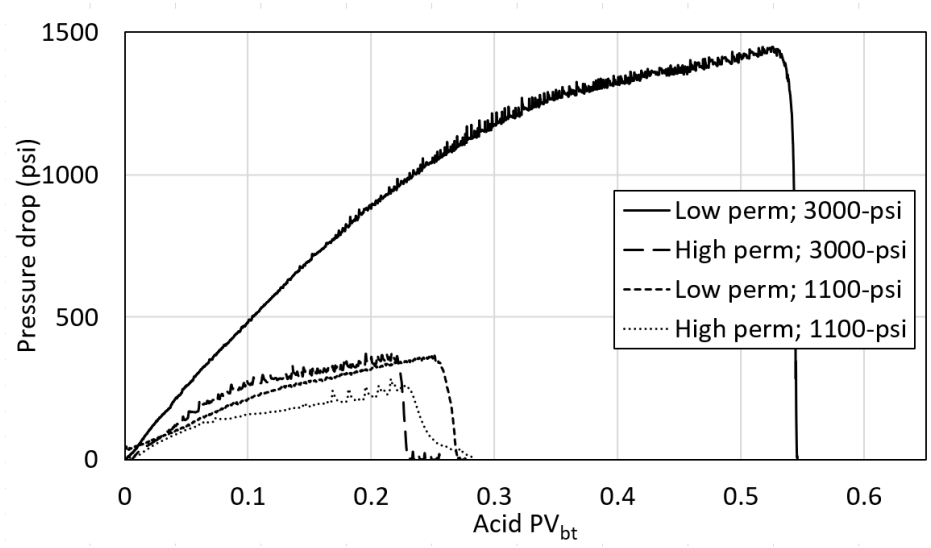

Figure 6.32: Pressure drop across oil-saturated cores during acid injection at 1 cm^3/min

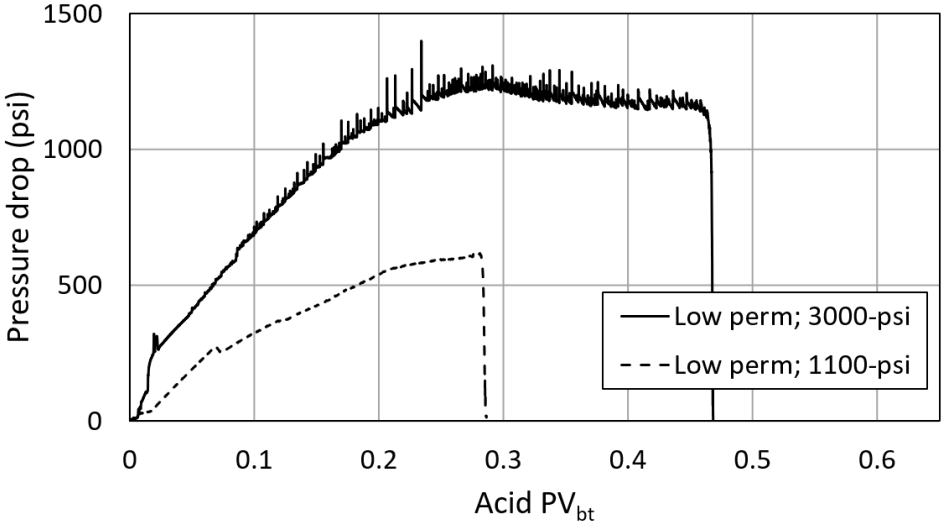

Figure 6.33: Pressure drop across oil-saturated cores during acid injection at 0.5 cm^3/min

6.4.3 Effect of Adding De-emulsifiers on Optimized Conditions

In this last experiment, we added a group of three Indiana Limestone cores (core 3, core 24, and core 43) presented in Table 6.13 and Figure 6.34. We applied the same procedure of measuring porosity, permeability, saturation, injecting water/oil, and aging. In addition, a de-emulsifier was added to HCl acid before injecting it into the cores. Our results from Chapter 4 confirm that acid-oil emulsions do form during matrix acidizing. The use of de-emulsifiers that limit the formation of emulsions, which is very common in the practice of matrix acidizing, lowers the efficiency of the acidizing process. When the backpressure was 1,100 psi, it takes more than double the volume of acid to propagate a wormhole in high-permeability (180-mD) core 43 when de-emulsifiers are used. It takes 25% more acid to propagate a wormhole in lower-permeability (49-mD) core 24 in the presence of de-emulsifiers. Similarly, at high backpressure of 3,000 psi, more volume of acid was required to breakthrough core 3 with de-emulsifier compared to exactly the same condition with the absence of de-emulsifier. Again, error bars show a slight range of certainties. These results reveal that the presence of acid-oil emulsions results in less acid-volume-to-breakthrough. However, casting reveals that wormholes created in the presence of de-emulsifier were much less in branching, as showing in Figure 6.35, which means less leak-off.

Table 6.13: Acid injection parameters for group H: oil-saturated cores; *at 1,100-psi and ^at 3,000-psi backpressure

Core	Perm., mD	Inj. rate, cm^3/min	AV_{bt}, cm^3	PV, cm^3	PV_{bt}
Core 3*	49.0	1	10.70	26.12	0.41
Core 24^	49.0	1	18.239	28.06	0.65
Core 43^	180.0	1	16.12	28.28	0.57

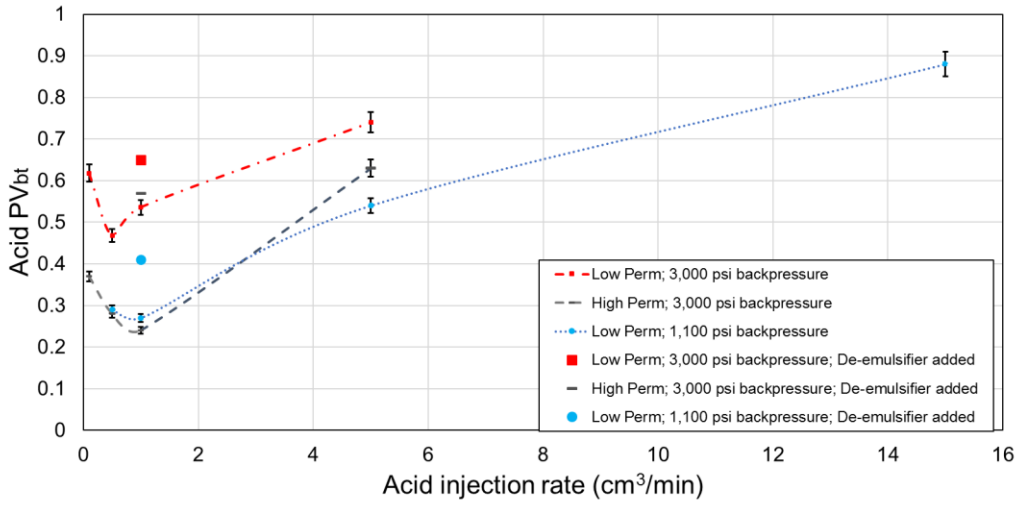

Figure 6.34: Acid injection data for oil-saturated cores, Group H

Figure 6.35: Image of casted wormhole of core 3

6.5 Error Analysis

Experimental work is always associated with measurements error. All data collected in these experiments are taken using an accurate data acquisition system with a minimum error range. However, for an experiment that includes multiple variables, there are always uncertainties in measurements. Combining these uncertainties from each measure to see how much error is

encountered is very important. Skoog et al. (2007) have derived a formula to calculate an error which is given by the standard deviation (σ_x) as showing in equation 6.2:

$$\frac{\sigma_x}{x} = \sqrt{\left(\frac{\sigma_a}{a}\right)^2 + \left(\frac{\sigma_b}{b}\right)^2 + \left(\frac{\sigma_c}{c}\right)^2} \qquad (6.2)$$

Where a, b, and c are measured data from the experiment while σ_x, σ_b, and σ_c are the standard deviations for each measured data. The final pore volume to breakthrough is calculated using equation 6.3. Using these two equations 6.2 and 6.3, the total error percentage with the assumed uncertainties values for each measurement for group A are shown in Table 6.13.

$$PV_{bt} = \frac{qt}{\emptyset\pi LD^2/4} \qquad (6.3)$$

Table 6.14: Measurement's error of group A

Property	Average value	Error	Error percentage, %
Time	14.0 min	0.05 min (3 sec)	0.36
Flow rate	1.0 cm^3/min	0.005 cm^3/min	0.5
Length	15.24 cm	0.025 cm	0.17
Diameter	3.81 cm	0.025 cm	0.67
Porosity	0.16	0.005	3.13
Pore volume to breakthrough	0.50	0.016	3.30

The error percentage for each group is presented in Table. 6.14. These percentages were used in computing the error bars that are presented throughout this document.

Table 6.15: Measurements error for all groups

Group	Error percentage, %
A	3.30
B	3.28
C	3.34
D	3.32
E	3.34
F	3.34
H	3.32

6.6 Assessing the Impact of Our Results on Field Applications Using Empirical Models

Using Pichler's empirical model, the radial wormhole penetration length is calculated. The resulting skin is then calculated using equation 6.4, assuming the wormhole passes the damaged zone area. To see how the productivity of a well would change, two cases of a large Kh and a small

Kh are assumed, and the productivity index is calculated using equation 6.5. The assumed inputs of cases parameters are showing in Table. 6.16. The laboratory data of the acid optimum injection rate and optimum pore volume to breakthrough for different injections conditions are listed in Table.6.17.

Table.6.16: Inputs values

Input	Value
Wellbore radius, r_w	0.325 ft
Porosity, φ	0.15
Volume of acid, V/l	10 cu. ft/ft
Oil viscosity, μ	26 cp
Oil formation volume factor, Bo	1.12 bbl/STB
Reservoir radius, r_e	750 ft
Kh (case 1)	100,000 md-ft
Kh (case 2)	2,000 md-ft

Table6.17: Experimental data for different injection conditions

Acid injection conditions	Pore volume to breakthrough, PV_{bt}	Optimum injection rate, q (cc/min)
Water saturated cores, 3000 psi backpressure	0.72	5
Oil saturated cores, 3000 psi backpressure	0.47	0.5
Oil saturated cores, 1100 psi backpressure	0.27	1
Oil saturated cores, 3000 psi backpressure, De-emulsifier used	0.65	1
Oil saturated cores, 1100 psi backpressure, De-emulsifier used	0.57	1

$$S = Ln\left(\frac{r_{wh}}{r_w}\right) \qquad (6.4)$$

$$J = \frac{Kh}{141.2B_o\mu Ln(\frac{r_e}{r_w} + S)} \qquad (6.5)$$

As shown in Figures 6.36 and 6.37, for the case of high kh of 10,0000 mD.ft, the wormhole propagation was at a maximum at the presence of oil with the condition of 1,100 psi backpressure, resulted in a skin factor of -3.3 and productivity index of 6.15 STB/day/psi. The increase in

productivity between the water-saturated and oil-saturated cases for the same backpressure of 3,000 psi is approximately 5.36 %. In the case of 1,100 psi backpressure, productivity is badly reduced by 9.18 %. The addition of De-emulsifiers to the acid results in 11% lower productivity compared to not adding De-emulsifiers in high-permeability formations. This loss goes down to 5% in low-permeability formations. This proves our conclusion of the advantage of the presence of oil in reducing fluid loss around the wormhole by creating an emulsion. A similar conclusion can be drawn for case 2, as shown in Figure 6.38.

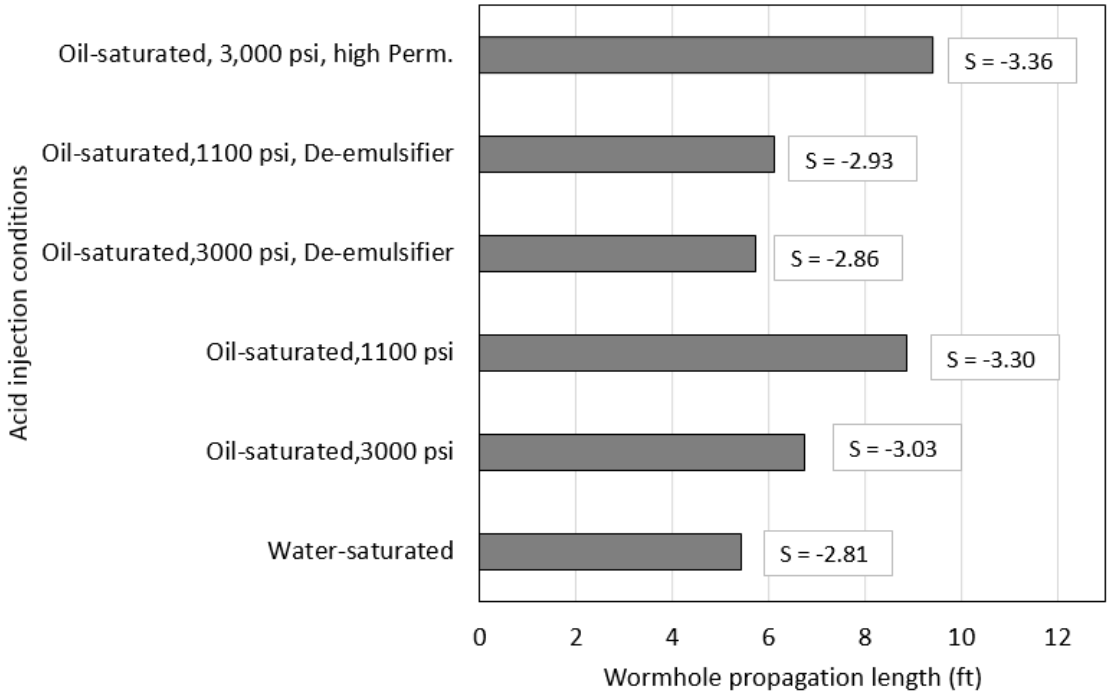

Figure 6.36: Wormhole propagation for different injection conditions

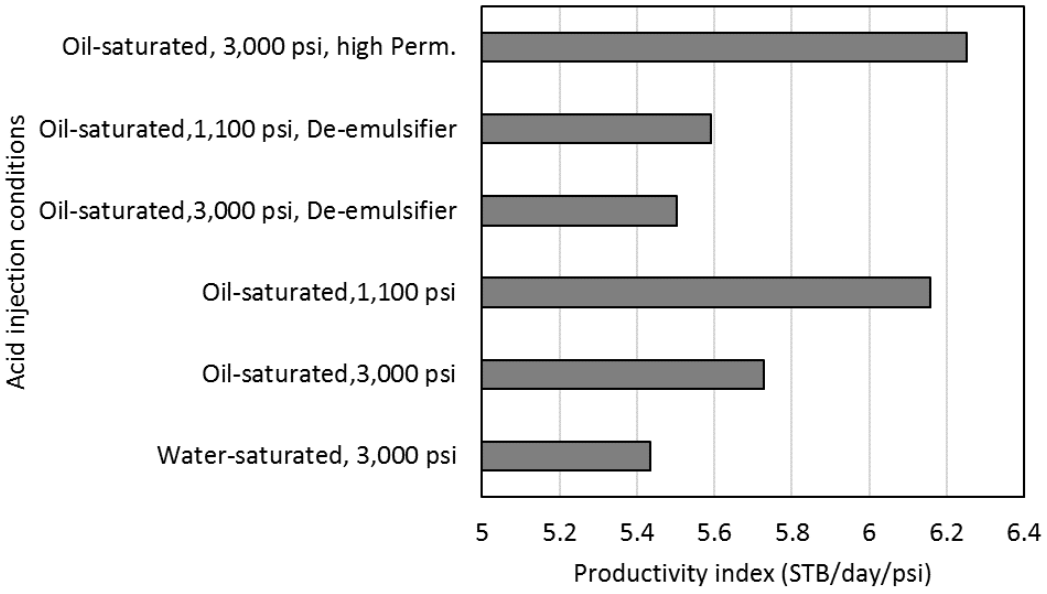

Figure 6.37: Productivity index for case 1 (kh=10,0000) different acid injection conditions

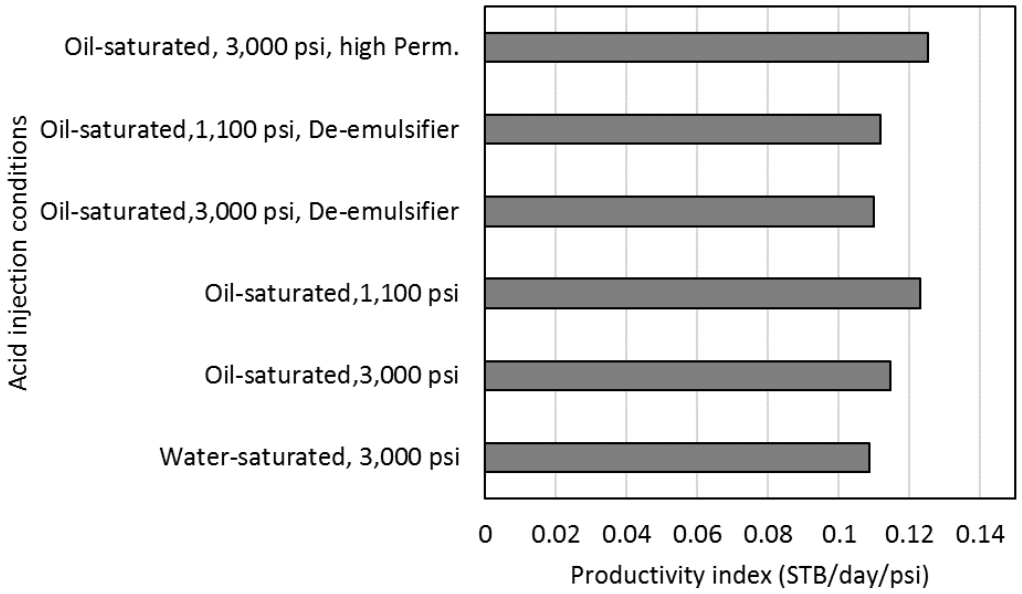

Figure 6.38: Productivity index of case 2 (kh=2,000) for different acid injection conditions

Furui's model (equation 6.6) calculates the fluid-loss coefficient (γ) for different injection conditions from the experimental results. An assumption of wormhole diameter of 0.4 cm for

water-saturated case, and 0.2 cm for oil-saturated case, is made. Pictures in figures 6.39 and 6.40 showing how the wormhole diameter for the water-saturated core is approximately double the size of the oil-saturated one with the same injection conditions.

$$v_{wh} = v_{i,tip} N_{Ac} \left(\frac{v_{i,tip} PV_{bt,opt} N_{Ac}}{v_{i,opt}} \right)^{-\gamma} \left\{ 1 - exp\left[-4 \left(\frac{v_{i,opt} PV_{bt,opt} N_{Ac} L_{core}}{v_{i,opt} r_{wh}} \right) \right] \right\}^2 \qquad (6.6)$$

Figure 6.39: Wormhole of water-saturated core

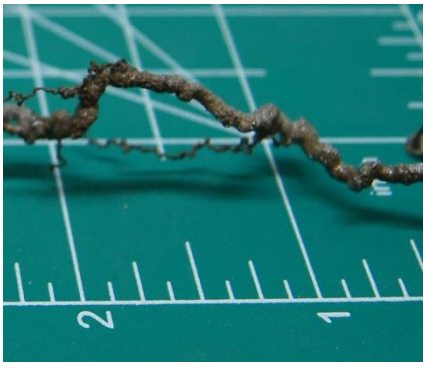

Figure 6.40: Wormhole of oil-saturated core

The corresponding fluid-loss coefficient showing in Figure 6.41 was at its minimum at 0.75 compared to 0.99 for the water-saturated cores.

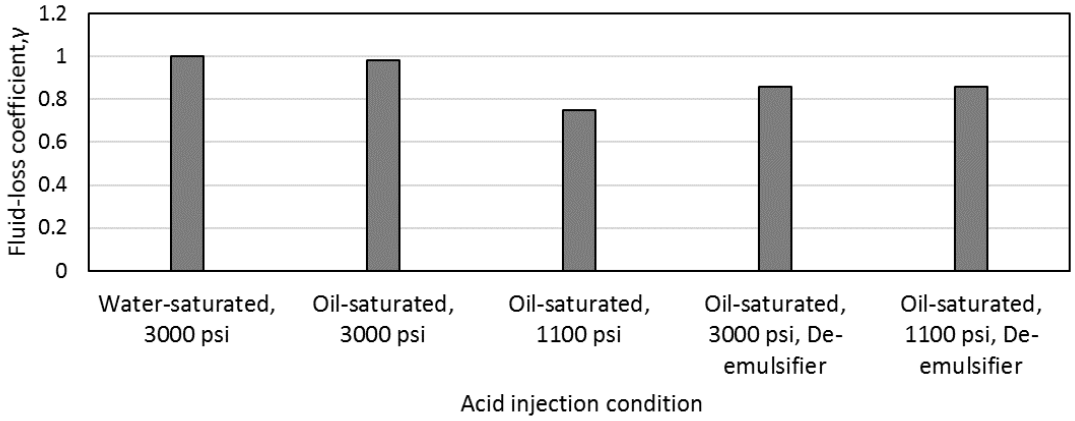

Figure 6.41: Fluid-loss coefficient (γ) for different acid injection conditions

6.7 Conclusions

- Saturation conditions significantly impact wormhole propagation during acidizing, where leak-off and inefficient propagation is observed in water-saturated cores, wormhole branching is observed in partially oil-saturated cores, and a single efficient wormhole is observed in cores that have zero water saturation.
- Acidizing partially oil-saturated high-permeability rocks at a pressure high-enough to keep CO_2 in solution (3,000 psi) results in more efficient wormhole propagation than in low-permeability rocks acidized under the same conditions.
- Acidizing at a low-pressure that limits CO_2 solubility in spent acid (1,100 psi) results in a substantially more efficient propagation of wormholes in low-permeability cores while resulting in a slightly less efficient wormhole propagation in high-permeability cores. Limited impact of pressure is observed on the optimum acid injection rate.
- The addition of de-emulsifier resulted in more acid needed to breakthrough; however, less wormhole branching was observed.

7. Chapter 7: Summary & Conclusions and Future Work

7.1 Summary

Matrix acidizing has been used for a long time in the oil and gas industry with great success in enhancing the productivity of damaged wells. However, with the current low oil prices, improving the acidizing process is essential to overcome issues associated with acid treatment. One crucial aspect that would help such an improvement is the study of the impact of the presence of oil in acidized formations and its potential in forming acid-oil emulsions. While these emulsions have shown high stability over time, causing many obstacles to the production system and forcing companies to use de-emulsifiers, our results show that emulsions prove to help in reducing the volume of acid needed and extending created wormholes by reducing fluid-loss during acidizing. Oil companies need to balance the use of de-emulsifiers in a way to avoid emulsions' effect on the flow assurance, but also utilize the advantage from the emulsions capability of improving created wormholes when the risk on flow assurance problems can be easily mitigated.

7.2 Conclusions

The following conclusions are drawn from the results of the three experimental approaches reported in this study:

- The acid-oil emulsions are can indeed form during acidizing treatment, and their behavior is time-sensitive. These emulsions could develop in a very viscous sludge with a viscosity value of up to 120 times the oil's viscosity after 5 days. The viscosity of these emulsions increases with time as the oil separates out of the emulsion, and a higher acid fraction is entrapped in the remaining emulsion layer. While the 20% acid content emulsions are not highly susceptible to emulsions, 30% acid content resulted in very viscous sludge with 888-cp viscosity after 3 days, and 40% acid content formed a sludge with 3,190-cp viscosity

after 5 days. Although these emulsions are homogeneous right after mixing, they become heterogeneous with time due to gravity segregation. According to its droplet size distribution, these emulsions are categorized as macro-emulsions.

- Injecting acid at a pressure that allows CO_2 to be in a gaseous phase could aid in forming stable emulsions in the rock. Spent-acid also creates heavy emulsions that cause flow restriction of getting the spent acid out of formation and, therefore, the crude oil as well. Having a well-tested de-emulsifier and surfactant breaks the emulsion viscosity and stability, resulting in better flow performance of spent-acid and oil by requiring lower pressure.
- Saturation conditions significantly impact wormhole propagation during acidizing. The process of creating wormholes during acid injection is more efficient in crude-saturated cores than it is in water-saturated or air-saturated cores. More efficiency means longer, thinner, and less branched wormholes are created in the presence of oil. The main reason for such better efficiency is the ability of the oil to reduce the fluid leak-off at the wormhole walls and reduce relative permeability in the area around it. The presence of oil saves more than half the amount of acid needed and reduces the rate by half as well.
- Contradictory to the common practice that is based on published literature on water-saturated cores, this work shows for the first time that acidizing partially oil-saturated high-permeability rocks required less acid volume needed to breakthrough than low-permeability rocks.
- Emulsions play a positive role in reducing the acid volume needed and improving the created wormhole structure, resulting in thinner wormholes with less leak-off. This work shows for the first time that the addition of De-emulsifiers to the acid results in 11% lower

productivity compared to not adding De-emulsifiers in high-permeability formations. This loss goes down to 5% in low-permeability formations. The economic impact of this loss needs to be assessed for each case to justify the use of de-emulsifiers.

- Acidizing at a low-pressure that limits CO_2 solubility in spent-acid (1,100 psi) results in a substantially more efficient propagation of wormholes in low-permeability cores, lowering the acid volume in half, while this low pressure does not impact wormhole propagation in high-permeability cores. Limited impact of pressure is observed on the optimum acid injection rate.

7.3 Future Work

Recommended future work includes:

- Upscaling all collected laboratory results to a field-scale where they can become more helpful in optimizing acid treatment operations.
- Conduct additional core flooding experiments with the presence of de-emulsifiers with different injection conditions to capture the full profile of impact under different permeability and backpressure conditions.
- Pressure profiles during acid injection at the various conditions, illustrated in Appendix C, invite further experimentation and simulation studies to fully understand the impact of other factors such as heterogeneity on wormhole propagation and the mechanisms at play during the rate-optimization process.
- Document the impact of temperature on the process.

Bibliography

Abdel-Raouf, M.E. 2012. *Factors Affection the Stability of Crude Oil Emulsions*. Croatia: InTech. http://dx.doi.org/10.5772/35018.

Abdollahi, R., Esfandyari, H., Pari, M.N.; Davarpanah, A. 2021. Conventional diverting techniques and novel fibr-assisted self-diverting system in carbonate reservoir acidizing with successful case studies. *Pet. Res.* https://doi.org/10.1016/j.ptlrs.2021.01.003.

Abdulredha, M.M., Aslina, H.S., and Luqman, C.A. 2020. Overview on petroleum emulsions, formation, influence, and demulsification treatment techniques. *Arab. J. Chem.* **13** (01): 3403–3428. doi:10.1016/j.arabjc.2018.11.014.

Abhishek, V. D. 2014. *Impact of Fluid Saturation on Matrix Acidizing.* Ms. Thesis, University of Oklahoma, Norman, Oklahoma (December 2014).

Adewale, A., Olalekan, O., Kelani, B., and Abass, I. 2004. Effects of Peclet Number on Miscible Displacement Process through the Reservoir. Paper presented at the Nigeria Annual International Conference and Exhibition, Abuja, Nigeria, 2-4 August. SPE-88881-MS. https://doi.org/10.2118/88881-MS.

Akanni, O. O., Nasr-El-Din, H. A., and Deepak G. 2017. A Computational Navier-Stokes Fluid-Dynamics-Simulation Study of Wormhole Propagation in Carbonate-Matrix Acidizing and Analysis of Factors Influencing the Dissolution Process. *SPE J* **22** (06): 2049–2066. https://doi-org.ezproxy.lib.ou.edu/10.2118/187962-PA

Al-Mutairi, S.H., Al-Obied, M.A., Al-Yami, I. Shebatalhamd, A. M., and D. A. Al-Shehri. 2012. Wormhole Propagation in Tar During Matrix Acidizing of Carbonate Formation. Paper presented at the SPE International Symposium and Exhibition on Formation Damage Control, Lafayette, Louisiana, USA, 15-17 February. SPE-151560-MS. https://doi.org/10.2118/151560-MS

Alvarado, D.A. and Marsden, S.S. 1979. Flow of Oil-in-Water Emulsions Through Tubes and Porous Media. *SPE J.* **19** (6): 369-377. SPE-5859-PA. http://dx.doi.org/10.2118/5859-PA.

Alvarado, V., Wang, X., and Moradi, M. 2011. Role of Acid Components and Asphaltenes in Wyoming Water-in-Crude Oil Emulsions. *Energy and Fuels* **25** (10): 4606-4616. http://dx.doi.org/10.1021/ef2010805.

Aske, N., Kallevik, H., and Sjöblom, J. 2002. Water-in-crude Oil Emulsion Stability Studied by Critical Electric Field Measurements. Correlation to Physico-chemical Parameters and Near-Infrared Spectroscopy. *Journal of Petroleum Science and Engineering* **36** (1): 1-17. http://dx.doi.org/10.1016/S0920-4105(02)00247-4.

Atehortúa, C.M.G., Pérez, N., Andrade, M.A.B., Pereira, L.O.V., and Adamowski, J.C. 2019. Water-in-oil emulsions separation using an ultrasonic standing wave coalescence chamber. *Ultrason. Sonochemistry*. **57**: 57–61. doi:10.1016/j.ultsonch.2019.04.043.

Arirachakaran, S., Oglesby, K.D., Malinowsky, M.S., Shoham, O., and Brill, J.B. 1989. An Analysis of Oil/Water Flow Phenomena in Horizontal Pipes. Paper presented at the SPE Production Operations Symposium, Oklahoma City, Oklahoma, 13-14 March. SPE-18836-MS. https://doi-org.ezproxy.lib.ou.edu/10.2118/18836-MS

Aziz, H.M.A., Darwish, S.F., and Abdeen, F.M. 2002. Downhole Emulsion Problem, The Causes, and Remedy, Ras Budran Field. Paper presented at the SPE Asia Pacific Oil and Gas Conference and Exhibition, Melbourne, Australia, 8-10 October. SPE-77847-MS. https://doi.org/10.2118/77847-MS

Bazin, B. 2001. From Matrix Acidizing to Acid Fracturing: A Laboratory Evaluation of Acid/Rock Interactions. *SPE J.* **16** (1): 22-29. SPE-66566-PA. https://doi.org/10.2118/66566-PA

Bhardwaj, A., and Hartland, S. 1994. Dynamics of Emulsification and Demulsification of Water in Crude Oil Emulsions. *Ind. Eng. Chem. Res.* **33**: 1271–1279. doi:10.1021/ie00029a025.

Buijse, M.A. 2000. Understanding Wormholing Mechanisms Can Improve Acid Treatments in Carbonate Formations. *SPE Prod & Fac* 15 (03): 168–175. SPE-65068-PA. https://doi-org.ezproxy.lib.ou.edu/10.2118/65068-PA

Buijse, M.A., and Gerard, G. A. 2005. Semi-Empirical Model to Calculate Wormhole Growth in Carbonate Acidizing. Paper presented at the SPE Annual Technical Conference and Exhibition, Dallas, Texas, 9-12 October. SPE-96892-MS. https://doi-org.ezproxy.lib.ou.edu/10.2118/96892-MS

Jeffrey W. B., Adam T. P., Edward J. G., and Nicos S. M. 2008. A Comparison of Viscosity-Concentration relationships for Emulsions. *Journal of Colloid and Interface Science*. **330** (1) 186-193. https://www.sciencedirect.com/science/article/pii/S0021979708013672

Cheng, H., Zhu, D., and Hill, A. D. 2016. The Effect of Evolved CO_2 on Wormhole Propagation in Carbonate Acidizing. Paper presented at SPE International Conference and Exhibition on Formation Damage Control, Lafayette, Louisiana, USA, 24-26 February. SPE-178962-MS. https://doi.org/10.2118/178962-MS

Coppel, C.P. 1975. Factors Causing Upsets to Surface Facilities Following Acid Stimulation. *J Pet Technol* **27** (9): 1060-1066. SPE-5154-PA. http://dx.doi.org/10.2118/5154-PA.

Czarnecki, J. and Moran, K. 2005. On the Stabilization Mechanism of Water-in-Oil Emulsions in Petroleum Systems. *Energy Fuels*. **19:** 2074–2079. doi:10.1021/ef0501400.

Daccord, G., Lenormand, R., and Lietard, O. 1993. Chemical Dissolution of a Porous Medium by a Reactive Fluid ¾ II. Convection vs. Reaction, Behavior Diagram. *Chem. Eng. Science*, **48** (1): 169-178. https://doi.org/10.1016/0009-2509(93)80293-Y

Daccord, G., Touboul, E. and Lenormand, R. 1989. Carbonate Acidizing: Toward a Quantitative Model of the Wormholing Phenomenon. *SPE Prod Eng* **4** (1): 63–68. SPE-16887-PA. https://doi.org/10.2118/16887-PA.doi:10.2118/16887-PA

DeZabala, E.F. and Radke, C.J. 1986. A Nonequilibrium Description of Alkaline Waterflooding. *SPE Res Eng* **1** (1): 29-43. SPE-11213-PA. http://dx.doi.org/10.2118/11213-PA.

Dickie, J.P. and Yen, T.F. 1967. Macrostructures of the Asphaltic Fractions by Various Instrumental Methods. *Analytical Chemistry*. **39** (14): 1847-1852. http://dx.doi.org/10.1021/ac50157a057.

Dong, K., Jin, X., Zhu, D., and Hill, A. D. 2014. The Effect of Core Dimensions on the Optimal Acid Flux in Carbonate Acidizing. Paper presented at SPE International Symposium and Exhibition on Formation Damage Control, Lafayette, Louisiana, USA, 26-28 February. SPE-168146-MS. https://doi.org/10.2118/168146-MS

Dong, K., Zhu, D., and Hill, A.D. 2017. Theoretical and Experimental Study on Optimal Injection Rates in Carbonate Acidizing. *SPE J.* **22**(3): 892–901. doi:10.2118/178961-pa.

Duan, Z., and Zhang, Z. 2006. Equation of state of the H2O, CO2, and H2O–CO2 systems up to 10 GPa and 2573.15 K: Molecular dynamics simulations with ab initio potential surface. *Geochimica et Cosmochimica Acta*, **70** (9): 2311– 2324. http://dx.doi.org/10.1016/j.gca.2006.02.009

Dubetz, D., Cheng, H., Zhu, D., and Hill, A. D. 2016. Characterization of Rock Pore-Size Distribution and Its Effects on Wormhole Propagation. Paper presented at SPE Annual Technical Conference and Exhibition, Dubai, UAE, 26-28 September. SPE-181725-MS. https://doi.org/10.2118/181725-MS

Dunlap, D.D. and Houchin, L.R. 1990. Evaluation of Acid System Design and Formation Damage Using Polarized Microscopy. Paper Presented at the SPE Formation Damage Control Symposium, 22-23 February, Lafayette, Louisiana. SPE-19425-MS. http://dx.doi.org/10.2118/19425-MS.

Economides, M. J., Hill, A. D., and Ehlig-Economides, C. 1994. *Petroleum Production Systems / Michael J. Economides, A. Daniel Hill, Christine Ehlig-Economides.* Englewood Cliffs, N.J.: PTR Prentice Hall.

Ehrenberg, S. N., Nadeau, P. H. 2005. Sandstone vs. Carbonate Petroleum Reservoirs: A Global Perspective on Porosity-Depth and Porosity-Permeability Relationships. *Bulletin* **89** (4), 435–445. https://doi.org/10.1306/11230404071.

Eley, D.D., Hey, M.J., and Symonds, J.D. 1988. Emulsions of Water in Asphaltene-Containing Oils. Droplet Size Distribution and Emulsification Rates. *Colloids and Surfaces* **32**: 87-101. http://dx.doi.org/10.1016/0166-6622(88)80006-4.

Elsafih, M., and Mashhad F. 2021 "Quantifying the Effect of Multiphase Flow on Matrix Acidizing in Oil-Bearing Carbonate Formations." *SPE Prod & Oper* (1-12). SPE-205397-PA. https://doi-org.ezproxy.lib.ou.edu/10.2118/205397-PA

Elsafih, M., Fahes, M., and Teodoriu, C. 2021. Quantifying the Effect of De-Emulsifiers on Acid Treatment in Carbonate Formations. *Energies* 14 (4): 1148. https://doi.org/10.3390/en14041148.

Etten, J., Zhu, D., and Hill, A. D. 2015. The Combined Effect of Permeability and Pore Structure on Carbonate Matrix Acidizing. Paper presented at EUROPEC, Madrid, Spain, 1-4 June. SPE-174314-MS. https://doi.org/10.2118/174314-MS

Fan, Z., Li, X., Ostermann, R.D., and Jiang, J. 2018. An Efficient Method to Determine Wormhole Propagation During Matrix Acidizing. Paper presented at the SPE/AAPG/SEG Unconventional Resources Technology Conference, Houston, Texas, USA, 23-25 July. URTEC-2902519-MS. https://doi.org/10.15530/urtec-2018-2902519.

Feazel, C., Byrnes, A., Honefenger, J., Leibrecht, R., Loucks, R., McCants, S., and Saller, A. 2004. Research Symposium Focuses on Complexity of Carbonate-Reservoir Characterization and Simulation. *Journal of Petroleum Technology* **56** (08), 26–34. https://doi.org/10.2118/0804-0026-JPT.

Fredd, C.N. 2000. Dynamic Model of Wormhole Formation Demonstrates Conditions for Effective Skin Reduction During Carbonate Matrix Acidizing." Paper presented at the SPE Permian Basin Oil and Gas Recovery Conference, Midland, Texas, 21-23 March. SPE-59537-MS. https://doi-org.ezproxy.lib.ou.edu/10.2118/59537-MS

Fredd, C. N. and Fogler, H. S. 1998. Alternative Stimulation Fluids and Their Impact on Carbonate Acidizing. *SPE Journal.* **3** (1): 34–41. SPE-31074-MS. https://doi.org/10.2118/31074-MS

Fredd, C. N., and Fogler, H. S. 1999. Optimum Conditions for Wormhole Formation in Carbonate Porous Media: Influence of Transport and Reaction. *SPE Journal* **4** (03): 196–205. SPE-56995-PA. https://doi.org/10.2118/56995-PA

Fredd, C.N., and M.J. Miller. 2000. Validation of Carbonate Matrix Stimulation Models. Paper presented at the SPE International Symposium on Formation Damage Control, Lafayette, Louisiana, 23-24 February. SPE-58713-MS. https://doi_org.ezproxy.lib.ou.edu/10.2118/58713-MS

Furui, K., Burton, R.C. C., Burkhead, D.W. W., Abdelmalek, N.A. A., Hill, A.D. D., Zhu, D., and M. Nozaki. A Comprehensive Model of High-Rate Matrix-Acid Stimulation for Long Horizontal Wells in Carbonate Reservoirs: Part I—Scaling Up Core-Level Acid Wormholing to Field Treatments. *SPE J* 17 (01): 271–279. SPE-134265-PA. https://doi-org.ezproxy.lib.ou.edu/10.2118/134265-PA

Gao, J., Feng, P., Wang, D, Shao, S., Cui, B., and Wang, G. 2019. Large Liquid Volume Deep Penetration Acidizing in Iraq Missan Oilfield – 3 Case Study. Paper Presented at the International Petroleum Technology Conference, Beijing, China, 26-28 March. IPTC-19549-MS. https://doi.org/10.2523/IPTC-19549-MS.

Gomez, S. 2018. *Experimental Characterization of Brine in Crude Oil Emulsions and Its Performance in Artificial Lift Systems*. Ms. Thesis, University of Oklahoma, Norman, Oklahoma (December 2018). https://shareok.org/handle/11244/316785

Helene, K. 2019. *Experimental Study of Flow and Rheology of Water-In-Crude Oil Emulsions*. Ms. Thesis, University of Oklahoma, Norman, Oklahoma (May 2019). https://shareok.org/handle/11244/319575

Hashmi, S.M. and Firoozabadi, A. 2011. Tuning size and Electrostatics in Non-Polar Colloidal Asphaltene Suspensions by Polymeric Adsorption. *Soft Matter* **7** (18): 8384-8391. http://dx.doi.org/10.1039/c1sm05384a.

Hoefner, M. L. and Fogler, H. S. 1989. Fluid-Velocity and Reaction-Rate Effects During Carbonate Acidizing: Application of Network Model. *SPE Prod Eng* **4** (01): 56-62. SPE-15573-PA. doi:10.2118/15573-PA

Hoefner, M.L. and Fogler, H. S. 1988. Pore Evolution and Channel Formation During Flow and Reaction in Porous Media", *AIChE J*. **34** (1), 45-54. http://hdl.handle.net/2027.42/37401

Houchin, L., Dunlap, D., Arnold, B., and Domke, K. 1990. The Occurrence and Control of Acid-Induced Asphaltene Sludge. Paper presented at the SPE Formation Damage Control Symposium, Lafayette, Louisiana, 22-23 February. SPE-19410-MS. https://doi.org/10.2118/19410-MS.

Huang, T., Hill, A. D., and Schechter, R. S. 1997. Reaction Rate and Fluid Loss: The Keys to Wormhole Initiation and Propagation in Carbonate Acidizing. Paper presented at the International Symposium on Oilfield Chemistry, Houston, Texas, 18-21 February. SPE-37312-MS. https://doi.org/10.2118/37312-MS

Hung, K. M., Hill, A. D., and Sepehrnoori, K. 1989. A Mechanistic Model of Wormhole Growth in Carbonate Matrix Acidizing and Acid Fracturing. *JPT* **41** (1): 45-66

Jacobs, I.C. 1989. Chemical Systems for the Control of Asphaltene Sludge During Oilwell Acidizing Treatments. Paper presented at the SPE International Symposium on Oilfield Chemistry, Houston, Texas, USA, 8-10 February. SPE-18475-MS. http://dx.doi.org/10.2118/18475-MS.

Jacobs, I.C. and Thorne, M.A. 1986. Asphaltene Precipitation During Acid Stimulation Treatments. Paper presented at the SPE Formation Damage Control Symposium, Lafayette, Louisiana, 26-27 February. SPE-14823-MS. http://dx.doi.org/10.2118/14823-MS.

Jones, T.J., Neustadter, E.L., and Wittingham, K.P. 1978. Water-in-Crude Oil Emulsion Stability and Emulsion Destabilization by Chemical Demulsifiers. *J Can Pet Technol* **17** (2): 100-108. PETSOC-78-02-08. http://dx.doi.org/10.2118/78-02-08.

Kalfayan, Leonard. 2008. *Production enhancement with acid stimulation*. Tulsa, Okla: PennWell. http://www.books24x7.com/marc.asp?bookid=17307.

Karale, C., Beuterbaugh, A., Pinto, M., Hipparge, G., and Prakash, A. 2016. HP/HT Carbonate Acidizing-Recent Discoveries and Contradictions in Wormhole Phenomenon. Paper presented at the Offshore Technology Conference Asia, Kuala Lumpur, Malaysia, 22-25 March. OTC-26714-MS. https://doi.org/10.4043/26714-MS.

Kilpatrick, p. 2012. Water-in-Crude Oil Emulsion Stabilization: Review and Unanswered Questions. *Energy& Fuels* **26** (07):4017-4026. https://pubs.acs.org/doi/10.1021/ef3003262

Kimbler, O.K., Reed, R.L., and Silberberg, I.H. 1966. Physical Characteristics of Natural Film Formed at Crude Oil-Water Interfaces. *J Pet Technol* **6** (2): 153-165. SPE-77497-PA. http://dx.doi.org/10.2118/1201-PA.

Knopp, M. 2009. Non-damaging Matrix and Fracturing Acids: Some Key Considerations, Richardson, Texas: Distinguished Lecturer Program, Society of Petroleum Engineers. http://www.spe.org/dl/docs/2009/Knopp.pdf.

Kokal, S. 2005. Crude Oil Emulsions: A State-of-the-Art Review. Paper presented at the SPE Annual Technical Conference and Exhibition, San Antonio, Texas, USA, 29 September – 2 October. SPE-77497-MS. http://dx.doi.org/10.2118/77497-MS.

Kokal, S., Al-Dawood, N., Fontanilla, J., Al-Ghamdi, A., Nasr-El-Din, H., and Al-Rufaie, Y. 2002. Productivity Decline in Oil Wells Related to Asphaltene Precipitation and Emulsion Blocks. Paper presented at the SPE Annual Technical Conference and Exhibition, San Antonio, Texas, 29 September – 2 October. 2002. SPE-77767-MS. https://doi.org/10.2118/77767-MS

Kokal, S.; Al-Juraid, J. 1998. Reducing Emulsion Problems by Controlling Asphaltene Solubility and Precipitation. Paper presented at the SPE Annual Technical Conference and Exhibition, New Orleans, Louisiana, 27-30 September 1998. SPE-48995-MS. https://doi.org/10.2118/48995-MSIn

Kokal, S. and Alvarez, C. 2003. Reducing Pressure Drop in Offshore Pipelines by Controlling the Viscosities of Pressurized Emulsions. Paper presented at the Middle East Oil Show, Bahrain, 5-8 April. SPE-81511-MS. https://doi.org/10.2118/81511-MS

Kokal, S., Al-Yousif, A., Meeranpillai, N., and Al-Awaisi, M. 2001. Very Thick Crude Emulsions: A Field Case Study of a Unique Crude Production Problem. Paper presented at the SPE Annual Technical Conference and Exhibition, New Orleans, Louisiana, USA, September. SPE-71467-MS. https://doi.org/10.2118/71467-MS

Kokal, S.L. 2006. *Crude Oil Emulsions. In Petroleum Engineering Handbook*, Vol. 1—General Engineering, ed. J.R. Fanchi. Rich-ardson, Texas: Society of Petroleum Engineers.

Kokal, S.L. 2005. Crude Oil Emulsions: A State-Of-The-Art Review. *SPE Prod. & Fac.* **20** (01): 5–13. SPE-77497-PA. doi:10.2118/77497-pa.

Kokal, S.L., Al-Dokhi, M. 2008. Case Studies of Emulsion Behavior at Reservoir Conditions. *SPE Prod. Oper.* **23** (03): 312–317. SPE-105534-PA. doi:10.2118/105534-pa.

Kokal, S.L., Al-Ghamdi, A., and Meeranpillai, N.S. 2007. An Investigative Study of Potential Emulsion Problems Before Field Development. *SPE Proj. Facil. Constr.* **2** (01): 1–10. SPE-102856-PA. https://doi.org/10.2118/102856-PA

Krueger, R.F. 1988. An Overview of Formation and Well Productivity in Oilfield Operations: An Update. Paper presented at the SPE California Regional Meeting, Long Beach, California, USA, 23-25 March. SPE-17459-MS. http://dx.doi.org/10.2118/17459-MS.

Kumar, R., He, J., Bataweel, M., and Nasr-El-Din, H. A. 2018. New Insights on the Effect of Oil Saturation on the Optimal Acid-Injection Rate in Carbonate Acidizing. *SPE J.* **23** (3): 969-984. SPE-169134-PA. https://doi.org/10.2118/169134-PA

Lake, L., Fanchi, John R. 2006. *Society of Petroleum Engineers. Petroleum engineering handbook* / Larry W. Lake, editor-in-chief. Richardson, TX: Society of Petroleum Engineers.

Langevin, D., Poteau, S., Hénaut, I., and Argillier, J. F. 2004. Crude Oil Emulsion Properties and their Application to Heavy Oil Transportation. *Oil & Gas Science and Technology* **59** (5): 511-521. https://doi.org/10.2516/ogst:2004036

Liu, J., Li, X., Jia, W., Li, Z., Zhao, Y., and Ren, S. 2015. Demulsification of Crude Oil-in-Water Emulsions Driven by Graphene Oxide Nanosheets. *Energy & Fuels* **29** (07): 4644–4653. https://doi.org/10.1021/acs.energyfuels.5b00966

Mahmoud, M. A., Nasr-El-Din, H. A., De Wolf, C. A., and A. K. Alex. 2011. Effect of Reservoir Fluid Type on the Stimulation of Carbonate Cores Using Chelating Agents." Paper presented at the Brasil Offshore, Macaé, Brazil, 14-17 June. SPE-143086-MS. https://doi-org.ezproxy.lib.ou.edu/10.2118/143086-MS

Mason, S., May, K., and Hartland, S. 1995. Drop size and concentration profile determination in petroleum emulsion separation. *Colloids Surfaces A: Physicochem. Eng. Asp.* **96** (1-2): 85–92. doi:10.1016/0927-7757(94)03030-4.

Mazzullo, S. J., Rieke, H. H., and Chilingarian, G. V. 1996. *Carbonate Reservoir Characterization: A Geologic-Engineering Analysis, Part II*; Elsevier.

McLean, J.D. and Kilpatrick, P.K. 1997. Effects of Asphaltene Solvency on Stability of Water-in-Crude Oil Emulsions. *Journal of Colloid and Interface Science* **189** (2): 242-253. http://dx.doi.org/10.1006/jcis.1997.4807.

Moore, E.W., Crowe, C.W., and Hendrickson, A.R. 1965. Formation, Effect, and Prevention of Asphaltene Sludges During Stimulation Treatments. *J Pet Technol* **17** (09): 1023-1028. SPE-1163-PA. http://dx.doi.org/10.2118/1163-PA.

Mostofizadeh, B. and Economides, M. J. 1994. Optimum Injection Rate from Radial Acidizing Experiments. Paper presented at SPE Annual Technical Conference and Exhibition, New Orleans, Louisiana, 25-28 September. SPE-28547-MS. https://doi.org/10.2118/28547-MS

Mullins, O.C. 2011. The Asphaltenes. *Annu. Rev. Anal. Chem.* **4** (1): 393-418. 21689047. https://doi.org/10.1146/annurev-anchem-061010-113849

Nasr-El-Din, H.A., Al-Dirweesh, S., Samuel, M.M. 2008. Development and Field Application of a New, Highly Stable Emulsified Acid. Paper presented at the SPE Annual Technical Conference and Exhibition, Denver, Colorado, USA, 21-24 September 2008. SPE-115926-MS. https://doi.org/10.2118/115926-MS

O'Niel, B., Maley, D., and Lalchan, C. 2015. Prevention of Acid-Induced Asphaltene Precipitation: A Comparison of Anionic vs. Cationic Surfactants. *J Can Pet Technol* **54** (1): 49-62. SPE-164087-PA. http://dx.doi.org/10.2118/164087-PA.

Oluwatosin, I. 2016. *Experimental Study of the Rheology and Stability Behavior of Surfactant Stabilized Water-in-oil Emulsion*. MS Thesis, University of Oklahoma, Norman, Oklahoma (December 2016). https://hdl.handle.net/11244/47076.

Omole, O. and Falode, O.A. 2005. Effects of Mixing Conditions, Oil Type and Aqueous Phase Composition on Some Crude Oil Emulsions. *Journal of Applied Sciences* **5** (5): 873-877. http://198.170.104.138/jas/2005/873-877.pdf.

Oneil, B.J., Maley, D.M., and Lalchan, C.A. 2015. Prevention of Acid-Induced Asphaltene Precipitation: A Comparison of Anionic Vs. Cationic Surfactants. *J. Can. Pet. Technol.* **54** (01): 49–62. SPE-164087-PA. doi:10.2118/164087-pa.

Opawale, A.O. and Osisanya, S.O. 2013. Tool for Troubleshooting Emulsion Problems in Producing Oilfields. Paper presented at the SPE Production and Operations Symposium, Oklahoma City, Oklahoma, USA, 23-26 March. SPE-164512-MS. https://doi.org/10.2118/164512-MS

Paccaloni, G. and Tambini, M. 1993. Advances in Matrix Stimulation Technology. *J Pet Technol* **45** (03): 256–263. SPE-20623-PA. https://doi.org/10.2118/20623-PA

Panait, E., Isac, C., Marton, C., Dos Santos, A., and Girardi, S. 2018. Effective Matrix Acidizing Based in Chelating Agents: A Case Study in Romanian Heavy Oil Reservoirs. Paper presented at the SPE International Heavy Oil Conference and Exhibition Kuwait City, Kuwait, 10-12 December. SPE-193723-MS. https://doi.org/10.2118/193723-MS.

Paulis, J.B., Sharma, M.M. 1997. A New Family of Demulsifies for Treating Oilfield Emulsions. Paper presented at the International Symposium on Oilfield Chemistry, Houston, Texas, USA, 18-21 February. SPE-37269-MS. https://doi.org/10.2118/37269-MS

Picou, R.A., Ricketts, K., Luquette, M., and Hudson, L. M. 1992. Successful Stimulation of Acid-Sensitive Crude Producers in the Gulf of Mexico. Paper presented at the SPE Formation Damage Control Symposium, Lafayette, 26-27 February. SPE-23818-MS. http://dx.doi.org/10.2118/23818-MS.

Prutton, C. F. and Savage, R. L. 1945. The Solubility of Carbon Dioxide in Calcium Chloride-Water Solutions at 75, 100, 120° and High Pressures. *J. Am. Chem. Soc.* **67** (9): 1550–1554. https://doi.org/10.1021/ja01225a047

Qiu, X. W., Zhao, W., Dyer, S. J., Al Dossary, A., Khan, S., and Sultan, A. S. 2014. Revisiting Reaction Kinetics and Wormholing Phenomena During Carbonate Acidizing. Paper presented at International Petroleum Technology Conference, Doha, Qatar, 19-22 January. IPTC-17285-MS. https://doi.org/10.2523/IPTC-17285-MS

Qiu, X., Zhao, W., Chang, F., and Dyer, S. 2013. Quantitative Modeling of Acid Wormholing in Carbonates What Are the Gaps to Bridge. Paper presented at the SPE Middle East Oil and Gas Show and Conference, Manama, Bahrain, March. SPE-164245-MS. https://doi.org/10.2118/164245-MS

Rabbani, E., Davarpanah, A., and Memariani, M. 2018. An experimental study of acidizing operation performances on the wellbore productivity index enhancement. *J. Pet. Explor. Prod. Technol.* **8:** *8*1243–1253. doi:10.1007/s13202-018-0441-8.

Rae, P. and Di Lullo, G. 2003. Matrix Acid Stimulation: A State-of-the-Art Review. Paper presented at the SPE European Formation Damage Conference, The Hague, Netherlands, 13-14 May. SPE-82260-MS. http://dx.doi.org/10.2118/82260-MS.

Rietjens, M. 1997. Sense and Non-Sense about Acid-Induced Sludge. Paper presented at the SPE European Formation Damage Conference, The Hague, Netherlands, 2-3 June. SPE-38163-MS. https://doi.org/10.2118/38163-MS

Salager, J. L. and Forgiarini, A.M. 2012. Emulsion Stabilization, Breaking, and Inversion Depends upon Formulation: Advantage or Inconvenience in Flow Assurance. *Energy & Fuels* **26** (7): 4027–4033. doi:10.1021/ef3001604.

Saneifar, M., Fahes, M.M., Lewis-Hosein, R., Hassna, B.O., and Hill, D. 2010. The Effect of Spent Acid on Carbonate Rock Wettability. Paper presented at the Trinidad and Tobago Energy Resources Conference, Port of Spain, Trinidad, 27-30 June. SPE-133166-MS. https://doi.org/10.2118/133166-MS

Scarborough, B. 2016. *Impact of Viscous Acid-in-Oil Emulsion Formation on Well Productivity Following Acid Stimulation.* MS Thesis, University of Oklahoma, Norman, Oklahoma (December 2016). https://hdl.handle.net/11244/47106.

Scarborough, B., Elsafih, M., Fahes, M., and Pournik, M. Characterizing Time-Dependent Stability and Viscosity of Acid–Crude Emulsions for Matrix-Acidizing Applications. *Energy Fuels* **33** (11): 10508–10518, doi:10.1021/acs.energyfuels.9b01996.

Schectter, R. S. 1992. *Oil Well Stimulation*, Prentice Hall, Englewood Cliffs, NJ.

Sharma, M.K., Shah, D.O. 1985. Introduction to Macro- and Microemulsions. In Proceedings of the ACS Symposium Series; American Chemical Society (ACS), 1985; Vol. 272, pp. 1–18.

Shirley, R.M., Zhu, D., Hill, A.D., and Da Motta, E.P. 2017. Maximizing the Value of Matrix Acidizing Treatments in Carbonate Reservoirs. Paper presented at the SPE Europec/EAGE Conference and Exhibition, Paris, France, 12-15 June. SPE-185812-MS. https://doi.org/10.2118/185812-MS

Shukla, S., Zhu, D., and Hill, A. D. 2006. The Effect of Phase Saturation Conditions on Wormhole Propagation in Carbonate Acidizing. *SPE J.* **11** (3): 273-281. SPE-82273-PA. https://doi.org/10.2118/82273-PA

Sidaoui, Z., Sultan, A.S. 2016. Formulating a Stable Emulsified Acid at High Temperatures: Stability and Rheology Study. Paper presented at the International Petroleum Technology Conference, Bangkok, Thailand, 14-16 November. IPTC-19012-MS. https://doi.org/10.2523/IPTC-19012-MS

Sjöblom, J., Mingyuan, L., Christy, A. A., and Gu, T. 1992. Water-in-crude-oil emulsions from the Norwegian continental shelf 7. Interfacial pressure and emulsion stability. *Colloids Surfaces* **66** (01): 55–62. doi:10.1016/0166-6622(92)80120-q.

Skoog, D., Holler, J., Crouch, S. 2007. *Principles of Instrumental Analysis*; 6th Ed., Thomson Brooks/Cole: Belmont.

Soo, H. and Radke, C.J. 1984. The Flow Mechanism of Dilute Stable Emulsions in Porous Media. *Ind. Eng. Chem. Fundamen.* **23** (2): 342-347. http://dx.doi.org/10.1021/i100015a014.

Strassner, J.E. 1968. Effect of pH on Interfacial Films and Stability of Crude Oil-Water Emulsions. *J Pet Technol* **20** (3): 303-312. SPE-1939-PA. http://dx.doi.org/10.2118/1939-PA.

Swanson, B. 1981. A Simple Correlation Between Permeabilities and Mercury Capillary Pressures. *J Pet Technol*. **33** (12): 2498-2504. https://doi.org/10.2118/8234-PA

Sztukowski, D.M., Jafari, M., Alboudwarej, H., and Yarranton, H.W. 2002. Asphaltene Self-Association and Water-in-Hydrocarbon Emulsions. *Journal of Colloid and Interface Science* **265** (1): 179-186. http://dx.doi.org/10.1016/S0021-9797(03)00189-9.

Umar, A.A., Saaid, I.B.M., Sulaimon, A.A., and Pilus, R.B.M. 2018. A review of petroleum emulsions and recent progress on water-in-crude oil emulsions stabilized by natural surfactants and solids. *J. Pet. Sci. Eng.* **165**: 673–690. doi:10.1016/j.petrol.2018.03.014.

Wang, Y. 1993. *Existence of an Optimum Rate in Carbonate Acidizing and the Effect of Rock Heterogeneity on Wormhole Patterns*. Ph.D. dissertation, The University of Texas at Austin. (May 1993).

Wang, Y., Hill, A. D., and Schechter, R. S. 1993. The Optimum Injection Rate for Matrix Acidizing of Carbonate Formations. Paper presented at the SPE Annual Technical Conference and Exhibition, Houston, Texas. 3-6 October. SPE-26578-MS. https://doi.org/10.2118/26578-MS

Wanli, K., Yi, L., Baoyan, Q., Guangzhi, L., Zhenyu, Y., and Jichun, H. 2000. Interactions between alkali/surfactant/polymer and their effects on emulsion stability. *Colloids Surfaces A: Physicochem. Eng. Asp.* **175** (1-2): 243–247. doi:10.1016/s0927-7757(00)00461-1.

Williams, B. B., Gidley, J. L., Schechter, R. S. 1979. *Acidizing Fundamentals.* Society of petroleum engineers, Richardson, TX.

William, E. 1962. *Classification of Carbonate Rocks*, Memoir 1, AAPG, Tulsa, Oklahoma

Xue, H., Huang, Z.X., Zhao, L.Q., Wang, H.H. and Liu, P.L. 2019. Wormholing Influenced by Injection Temperature in Carbonate Rocks. *Open Journal of Yangtze Gas and Oil*. **4** (1): 12-30. https://doi.org/10.4236/ojogas.2019.41002

Yang, X., Verruto, V.J., and Kilpatrick, P.K. 2007. Dynamic Asphaltene Resin Exchange at the Oil-Water Interface: Time-Dependent W/O Emulsion Stability for Asphaltene/Resin Model Oils. *Energy and Fuels* **21** (3): 1343-1349. http://dx.doi.org/10.1021/ef060465w.

Yarranton, H.W., Hussein, H., and Masliyah, J.H. 2000. Water-in-Hydrocarbon Emulsions Stabilized by Asphaltenes at Low Concentrations. *Journal of Colloid and Interface Science* **228** (1): 52-63. https://doi.org/10.1006/jcis.2000.6938.

Zakaria, A.S., Nasr-El-Din, H.A., and Ziauddin, M. 2015. Predicting the Performance of the Acid-Stimulation Treatments in Carbonate Reservoirs With Nondestructive Tracer Tests. *SPE J.* **20** (06): 1238–1253. https://doi-org.ezproxy.lib.ou.edu/10.2118/174084-PA

Zolfaghari, R., Fakhru'L-Razi, A., Abdullah, L.C., Elnashaie, S.S., and Pendashteh, A. 2016. Demulsification techniques of water-in-oil and oil-in-water emulsions in petroleum industry. *Sep. Purif. Technol.* **170:** 377–407. doi:10.1016/j.seppur.2016.06.026.

Appendix A: Wormhole Propagation Models

Models in literature can be classified into five categories: simple models, network models, chemical models, flow models, and empirical models. The following section gives a brief summary and some examples of models in each category.

❖ ***Simple Models***

The first models to simulate the worm-holing process were built assuming the shape of the wormhole is cylindrical. Wang et al. (1993), Hung et al. (1989), Buijse (2000), and Gdansky (1999) idealized the wormhole to a cylinder shape and used transport equations as if the flow was inside a tube, represented by Stoke's equation. Huang et al. (1997) provided a more detailed model based on the same assumption but considering fluid loss across the cylinder. Then, they extended that model in 1999 to investigate the wormhole density. The same model was improved by Schechter (1992), where the wormhole is still assumed to be idealized. Their final expression of wormhole-length growth with time is:

$$\frac{dL}{dt} = \frac{\beta_{100}\rho_{acid}C_{end}U_{end}}{(1-\emptyset)\rho_{rock}} \qquad (A.1)$$

Where:

β_{100}: Dissolving power at 100% HCL

ρ_{acid}: Acid density

C_{end}: Acid concentration at the wormhole's tip

U_{end}: Acid flux at the wormhole's tip

ρ_{rock}: Rock matrix density, 2.71 g/cc for limestone

∅: Porosity

❖ ***Models based on a network approach***

These models rely on the physical aspect of the acidizing process. Hoefner and Fogler (1998) developed a model based on the dissolution of rock grains. They assumed the space between any two pores is a cylindrical capillary tube, and Poiseuille's' law represents flow. The dissolution of grains is considered to be proportional to flow velocity and concentration. Although they were able to optimize the acid injection rate, many difficulties were faced applying the model. Complications include the large-scale systems and not accounting for the merging of pores. This model assumes that acid diffusive flow to the wall of the pore is laminar and is calculated using the following equations:

$$C = C_0 \exp\left(-\pi k_s \frac{dl}{q}\right) \qquad (A.2)$$

Where:

C: Acid concentration

C_o: Inlet acid concentration

K_s = Mass-transfer coefficient

L: Bond length

q: Volumetric flow rate

$$C = C_0 exp\left\{-a\left[\frac{D_{ab}^{2/3} L}{(q^{1-b} d^b \nu^{b-0.33})}\right]\right\} \qquad (A.3)$$

Where:

D_{ab}: Acid diffusion rate

d: Bond diameter

v: Kinematic viscosity

a and b are Constants

After a series of derivations, the overall growth of a single pore is given by the following equation:

$$\frac{\Delta d}{d} = \left(\frac{C_0}{\vartheta}\right)\left(\frac{q\Delta t}{d^2 L}\right)\left\{1 - exp\left\{-a\left[\frac{D_{ab}^{\frac{2}{3}} L}{(q^{1-b} d^b v^{b-0.33})}\right]\right\}\right\} \qquad (A.4)$$

Where:

t: time

ϑ: Stoichiometric coefficient

❖ ***Models based on chemical process***

These models are built based on chemical and thermal correlations applied at the core scale. Daccord et al. (1993) and Frick et al. (1994) converted all parameters included in the chemical reaction of the acid with limestone into correlated constants derived theoretically or experimentally. Similar approaches were developed by Fredd et al. (1999), where the acid injection rate was optimized based on the Damkohler number. Buisje and Glasbergen (2005) were able to extend the work of Daccord et al. (1993), which was a linear and radial water injection model in a plaster core, to an empirical model that can be used at reservoir conditions based on the chemical reaction. Another model that is based on the chemical process is introduced by Mostofizadeh and

Economides (1994). Their definition of Peclet number and acid capacity number are given by equations A.5, A.6.

$$N_{pe} = \frac{i\sqrt{k}}{2\pi r_w L \varphi D} \qquad (A.5)$$

Where:

k: Permeability

i: Injection rate

L: Injection length

D: Diffusivity coefficient

r_w: Wellbore radius

φ: Porosity

$$N_{ac} = \frac{X}{1-\varphi} \qquad (A.6)$$

$$X = \frac{M_{Min}\rho_{acid}C_{acid}}{\lambda\, M_{HCl}\, \rho_{Min} * 100} \qquad (A.7)$$

Where:

λ: Stoichiometric coefficient

The wormhole propagation length is then calculated from equation A.8.

$$V_{acid} = \left(r_{eq}^{df} - r_w^{df}\right) L \frac{N_{pe}^{0.333}}{N_{ac}} \frac{1}{B} \qquad (A.8)$$

$$B = 9.2\, N_{pe}^{0.333} \frac{r_w RL}{V_{bt} N_{ac}} \qquad (A.9)$$

Where:

d_f: Fractal dimension = 1.6

R: Sample radius

❖ ***Models based on flow in porous media***

These models were built based on applying the continuum equation in porous media. Liu et al. (1997) and Chen et al. (1997) developed a model that resolves Darcy-scale equations of fluid flow in porous media while considering acid reaction and acid transport phenomena. These models are also based on some assumptions that limit their applications, such as reaction rate is what controls the acid dissolution, and the effect of mass transfer is negligible.

❖ ***Empirical models:***

A volumetric, empirical model was developed by Pichler et al. (1992). This model is based on the assumption that a constant fraction of the rock volume is dissolved in the wormhole area. The radius of the wormhole in radial flow is given by:

$$r_{wh} = \sqrt{r_w^2 + \frac{V/l}{\pi \varphi P V_{bt}}} \qquad (A.10)$$

Where:

r_w: Wellbore radius, ft

V/l: Volume of acid injected per unit of formation thickness

PV_{bt}: Number of pore volumes of acid needed to breakthrough

Another semiempirical model is Buijse's Model, which was developed in 2005. In this model, the wormhole growth rate is modeled as a function of acid velocity in pores. The average interstitial velocity is given by:

$$V_i = \frac{Q}{2\pi r l \varphi} \qquad (A.11)$$

Where:

Q: Volumetric flow rate

r: Wormhole penetration distance

Then, the wormhole growth velocity is calculated using equation A.12, where parameters that account for temperature, acid concentration, permeability, and mineralogy are computed using equations A.13, A.14, and A.15.

$$V_{wh} = W_{eff} V_i^{2/3} B \qquad (A.12)$$

$$B = \left(1 - exp\left(-W_B V_i^2\right)\right)^2 \qquad (A.13)$$

$$W_{eff} = \frac{V_{i-opt}^{0.333}}{P V_{bt-opt}} \qquad (A.14)$$

$$W_B = \frac{4}{V_{i-opt}^2} \qquad (A.15)$$

Where:

$V_{i\text{-}opt}$: Optimum acid velocity

Furui et al. (2010) combined the two models of Hung et al. (1989) and Buijse et al. (2005). They introduce the fluid-loss effect coefficient (γ), which was set to be 1/3 for Buijse's model. The following equations are used:

$$v_{wh} = v_{i,tip} N_{Ac} \left(\frac{v_{i,tip} PV_{bt,opt} N_{Ac}}{v_{i,opt}} \right)^{-\gamma} \left\{ 1 - exp\left[-4 \left(\frac{v_{i,opt} PV_{bt,opt} N_{Ac} L_{core}}{v_{i,opt} r_{wh}} \right) \right] \right\}^2 \qquad (A.16)$$

$$v_{i,tip} = \frac{q}{\varphi h \sqrt{\pi m_{wh}}} \left[(1 - \alpha_z) \frac{1}{\sqrt{d_{e,wh} r_{wh}}} + \alpha_z \left(\frac{1}{d_{e,wh}} \right) \right] \qquad (A.17)$$

$$d_{e,wh} = d_{core} PV_{bt,opt} N_{Ac} \qquad (A.18)$$

$$N_{Ac} = \frac{\varphi \beta C_0 \rho_{acid}}{(1 - \varphi) \rho_{rock}} \qquad (A.19)$$

Where:

$V_{i.tip}$: Interstitial velocity at the wormhole tip

N_{Ac}: Acid capacity number

L_{core}: Core length

α_z: Wormhole axial spacing coefficient

$d_{e,wh}$: Effective wormhole radius

d_{core}: Core diameter

β: acid dissolving power

C_0: Injection acid concentration

ρ_{acid}: Acid density

ρ_{rock}: Rock density

γ: Fluid-loss coefficient

Appendix B: An Example of Water and Oil Injection Pressure Responses

Group D: Water and oil injection pressure responses

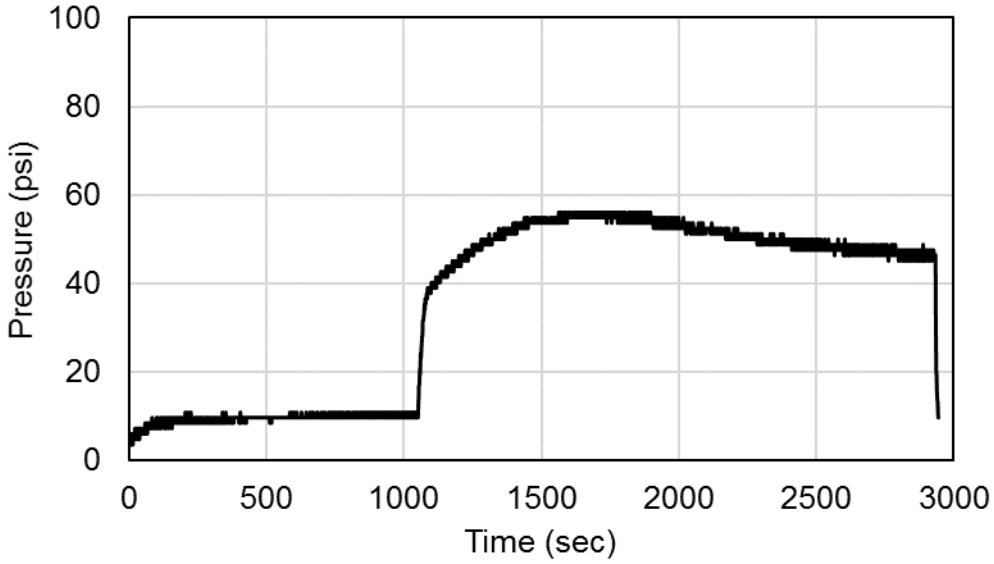

Figure B.1: Pressure responses of water injection of core 1

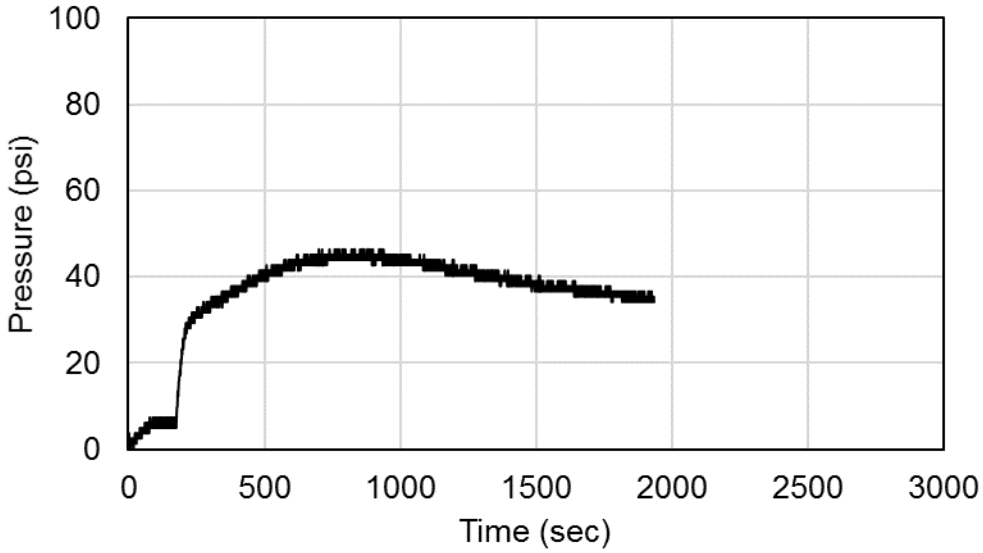

Figure B.2: Pressure responses of water injection of core 2

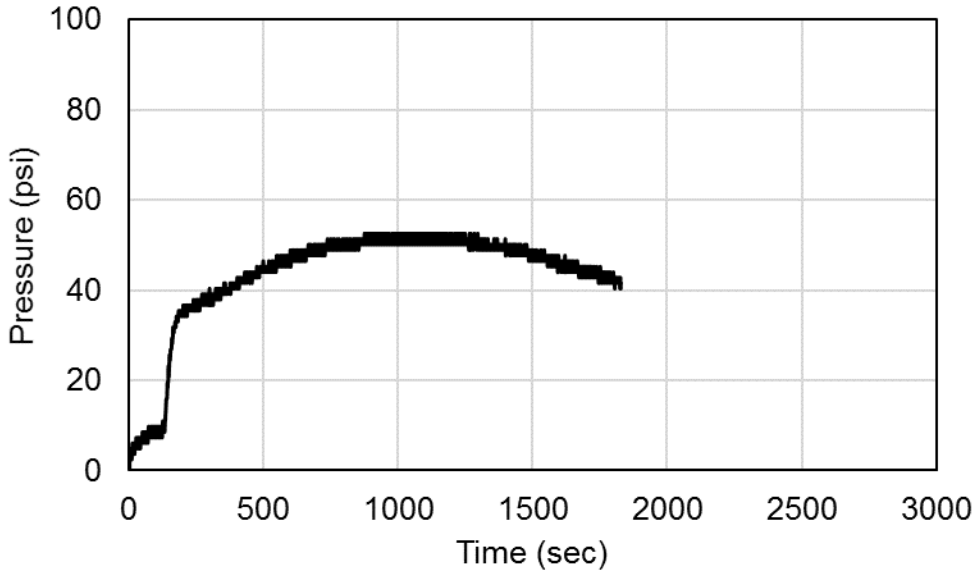

Figure B.3: Pressure responses of water injection of core 4

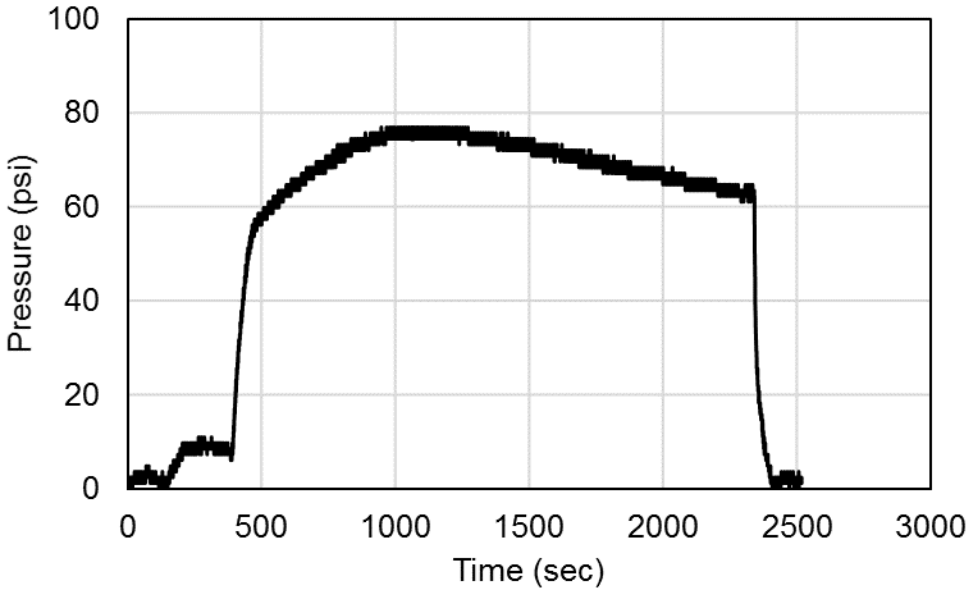

Figure B.4: Pressure responses of water injection of core 11

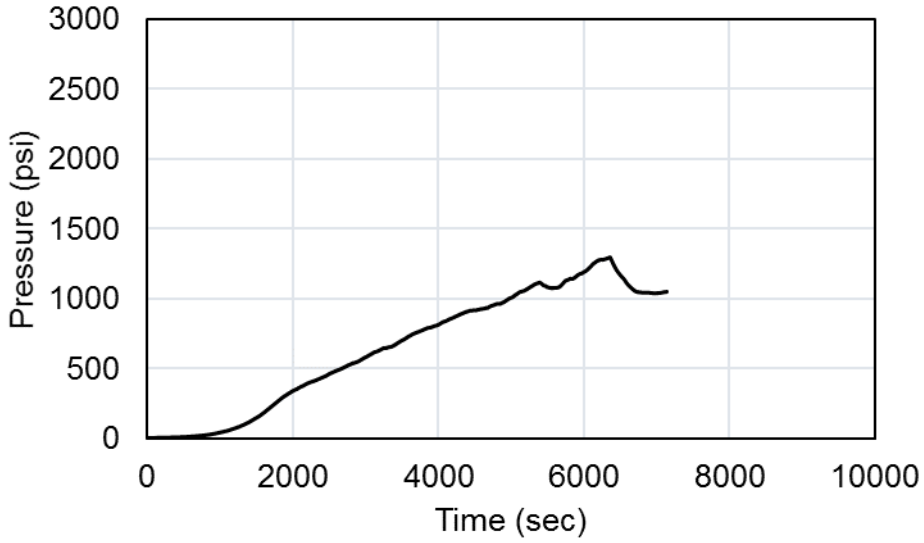

Figure B.5: Pressure responses of oil injection of core 1

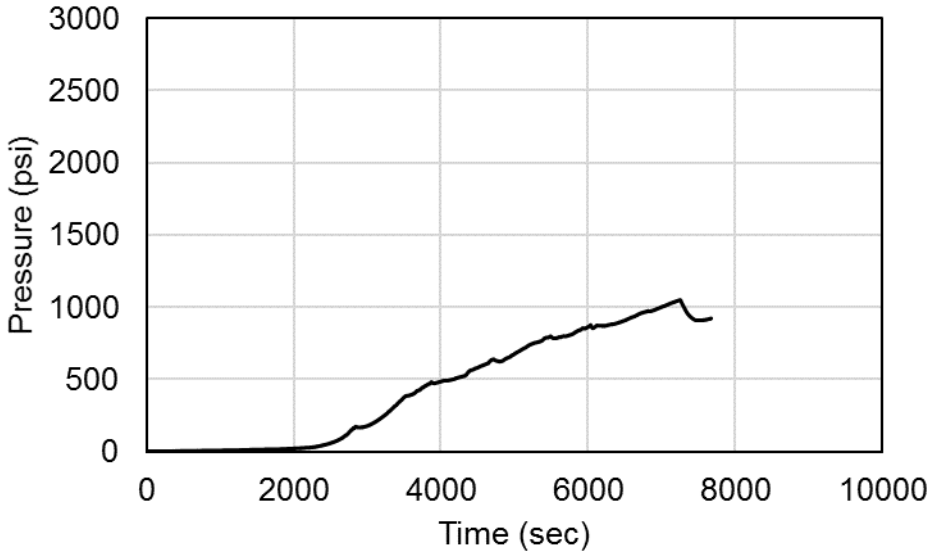

Figure B.6: Pressure responses of oil injection of core 2

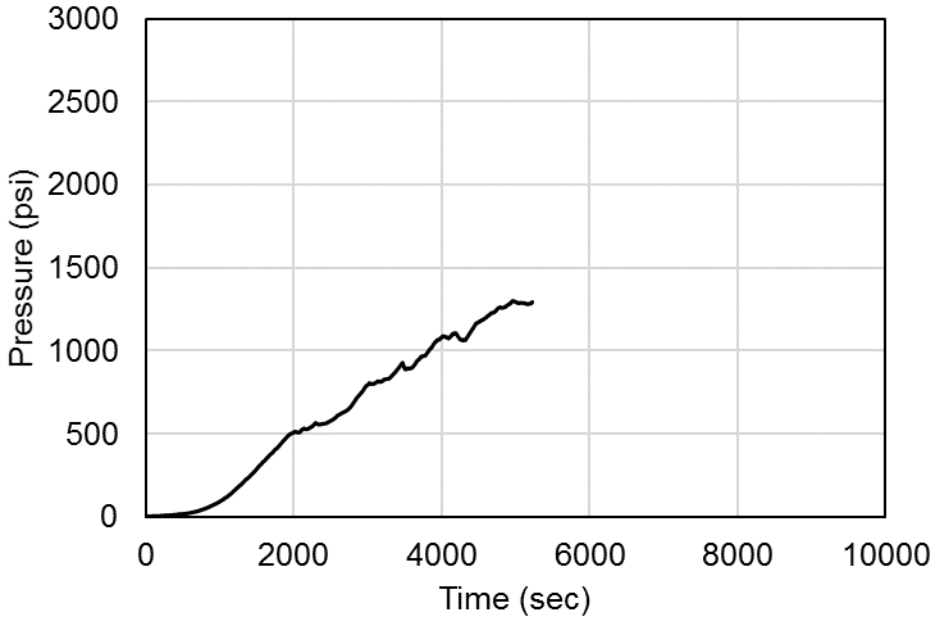

Figure B.7: Pressure responses of oil injection of core 4

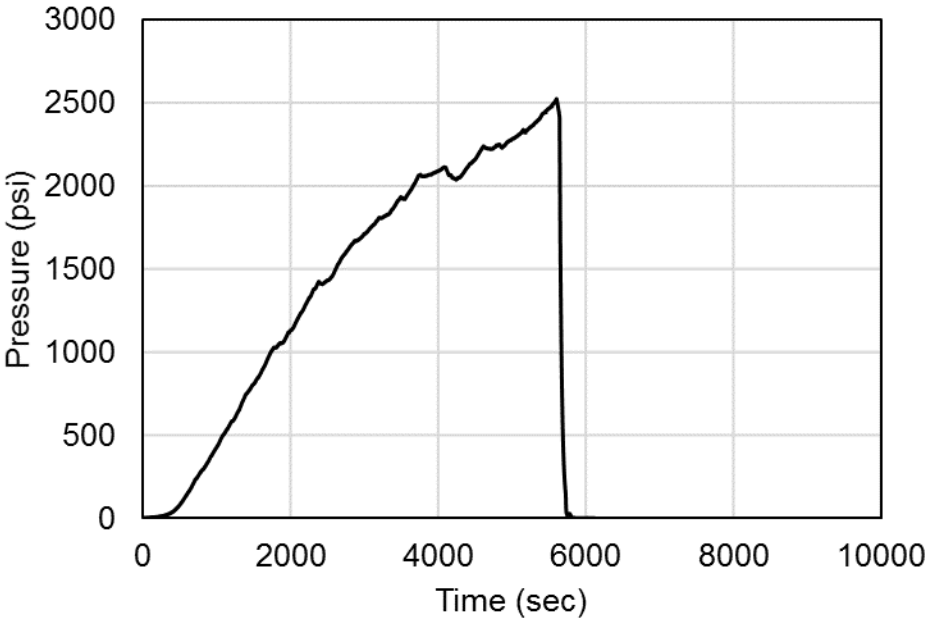

Figure B.8: Pressure responses of oil injection of core 11

Appendix C: Pressure Responses of Acid Injection

Group A: Acid injection pressure responses

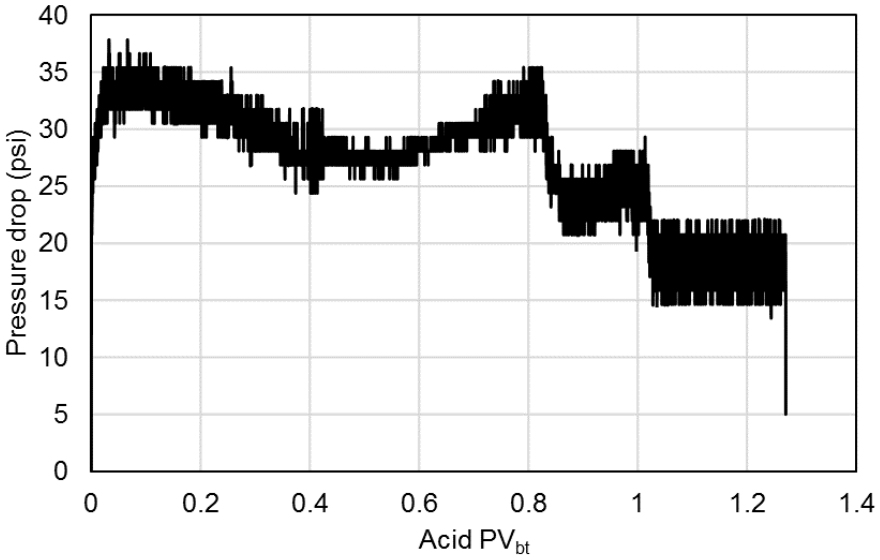

Figure C.1: Pressure responses of acid injection of core 26

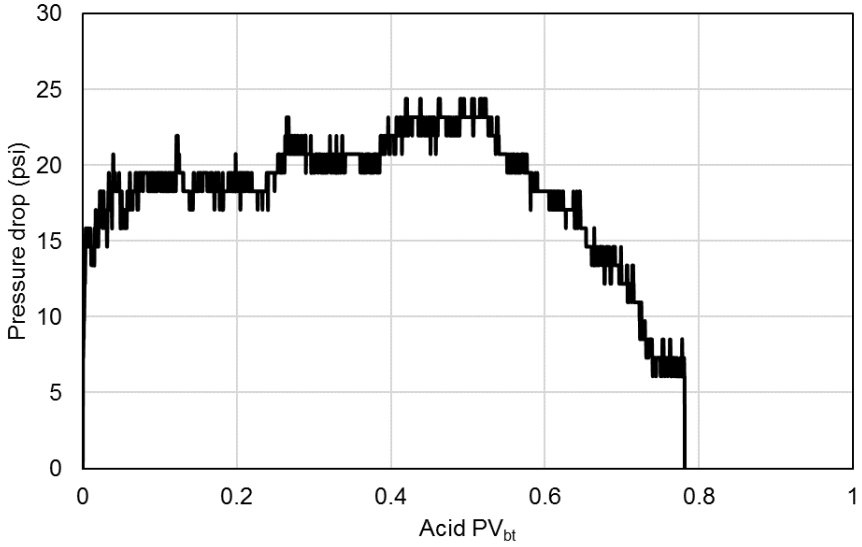

Figure C.2: Pressure responses of acid injection of core 30

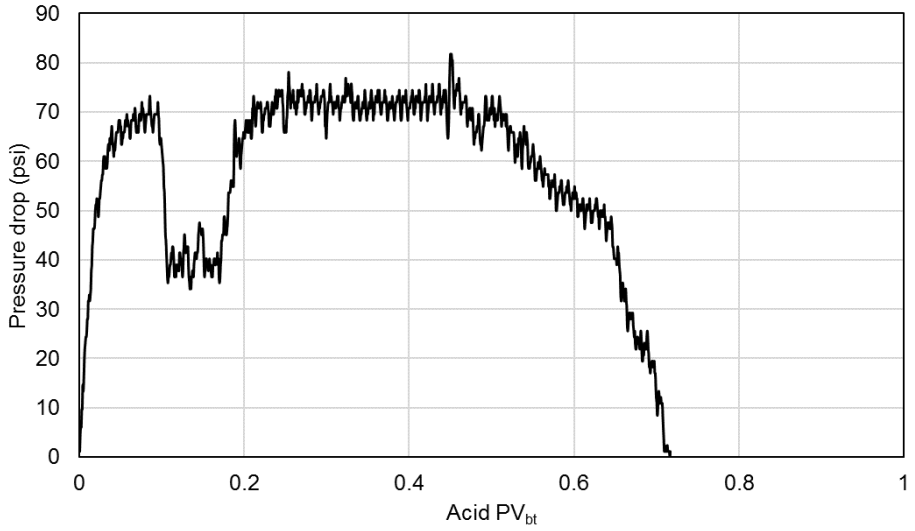

Figure C.3: Pressure responses of acid injection of core 7

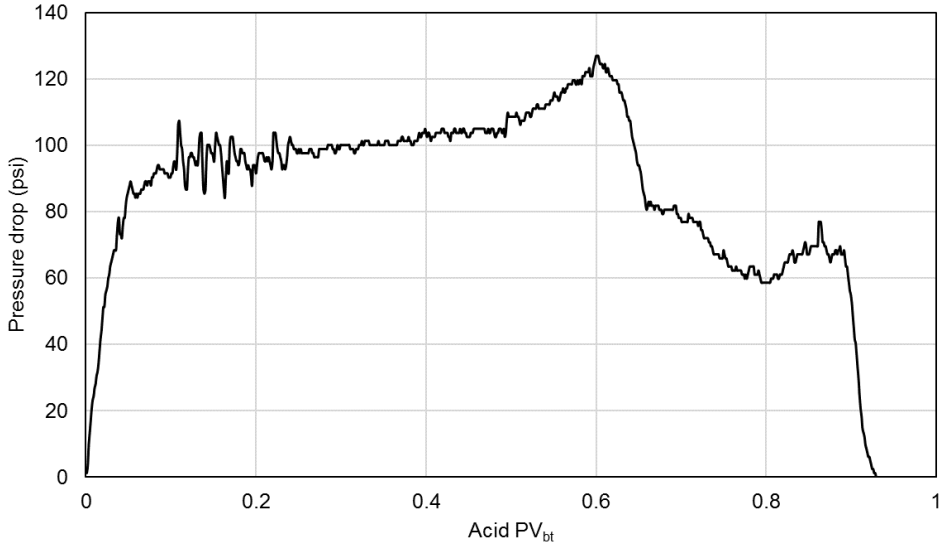

Figure C.4: Pressure responses of acid injection of core 29

Group B: Acid injection pressure responses

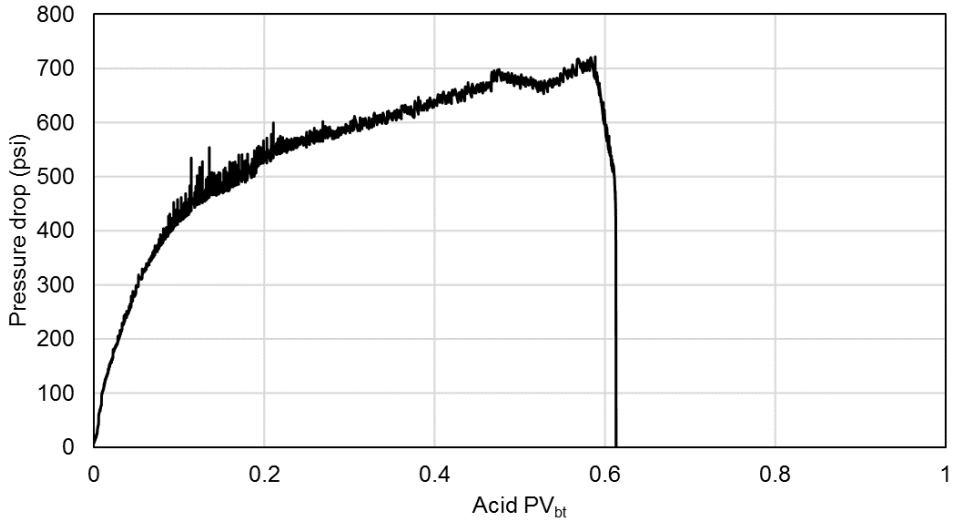

Figure C.5: Pressure responses of acid injection of core 9

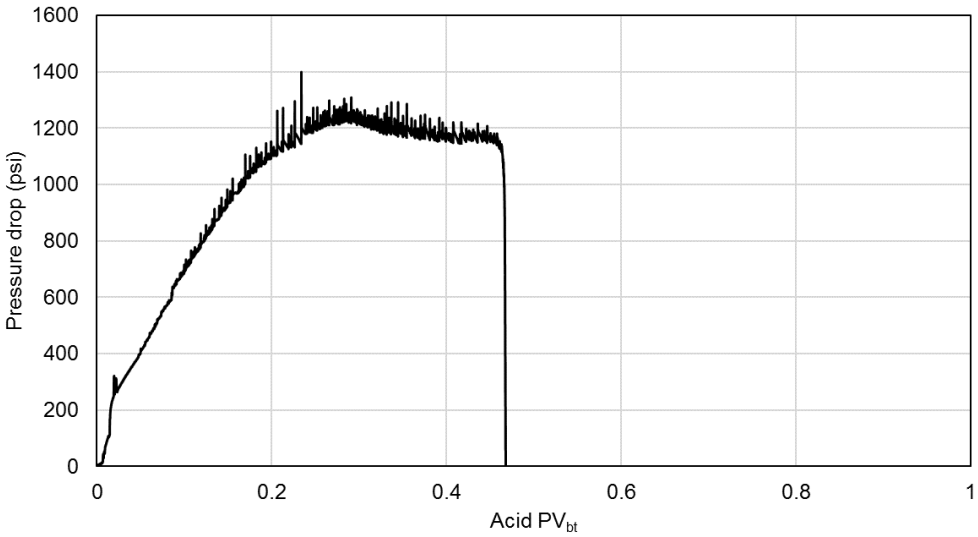

Figure C.6: Pressure responses of acid injection of core 17

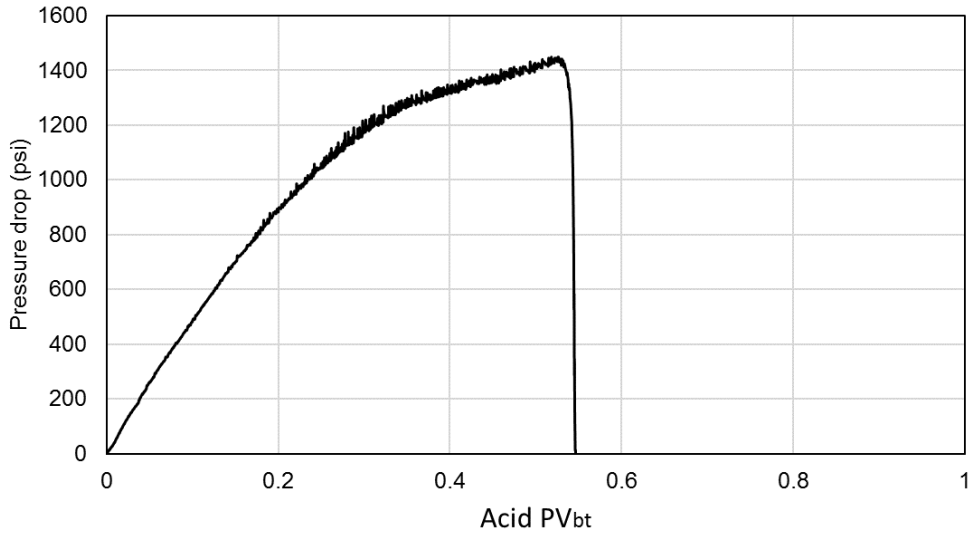

Figure C.7: Pressure responses of acid injection of core 6

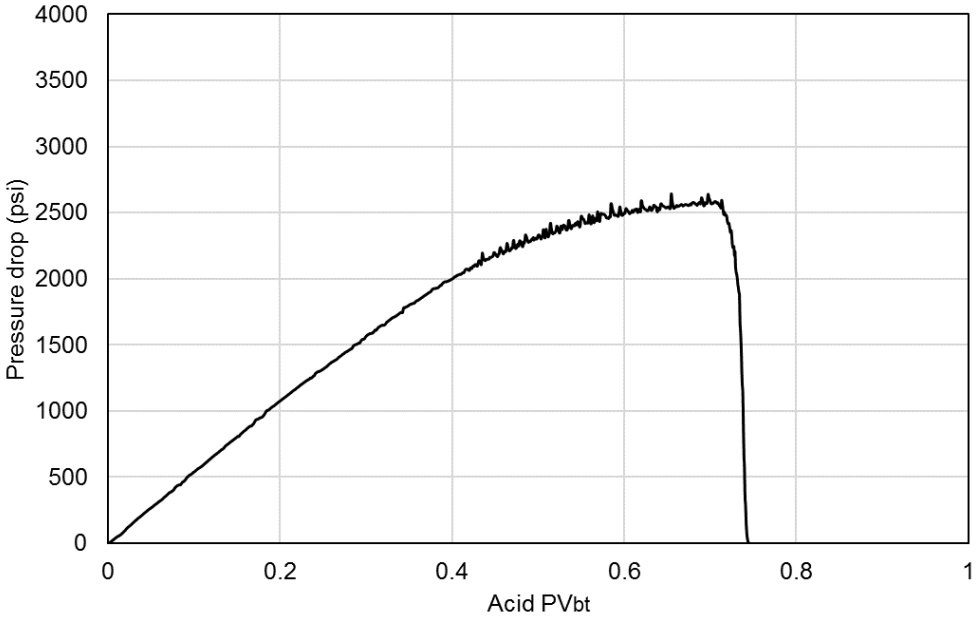

Figure C.8: Pressure responses of acid injection of core 8

Group C: Acid injection pressure responses

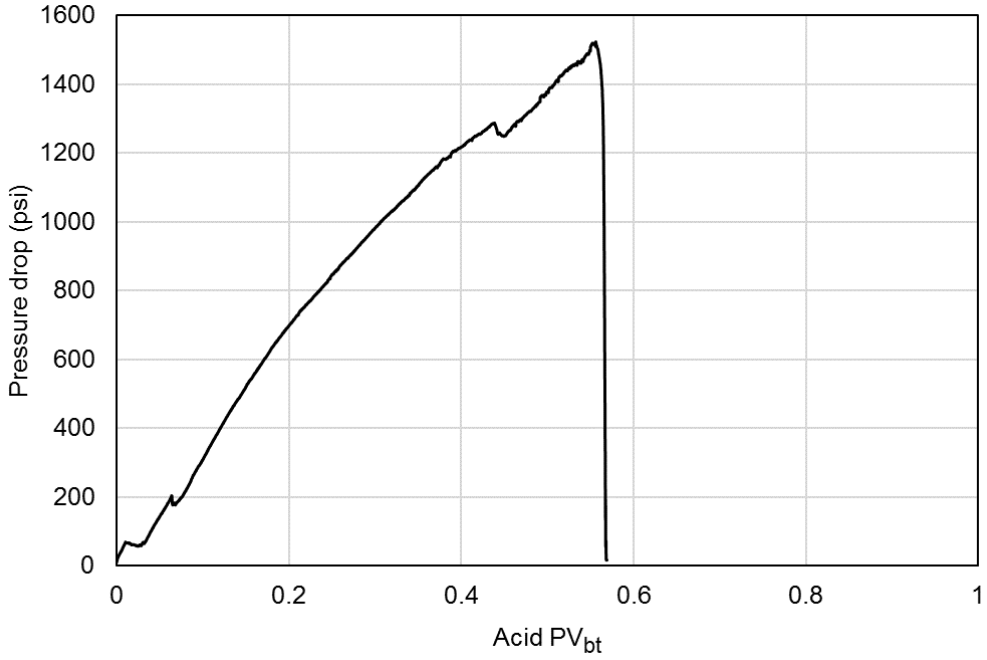

Figure C.9: Pressure responses of acid injection of core 16

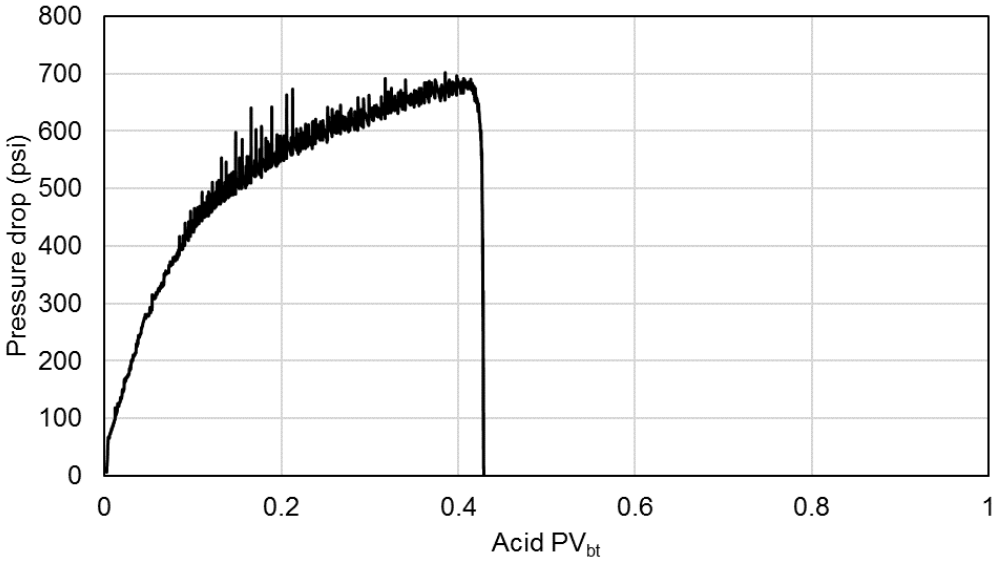

Figure C.10: Pressure responses of acid injection of core 27

Group D: Acid injection pressure responses

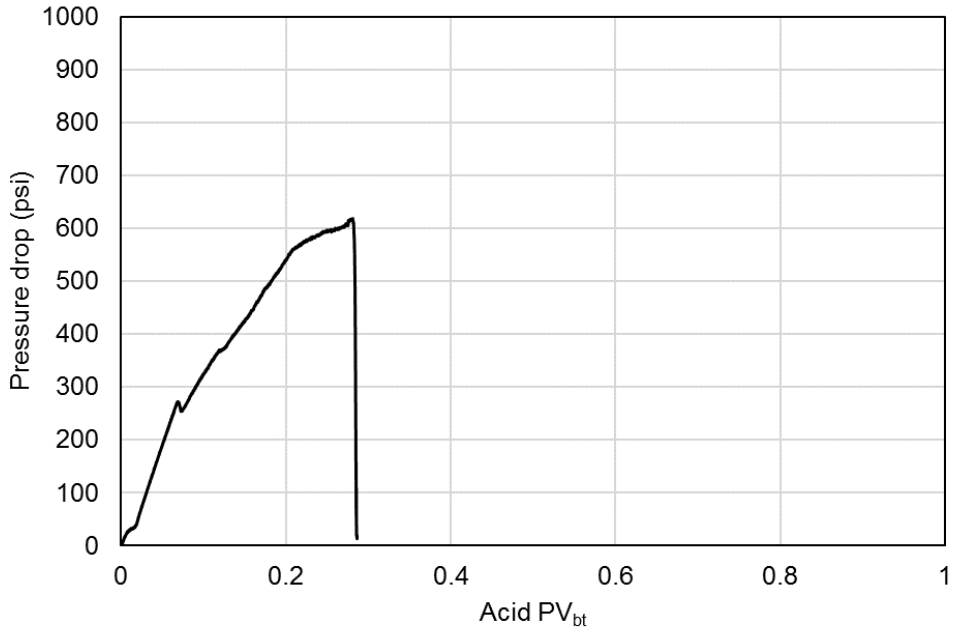

Figure C.11: Pressure responses of acid injection of core 11

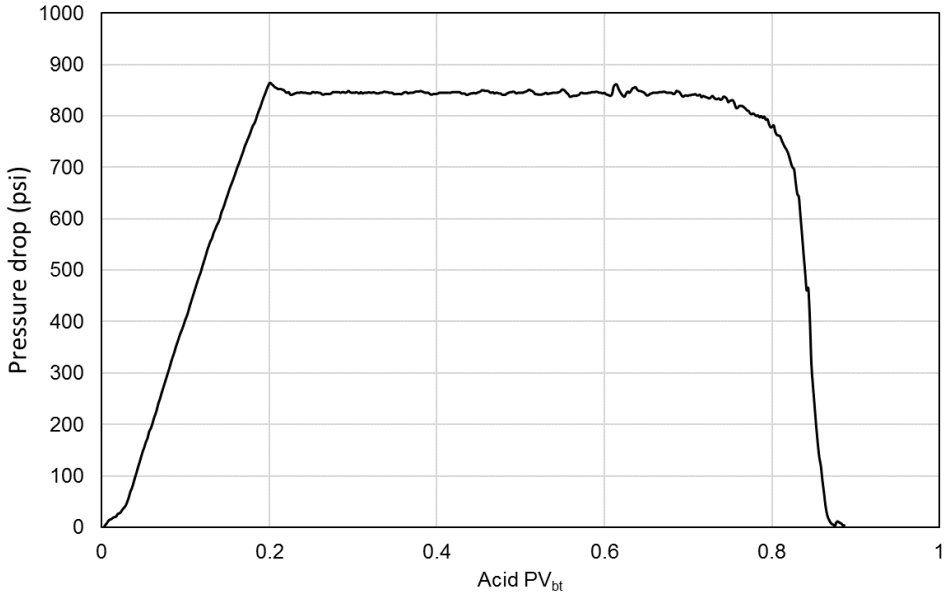

Figure C.12: Pressure responses of acid injection of core 2

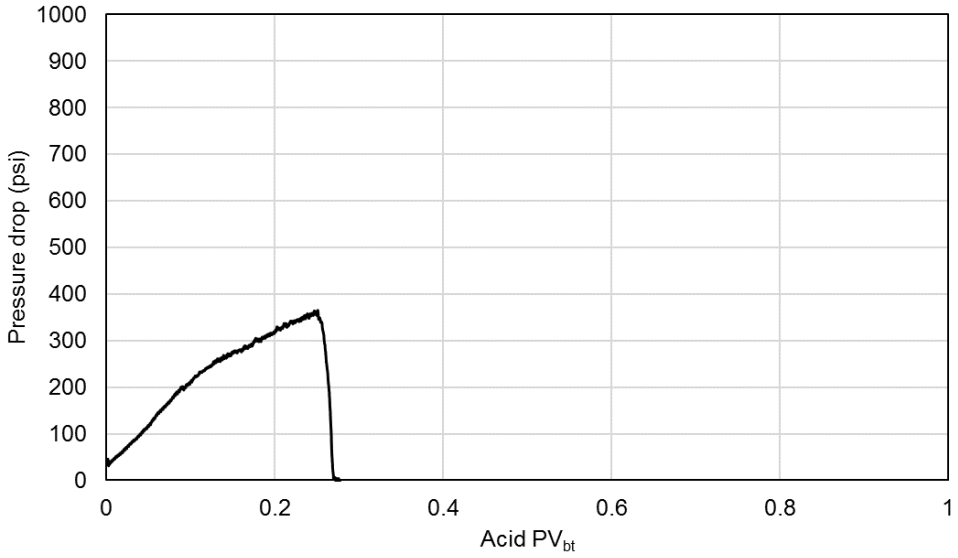

Figure C.13: Pressure responses of acid injection of core 1

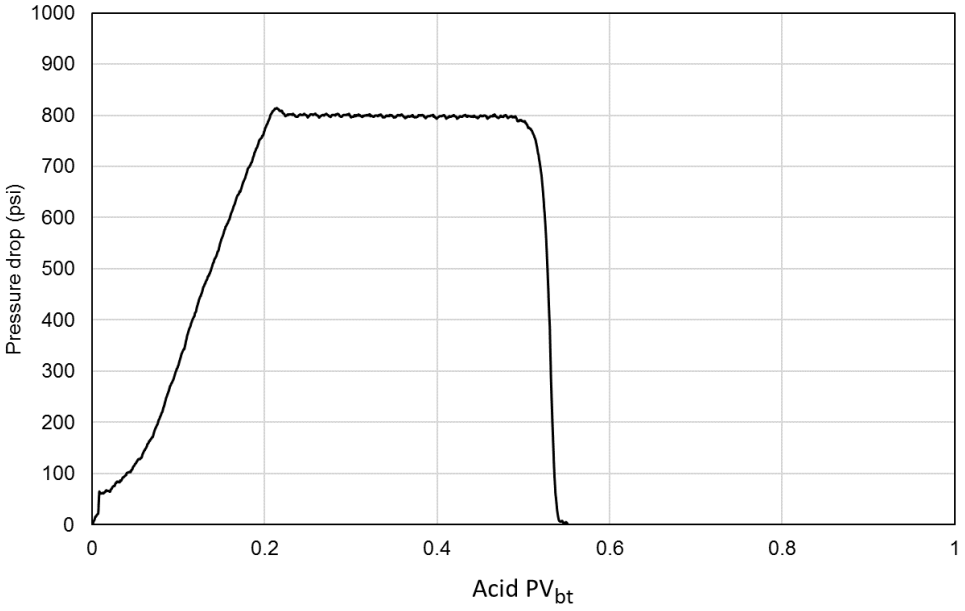

Figure C.14: Pressure responses of acid injection of core 4

Group E: Acid injection pressure responses

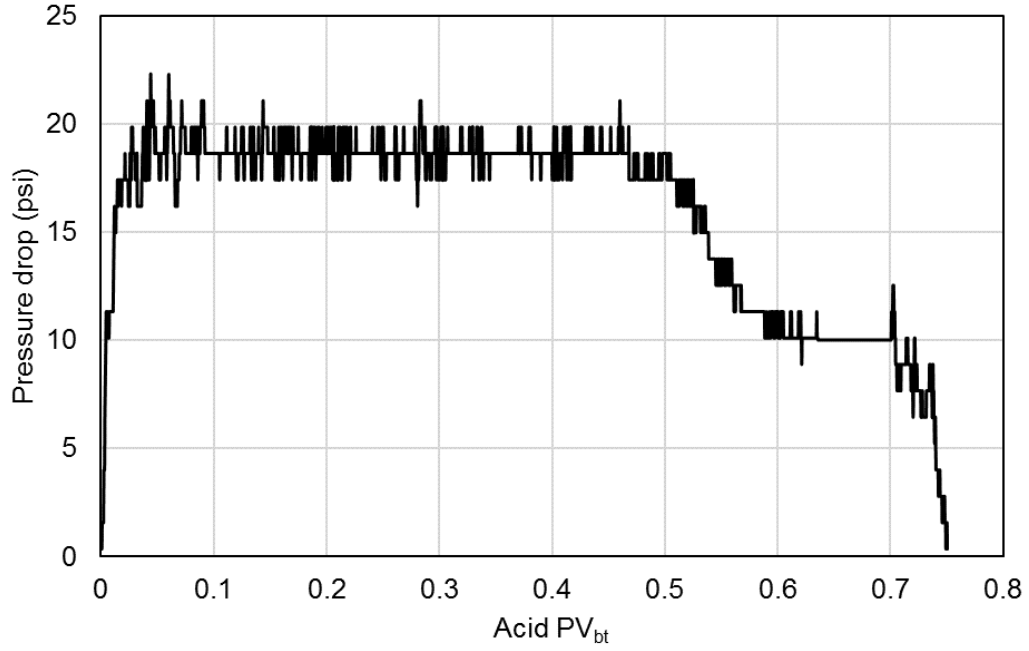

Figure C.15: Pressure responses of acid injection of core 23

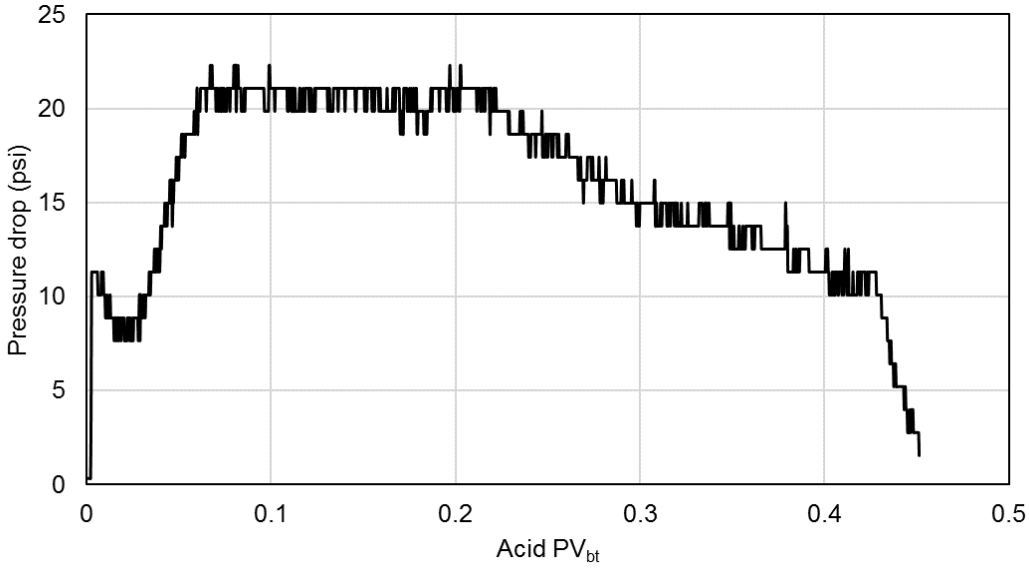

Figure C.16: Pressure responses of acid injection of core 25

Group F: Acid injection pressure responses

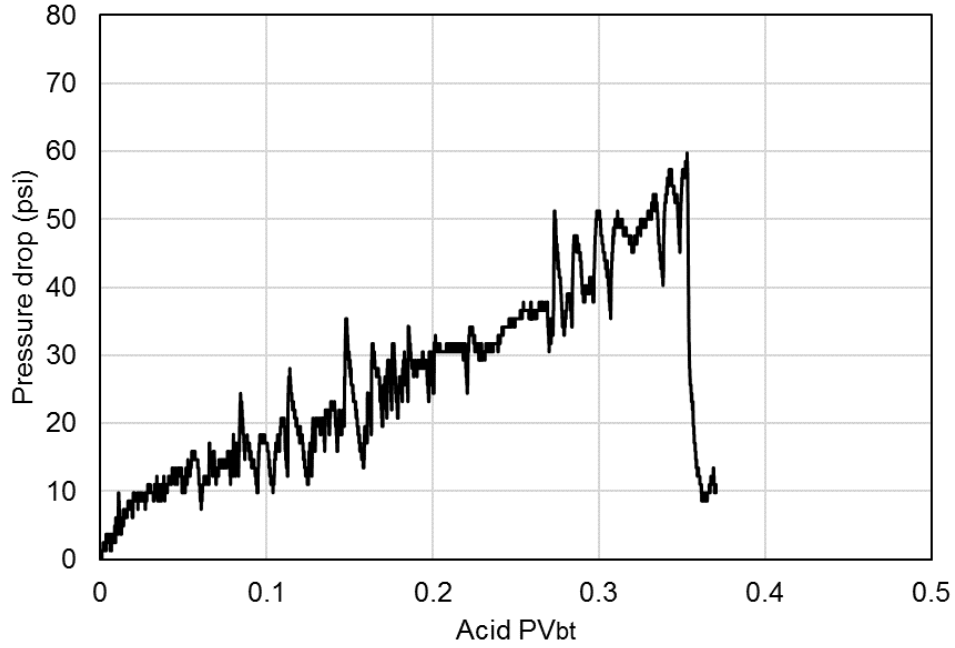

Figure C.17: Pressure responses of acid injection of core 44

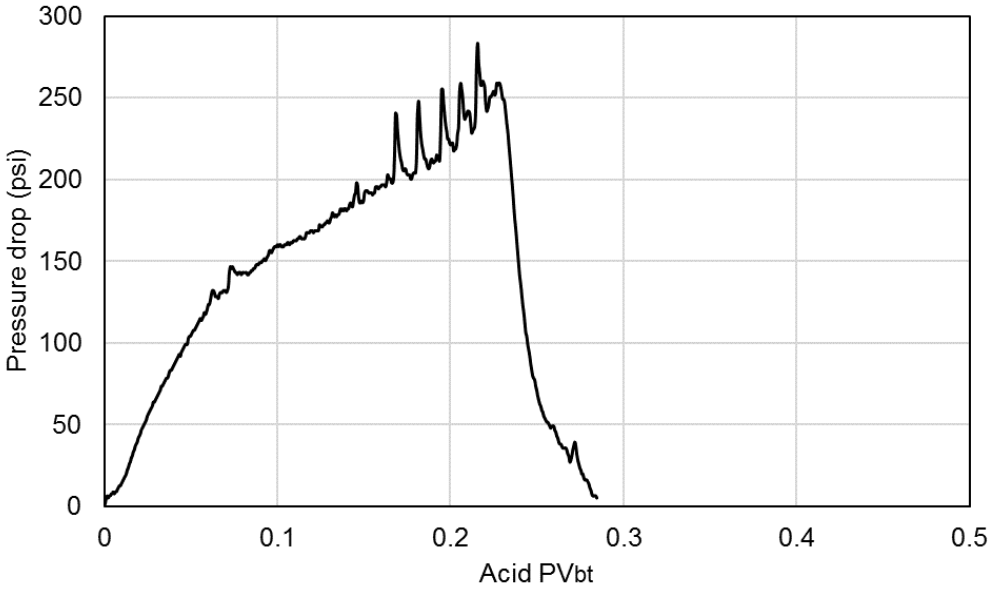

Figure C.18: Pressure responses of acid injection of core 45

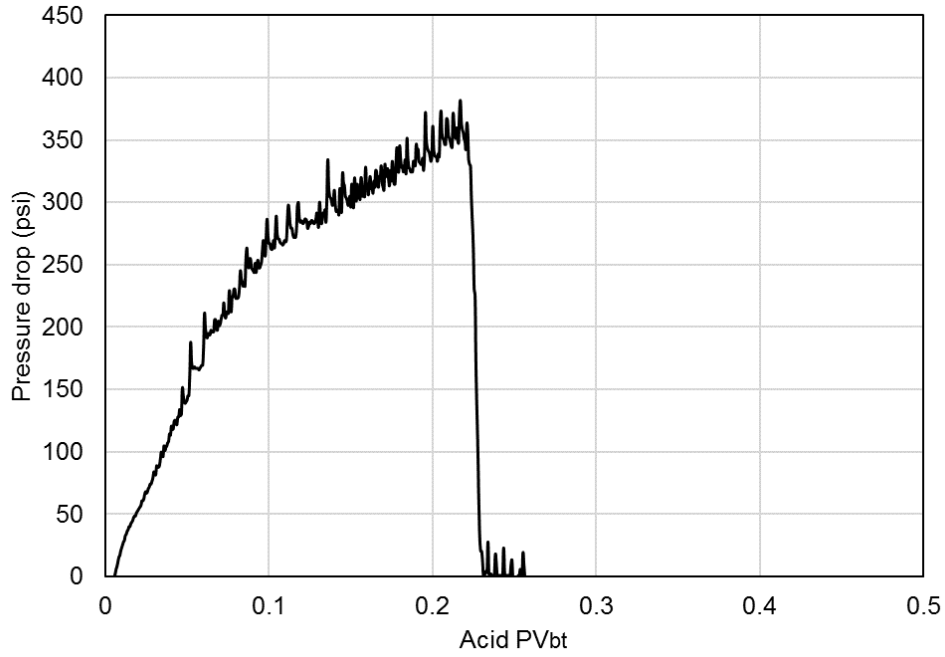

Figure C.19: Pressure responses of acid injection of core 42

Group H: Acid injection pressure responses

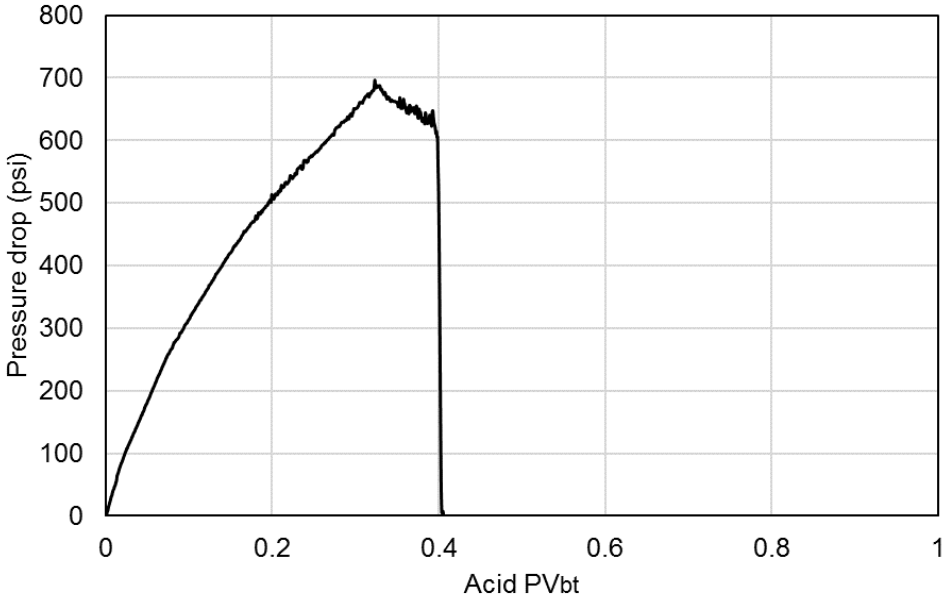

Figure C.20: Pressure responses of acid injection of core 3

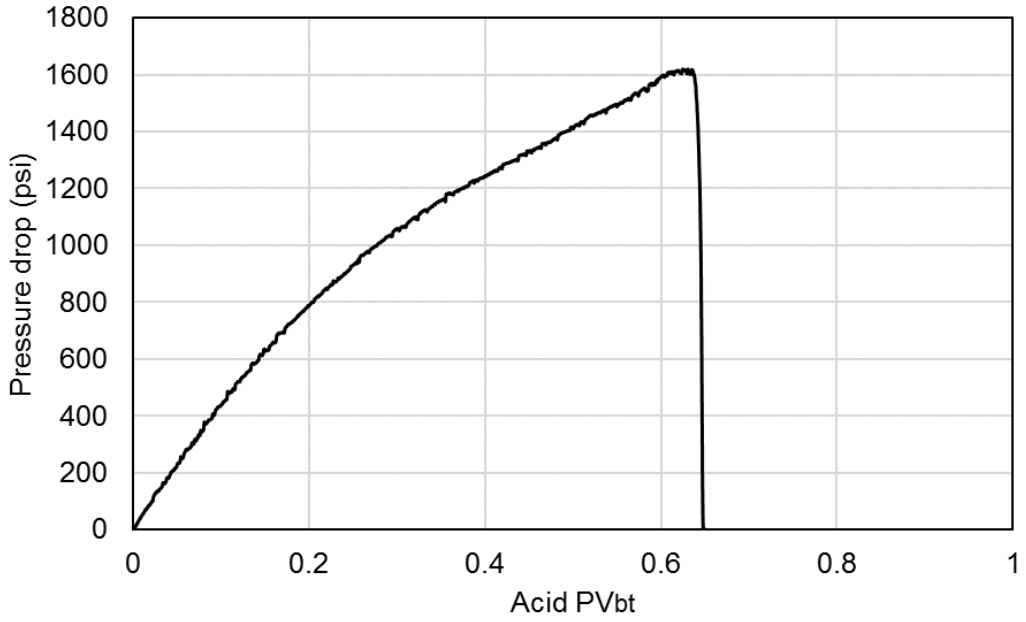

Figure C.21: Pressure responses of acid injection of core 24

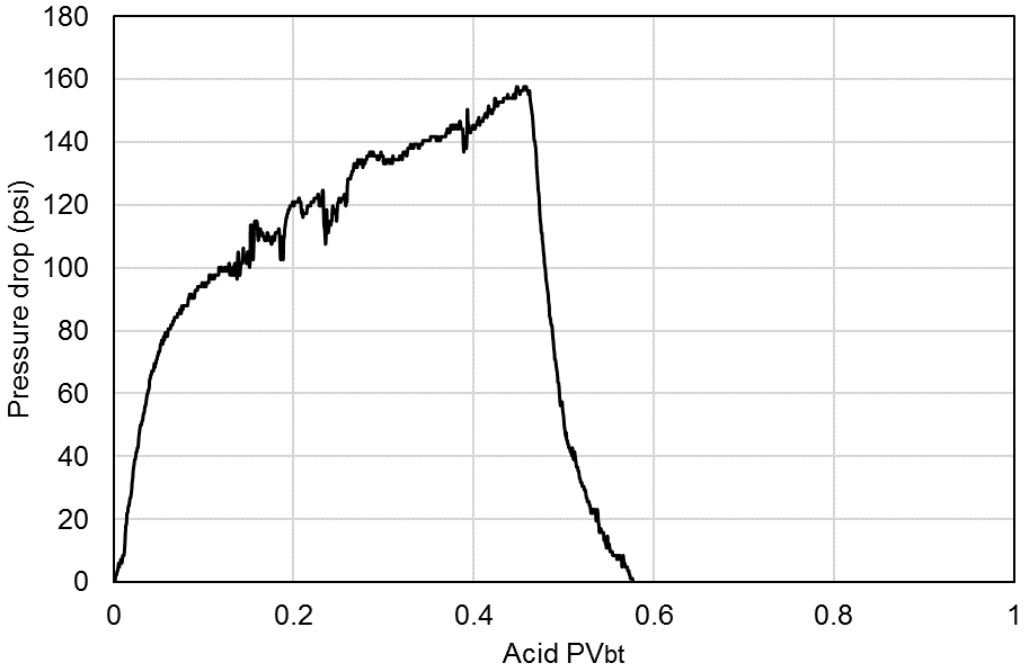

Figure C.22: Pressure responses of acid injection of core 43

Appendix D: Metal Casting Method of Injected Cores

Because the wormhole characterization is essential in evaluating the acid process, a metal casting method is used for distinguishing different wormholes for different acid flooding scenarios. The following procedure is applied:

- The cores were cased in a PVC pipe, and Wood's metal was placed on top of the core sample.
- Upon heating in an oven to approximately 200°F, the Wood's metal melted and then drained into the core.
- The core was then cooled to solidify the metal, all remaining carbonate rock was dissolved with acid, and the metal casting was recovered.

Figures D.1.a, D.1.b, and D.1.c show materials required for this method; Figure D.1.d is the core being dissolved by acid, while Figure D.1.e is an example of one of the cores being cast.

(a) wood's metal **(b) PVC pipe** **(c) Casing base** **(d) core dissolving** **(e) Resulted wormhole**

Figure D.1: Core casting process

Validation of the Casting Method

The following experiment procedure is conducted to make sure the metal casting method works properly of representing the wormhole created by acid, and the melted metal does not flow in porous media other than the wormhole itself (Figure D.2).

- A piece of the Indiana Limestone rock is cut from the same block used in this study.
- A hole of 1.5 in. length and 3/32 -in Diameter is drilled using a drilling bit.
- Metal is melted and poured into the hole.
- After the metal is cooled, the piece of rock is destroyed using live HCl.

Figure D.2: Drilling a piece of core and casting it

Nomenclature

Acronyms

A	Cross-sectional area
a	Experimental constant
AV_{bt}	Acid-Volume-to-Breakthrough
A_T	Transition pore area
b	Constant = $1.5 * 10^{-5}$ SI units
B_o	Formation volume factor
C	Acid concentration
Co	Initial concentration
CT	Computerized Tomography
C_{end}	Acid concentration at wormhole tip
D	Molecular diffusion coefficient
D_a	Damkohler number
D_{ab}	Acid diffusion rate
d	Bond diameter
d_{core}	Core diameter
$d_{e,wh}$	Effective wormhole radius
d_f	Fractal dimension
E_f	Forward reaction rate constant
h	Formation thickness
HCL	Hydrochloric acid
i	Injection rate
k	Kinetics reaction rate constant
K	Absolute permeability
K_d	Acid dissociation constant
K_f	Reaction rate constant
Ks	Damaged zone permeability
L	Wormhole length
L_a	Average length
L_{core}	Core length
MW_{acid}	Molecular weight of acid
MW_{rock}	Molecular weight of the rock

n	Reaction order
N_{ac}	Acid capacity number
P	kinetic parameter
Pe	Peclet number
PV_{bt}	Pore volume to breakthrough
$PV_{bt\text{-}opt}$	Optimum volume to breakthrough
q	Hydrocarbon flow rate
R	Pore radius
r_e	Reservoir radius
r_s	Radius of the damaged zone
r_T	Transition pore size
r_w	Wellbore radius
r_{wh}	Radius of worm-holed area
S	Skin factor
T	Temperature
t	Time
u	Acid flux
U_d	The diffusive flux
U_s	Molecular flux caused by surface reaction
U_{end}	Acid flux
V	Cumulative acid injected volume
v	Kinematic viscosity
V_{acid}	Volume of Acid
V_{rock}	Volume of rock
β_{100}	Dissolving power at 100% HCL
ρ_{acid}	Acid density
ρ_{rock}	Rock density
$\emptyset$	Porosity
β	Acid dissolving power
ϑ	Stoichiometric coefficient
α_z	Wormhole axial spacing coefficient
γ :	Fluid-loss coefficient